Université du Québec

INRS Institut national de la recherche scientifique

Centre Énergie Matériaux Télécommunications

NEW TYPES OF RECONFIGURABLE ORBITAL ANGULAR MOMENTUM ANTENNAS FOR INTELLIGENT WIRELESS SYSTEMS

Par

Hassan Naseri Gheisanab

Thèse présentée pour l'obtention du grade de
Philosophiae Doctor, Ph.D.
en Télécommunications

Jury d'évaluation

Examinateur interne	Prof. Serioja Tatu Institut national de la recherche scientifique
Examinateur externe	Prof. Mostafa Hefnawi Royal Military College of Canada
Examinateur externe	Prof. Rashid Mirzavand University of Alberta
Directeur de recherche	Prof. Tayeb A. Denidni Institut national de la recherche scientifique

ACKNOWLEDGMENT

First and foremost, I extend my deepest thanks to Allah, the Almighty, for granting me the health, strength, and perseverance necessary to complete this research.

I would like to express my profound gratitude to Professor Tayeb Denidni for his invaluable guidance and support throughout my academic journey. His wisdom and encouragement have played a crucial role in my progress.

To my dear wife, your unwavering love, patience, and understanding have been my greatest source of strength. Your sacrifices and constant support have inspired me to keep moving forward.

To my parents and my brother, your constant encouragement and belief in me have been a powerful driving force behind my achievements. Your support laid the foundation for my success.

I also wish to sincerely thank my friends, whose companionship and motivation have been a source of joy and comfort throughout this journey.

Finally, I express my heartfelt appreciation to my university, the *Institut National de la Recherche Scientifique (INRS–EMT), Université du Québec*, as well as to the *Fonds de Recherche du Québec–Nature et Technologies (FRQNT)* for their generous support of my doctoral studies through a full scholarship.

RÉSUMÉ

Traditionnellement, afin d'augmenter la capacité des canaux dans les systèmes de communication sans fil, tous les efforts ont été concentrés sur l'amélioration de la Bandwidth (BW) et du Signal to Noise Ratio (SNR). En effet, pour atteindre un débit élevé de transmission de données, une large bande d'impédance et un niveau de SNR acceptable sont requis. Toutefois, les systèmes actuels ne parviennent plus à répondre à la demande croissante des utilisateurs en matière de communications à haute vitesse, en raison des limitations liées à la BW et au SNR : la BW est parfois limitée par la bande passante du gain ou de l'Axial Ratio (AR), et le SNR chute à cause des variations environnementales ou d'autres paramètres incontrôlables. Ainsi, dans ce contexte, de nouvelles conceptions d'antennes doivent être envisagées pour améliorer la capacité des canaux.

Les antennes à Orbital Angular Momentum (OAM) peuvent générer plusieurs faisceaux orthogonaux en forme de "donut" à partir d'une seule ouverture. Cette orthogonalité provient des fronts de phase hélicoïdaux. Il est ainsi possible de transmettre simultanément plusieurs flux de données à la même fréquence.

Les antennes OAM reconfigurables jouent un rôle essentiel dans les systèmes sans fil avancés. Leur reconfigurabilité peut concerner les numéros de mode, la polarisation ou la fréquence de fonctionnement. Cette thèse vise principalement à développer de nouveaux systèmes d'antennes capables d'offrir ces types de reconfigurabilité. L'application principale de ces antennes se situe dans les systèmes intelligents basés sur l'OAM.

La première chapter présente une introduction approfondie aux principes fondamentaux des modes OAM et à leurs mécanismes de génération. Elle décrit également trois méthodes couramment utilisées pour l'excitation des modes OAM.

Dans la deuxième chapter, notre première conception d'antennes OAM reconfigurables en modes est discutée. Le design est basé sur une Uniform Circular Array (UCA) et un réseau d'alimentation 1×4. Grâce aux déphaseurs intégrés dans le réseau d'alimentation, il est possible de générer les modes OAM $+1$ ou -1. Le système proposé utilise des antenne patch comme éléments rayonnants, ce qui limite le contrôle de la polarisation après fabrication. De plus, comme le système ne comporte qu'un seul port d'entrée, il ne peut générer qu'un seul mode OAM à la fois. Cette limitation empêche l'utilisation simultanée de plusieurs modes, réduisant ainsi le potentiel des antennes OAM à améliorer la capacité du canal.

Dans la troisième chapter, un nouveau système d'antenne est présenté, permettant le contrôle à la fois de la polarisation de chaque mode OAM et de la fréquence de fonctionnement. Le système proposé peut en effet exciter simultanément plusieurs modes OAM avec des polarisations spécifiques, tout en offrant une capacité de syntonisation en fréquence. Une version modifiée de cette conception est évaluée dans la chapter 4. Ce nouveau design permet non seulement la propagation simultanée des modes, mais aussi la reconfiguration des numéros de mode assignés à chaque polarisation. La capacité de syntonisation en fréquence est également préservée. Ce système d'antenne répond à l'objectif principal de cette thèse : proposer des antennes OAM reconfigurables en modes, polarisation et fréquence.

Plus le nombre de modes OAM disponibles est élevé, plus les avantages liés à cette technologie sont importants. Dans cette optique, la chapter 5 présente un nouveau système capable

de générer trois modes OAM (0, -1, $+1$). Chaque mode peut se propager avec une polarisation verticale ou horizontale (sélectivité de polarisation), augmentant ainsi le degré de reconfigurabilité.

Après avoir exploré la conception d'antennes OAM reconfigurables pour des systèmes de communication intelligents, notre recherche a été étendue au développement d'antennes à gain élevé et multi-modes. Ces antennes sont essentielles pour les communications OAM à longue portée. Une présentation détaillée de ce travail est proposée également dans la chapter 6.

Enfin, la chapter 7 présente les conclusions tirées de quatre années de recherche dans le domaine des antennes OAM. Des pistes potentielles pour des travaux futurs y sont également proposées.

Mots-clés : Antennes OAM reconfigurables, Systèmes sans fil intelligents, Polarisation, Réseau d'alimentation

ABSTRACT

Traditionally, in order to increase the channel capacity of wireless communication systems, all attention has been on the enhancement of Bandwidth (BW) and Signal to Noise Ratio (SNR). In fact, to achieve a high-data transfer rate, a wide impedance BW and acceptable SNR level are required. However, nowadays, current systems are not able to satisfy user's growing demand for high-speed communications due to the fact that there are limitations regarding BW and SNR; the BW sometimes is restricted by gain or Axial Ratio (AR) BWs, and SNR drops as a result of change in environment conditions or other uncontrollable parameters. Therefore, with all this in mind, it should be a new antenna designs for improving the channel capacities.

Orbital Angular Momentum (OAM) antennas can generate various orthogonal donut-shaped beams from a shared aperture, orthogonality stems from helical phase fronts. Thus, it is possible to transfer several streams of data at the same frequency simultaneously.

Reconfigurable OAM antennas play a crucial role in advanced wireless systems. Their reconfigurability may involve mode numbers, polarization, or operating frequency. This thesis primarily aims to develop novel antenna systems capable of offering these types of reconfigurability. The main application of such antennas would be intelligent OAM systems.

The first chapter provides a comprehensive introduction to the fundamentals of OAM modes and their generation mechanisms. It also outlines and explains three commonly used methods for exciting OAM modes.

In the second chapter, our initial design focused on the mode reconfigurable OAM antennas are discussed. The design consists a Uniform Circular Array (UCA) and a 1×4 feeding network. Using the phase shifters embedded in the feeding network, there is a possibility to generate OAM mode +1 or -1. The proposed work has utilized patch antennas as the radiators, limiting the control on the polarization of system after fabrication. Additionally, since the system has only a single input port, it can generate only one OAM mode at a time. This limitation prevents the simultaneous use of multiple modes, thereby restricting the potential of the OAM antennas to enhance channel capacity.

In the third chapter, we provided a new antenna system with both control on polarization of each OAM mode as well as the operating frequency. In fact, the proposed system can simultaneously excite OAM modes with specific polarization and frequency-tunability capability. The modified version of this work has been evaluated in chapter 4. The new design not only has the benefit of simultaneous mode propagation but also can change the mode numbers assigned for each polarization. Frequency-tunability has preserved in the work as well. This antenna system has enabled us to reach the main goal of this thesis; OAM antenna systems with reconfigurability of modes, polarization and frequency.

The more we can increase the number of OAM modes, the more we can take advantage of their feature. To that end, we came up with a new system in chapter 5 which can generate three OAM modes (0,-1 and +1). Each mode can propagate with vertical or horizontal polarization (polarization selectivity), thus resulting in further increment of reconfigurability degree.

After completing our investigation into reconfigurable OAM antenna design for intelligent wireless communication systems, we extended our research to the development of high-gain, multi-

mode antenna systems. These antennas are crucial for enabling long-distance OAM communication. In chapter 6, detailed explanation on this work has been provided.

Finally, in chapter 7, the conclusions drawn from four years of research in the field of OAM antennas are presented. Furthermore, potential directions for future research are discussed.

Keywords : Reconfigrable OAM antennas, Intelligent wireless systems, Polarization, feeding network.

SOMMAIRE RECAPITULATIF

A.1 Titre de la Thèse en Français

NOUVEAUX TYPES D'ANTENNES RECONFIGURABLES À ORBITAL ANGULAR MOMENTUM POUR LES SYSTÈMES SANS FIL INTELLIGENTS

A.2 Introduction

En parlant des systèmes sans fil avancés, la communication à haut débit et l'imagerie haute résolution viennent à l'esprit. Ces caractéristiques ne peuvent pas être atteintes avec des antennes traditionnelles, car celles-ci sont limitées par la BW et le SNR. Plus précisément, la BW d'impédance est parfois restreinte par les BW de gain ou de AR, et le SNR diminue à cause de changements dans les conditions environnementales ou d'autres paramètres incontrôlables. Une solution consiste à utiliser des antennes Multiple-Input Multiple-Output (MIMO), qui peuvent introduire un degré de liberté supplémentaire afin d'améliorer le débit de données dans les systèmes de communication et la qualité des résultats dans les dispositifs d'imagerie [1, 2]. Cependant, des systèmes de beamforming sont nécessaires à cet effet [3]. Ces systèmes exigent un effort considérable lors de la phase de conception et d'implémentation. De plus, ils rendent les systèmes plus complexes.

La meilleure alternative pour les antennes mentionnées ci-dessus sont les antennes Orbital Angular Momentum (OAM). Les antennes OAM peuvent générer plusieurs faisceaux orthogonaux en forme de donut à partir d'une ouverture partagée, l'orthogonalité provient des fronts de phase héliques. Ainsi, il est possible de transférer plusieurs flux de données à la même fréquence simultanément. Pour démontrer cela, supposons que l'objectif soit de transmettre trois flux vidéo à partir d'une antenne conventionnelle. À cette fin, la BW devrait être divisée en trois parties distinctes, chacune affectée à une donnée. Comme il est évident, la BW devient limitée, ce qui entraîne un taux de données plus faible. De plus, trois porteuses devraient être générées pour la modulation et le multiplexage, ce qui nécessite des circuits externes. Dans le cas où l'antenne est remplacée par une portant trois faisceaux OAM, chaque donnée pourrait être transférée par un faisceau OAM en même temps et à la même fréquence. Du côté récepteur, elles pourraient être séparées par leurs modes OAM correspondants, sans besoin de processus de démultiplexage sophistiqués. Comme autre exemple, les systèmes d'imagerie traditionnels traitent les signaux en fonction des ondes diffusées provenant des objets étant imagés. Il est évident que plus les ondes diffusées portent des informations, meilleure serait la qualité des images après traitement du signal. Ainsi, pour fournir plus d'informations aux ondes diffusées, les antennes OAM multimodes peuvent être très utiles [4, 5]. En fait, chaque mode porte ses propres informations.

Ayant acquis une connaissance générale des capacités des modes OAM, il convient maintenant d'expliquer comment ces derniers peuvent être générés. Si l'on considère une loop antenne ayant une distribution de courant $I = I_0.e^{jl\phi}$, le calcul du radiation pattern de l'antenne fait apparaître le terme $e^{jl\phi}$ dans le champ électrique sur le plan perpendiculaire à l'axe de propagation. Cela indique la présence d'un front de phase hélicoïdal dans le faisceau, où l représente le nu-

méro de mode OAM et ϕ l'angle azimutal transverse. Ce front de phase illustre en effet une onde de propagation de type vortex. Dans certains cas, à partir d'une aperture partagée, il est possible de générer plusieurs numéros de mode OAM orthogonaux entre eux. Pour ce faire, une circular array d'antennes est utilisée. En introduisant une différence de phase progressive $\Delta\phi = \frac{2\pi l}{N}$ — où N est le nombre d'antennes dans la circular array — entre les éléments adjacents, le mode OAM souhaité est généré [6]. Par exemple, pour produire le mode OAM $+2$ à l'aide d'une array comprenant 12 antennes, la différence de phase entre les éléments doit être $2\pi(+2)/12 = \pi/3$.

En ce qui concerne la littérature, trois principales méthodes existent pour générer des modes OAM. Il est tenté d'expliquer chaque catégorie en détail.

A.2.1 Génération de OAM utilisant des array circulaire

Dans [7], une solution efficace pour générer des faisceaux radio porteurs de OAM avec trois polarisations est proposée. Dix antennes horn sont disposées de manière circulaire comme illustré dans la figure 1.1. Chaque antenne a la capacité de produire trois polarisations : linéaire, circulaire gauche et circulaire droite. En excitant les éléments avec une différence de phase successive de 0, ±1, ±2, ±3 et ±4, des modes OAM sont générés. L'équation (1.1) indique les différences de phase successives requises.

$$\Delta\varphi = \frac{2\pi l}{N} \tag{A.1}$$

Où N indique le nombre d'éléments et montre le mode OAM. Par exemple, pour obtenir le mode -1, il est nécessaire d'exciter les éléments avec une différence de phase de -36°. Il est évident que +36° donne le mode +1. En théorie, un grand nombre de modes OAM peut être généré à l'aide de l'équation (1.1), mais le diagramme de rayonnement se dégrade à mesure que le nombre de modes augmente. Cela trouve son origine dans le nombre d'éléments ; le nombre de modes est inférieur à la moitié du nombre d'éléments de rayonnement. Ainsi, pour obtenir des modes d'ordre supérieur, il est nécessaire d'augmenter le nombre d'antennes horn. Il convient également de mentionner que plus le diamètre de l'array est agrandi, plus le gain maximum est élevé et plus son angle de direction devient large.

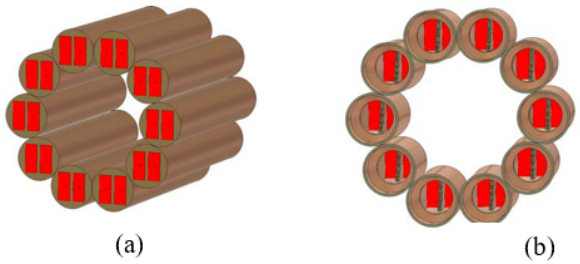

FIGURE A.1 : Géométrie de l'array d'antennes horn : (a) Vue arrière. (b) Vue avant [7].

Dans [6], trois arrangements différents d'array circulaire sont étudiés pour obtenir celui qui est le meilleur pour générer des modes OAM. Il est conclu qu'un UCA permet d'obtenir les résultats souhaités. La figure 1.2 montre les arrangements proposés.

De plus, dans cette référence, la condition de multiplexage ainsi que de démultiplexage est étudiée, et il est déduit que chaque mode OAM transportant de l'information peut être extrait faci-

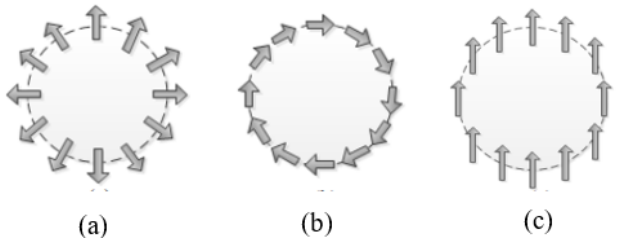

FIGURE A.2 : (a) Les structures de l'array radial, (b) de l'array tangentiel et (c) de l'uniform circular array [6].

lement par le récepteur à l'aide de la Discrete Fourier Transform (DFT). Cela est valable en raison du fait que les modes OAM sont orthogonaux les uns aux autres, et chaque motif avec un mode spécifique peut être multiplié par un signal séparé et transmis simultanément.

Dans [8], la réalisation de modes multiples OAM simultanément à travers un UCA à quatre dimensions est discutée. La quatrième dimension est liée aux interrupteurs : Single-Pole Single-Throw (SPST) et Single-Pole Double-Throw (SPDT). La performance de la structure repose sur les interrupteurs placés avant un diviseur de puissance $1\times N$ excitant les antennes. En fait, les interrupteurs induisent un délai dans l'excitation de chaque antenne. Si nous utilisons le SPST, comme les interrupteurs N-1 sont "désactivés", une grande quantité de puissance est absorbée par ceux-ci, et cela n'est pas efficace en termes d'énergie. D'autre part, en utilisant le SPDT, il n'y a pas d'état "désactivé", et tous les signaux divisés peuvent atteindre les antennes avec une différence de phase de 180° par rapport à un signal, qui est notre état préféré. Cela est valable, car l'autre état du SPDT induit une telle différence de phase au lieu de se désactiver.

Un autre point important dans [8] est lié à un nouveau setup pour mesurer le phase front. La figure 1.3 montre le setup.

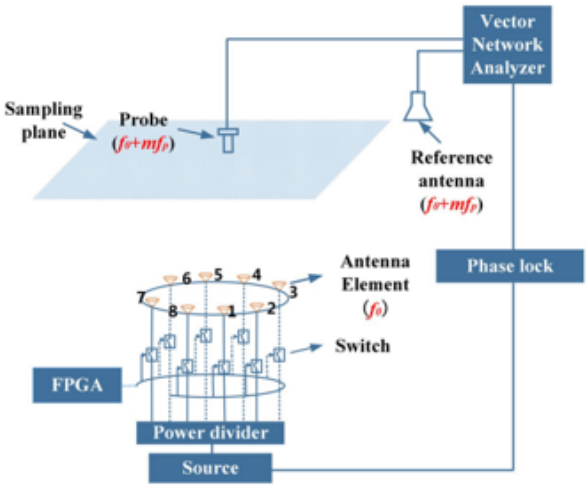

FIGURE A.3 : Mesure de la distribution de phase du Near-field pour l'antenne 4-D array [8].

Les ondes transportant de l'OAM générées simultanément par l'array circulaire 4-D sont réparties sur plusieurs fréquences harmoniques, et non uniquement à la fréquence centrale. Par conséquent, la plateforme expérimentale traditionnelle dans une anechoic chamber, où l'antenne émettrice et l'antenne sonde fonctionnent à la même fréquence, n'est pas applicable pour cette mesure. Dans l'expérience, le plan d'échantillonnage se situe à 200 mm au-dessus de l'array circulaire avec une plage de balayage de 500 mm $\times$ 500 mm. Pour obtenir la distribution du champ

proche, un guide d'ondes rectangulaire ouvert est utilisé comme sonde. Ici, la question clé est de résoudre la difficulté de la mesure de la distribution de phase. Parce que la phase des champs est une valeur relative et non une valeur absolue, une antenne de référence est ajoutée pour fournir une phase de référence. L'antenne de référence est fixée tandis que l'antenne sonde scanne dans le plan d'échantillonnage. Parallèlement, les deux terminaux récepteurs du guide d'ondes rectangulaire ouvert et de l'antenne de référence sont connectés à un Vector Network Analyzer (VNA) à deux ports. Le VNA effectue la fonction de comparaison des deux signaux provenant du guide d'ondes rectangulaire ouvert et de l'antenne de référence. Ainsi, la distribution de phase du champ proche peut être directement extraite du $\angle$S21 mesuré par le VNA. De plus, une boucle à verrouillage de phase est utilisée pour garantir que VNA et la signal source sont synchronisés.

A.2.2 Génération de modes OAM avec des métamatériaux

Dans [14], un Planar-Spiral Phase Plate (PSPP) est conçu pour créer des modes OAM mélangés. À cet effet, un grand nombre de cellules unitaires, comprenant 4 trous dans un substrat carré, sont utilisées. Pour convertir l'onde sphérique entrante (provenant d'un guide d'ondes ouvert) en une onde de type spirale avec différents modes, chaque unité du plancher-SPP transforme la phase entrante en la phase de sortie requise. En fait, les cellules unitaires compensent la différence de phase entre la phase requise et la phase entrante. Les équations (A.2) to (A.4) clarifient l'assertion mentionnée ci-dessus.

$$\text{outphase}(\phi) = \phi l \tag{A.2}$$

$$\text{inphase}(\theta) = \frac{2\pi F}{\lambda_0} \left(1 - \cos(\theta)\right) / \cos(\theta) \tag{A.3}$$

$$\text{Phase}(\theta, \phi) = \text{outphase}(\phi) - \text{inphase}(\theta) \tag{A.4}$$

L'équation (A.2) montre la phase de sortie requise. L'équation (A.3), qui calcule la phase entrante, est déterminée en utilisant une approximation d'optique géométrique [15] sous l'hypothèse que l'onde sphérique provient du centre de phase de l'antenne. Enfin, l'équation (A.4) génère la phase de compensation requise, qui doit être obtenue par chaque cellule unitaire en fonction de sa position.

La figure A.4 montre la structure du PSPP capable de générer les 3 modes mentionnés dans la figure.

Dans [16], une Split-Ring Frequency Selective Surfaces (FSS) Spiral Phase Plate est utilisée pour créer le premier ordre d'une onde porteuse de OAM. Elle est conçue à partir de cellules unitaires à deux couches, comprenant deux split-ring orthogonaux. En ce qui concerne l'angle entre les anneaux, θ_r, un déphasage spécifique est obtenu. Par exemple, si les anneaux sont orthogonaux entre eux, un déphasage de 180°, soit deux fois l'angle entre les anneaux, est atteint. Ainsi, une onde polarisée circulairement à gauche est transformée en son homologue à droite. La figure A.5 illustre les cellules unitaires.

Afin d'utiliser une telle structure pour une onde porteuse de OAM, un array 10×10 est conçu. Chaque élément de l'array doit générer un déphasage en fonction de sa coordonnée angulaire.

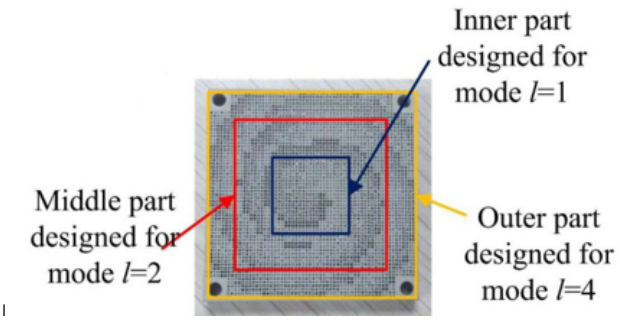

FIGURE A.4 : L'antenne OAM à trois modes mélangés [14].

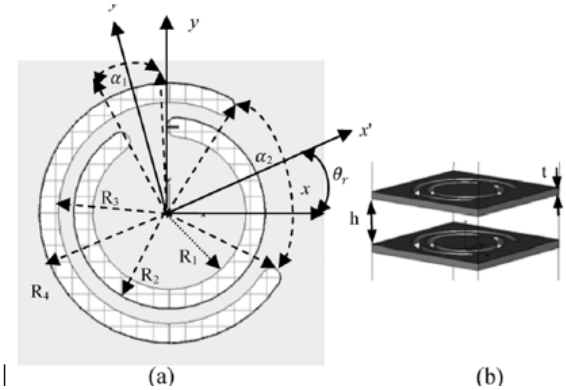

FIGURE A.5 : Structure FSS à double couche : (a) vue de dessus ; (b) vue en coupe [16].

Une Flat-Lensed Spiral Phase Plate basée sur une Phase-Shifting Surface pour la génération d'un faisceau OAM en ondes millimétriques est étudiée dans [17]. La cellule unitaire, présentée dans la figure A.6, comprend quatre substrats empilés avec cinq patchs métalliques. En modifiant la largeur et la longueur de la fente, un déphasage spatial est obtenu. En déterminant la phase requise pour chaque cellule unitaire en fonction de sa position angulaire dans l'array, un mode OAM est généré. Il convient de mentionner que les patchs rectangulaires agissent comme une lentille plate, ce qui permet de recentrer les deux faisceaux séparés du mode OAM vers l'axe, car ils compensent la différence de phase d'une onde incidente sphérique. En effet, cela produit un effet de focalisation dans l'array.

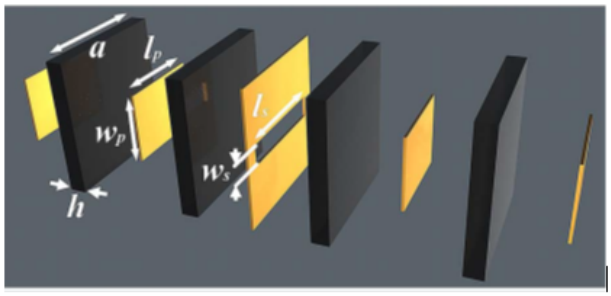

FIGURE A.6 : Vue éclatée d'une unit cell PSS multicouche [17].

A.2.3 Génération de modes OAM à l'aide de single antenna elements

Il existe également une méthode simple pour générer des modes OAM à l'aide d'un single element. Cela permet également de réduire la complexité du réseau d'alimentation. Dans [22], il est démontré qu'en excitant une circular patch antenna avec une différence de phase de $90°$ depuis deux points spécifiques, des modes OAM sont générés dans des modes de cavité d'ordre supérieur. Il est également conclu qu'il est possible d'exciter des modes OAM en utilisant une elliptical patch antenna. Ce faisant, deux points d'excitation avec une différence de phase de $90°$ ne sont plus nécessaires, et un seul port d'entrée suffit. Le problème associé à cette technique est sa bande passante étroite. Pour résoudre ce problème, les auteurs de [23] ont excité les circular patch antennas à partir de quatre points, rendant ainsi la structure large bande. La figure A.7 illustre une telle structure ainsi que son réseau d'alimentation.

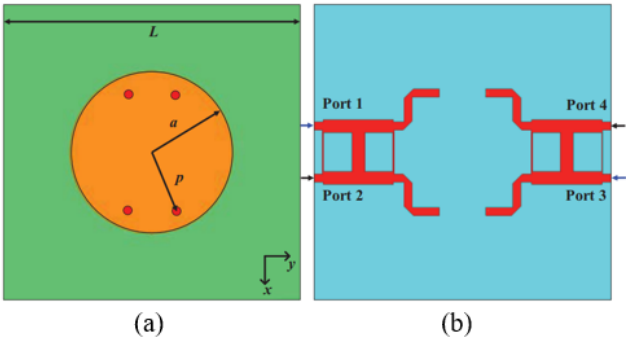

FIGURE A.7 : Configuration de la single patch antenna et de son réseau d'alimentation pour la génération d'une onde porteuse de OAM [22].

Comme il est évident, deux hybrid couplers excitent le patch à partir de deux points de manière indépendante. Lorsque le port d'excitation du coupler est modifié, l'ordre du mode OAM change de -1 à +1 et de -2 à +2, ou vice versa. Il convient également de mentionner que la distance radiale entre les deux points reliés à chaque coupler est de 135 degrés. Cela trouve son origine dans le fait de placer l'alimentation dans le point nul de l'autre alimentation. En d'autres termes, comme nous souhaitons tirer parti des modes supérieurs, en fonction du nombre de modes, des champs se formeront sous le patch. En examinant le motif des champs, on peut remarquer que le mode TM_{21} présente une distribution de champ illustrée dans la figure A.8. Ainsi, la distance radiale entre les deux alimentations devrait être de 135 degrés. Afin d'exciter d'autres modes, la même méthode est utilisée.

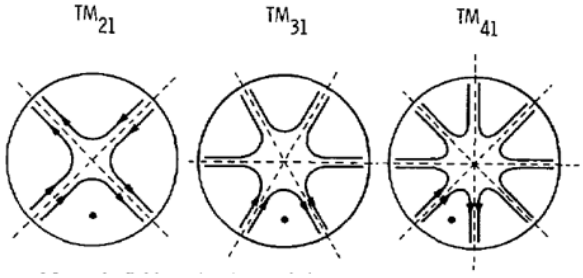

FIGURE A.8 : Field distribution des modes supérieurs sous le circular patch [23].

Une cavité half-mode Substrate Integrated Waveguide (SIW) est présentée, avec la capacité de générer des modes OAM à l'aide d'une seule alimentation [24]. Un résonateur de cavité en anneau avec deux fentes rectangulaires sur la surface métallique est utilisé à cette fin. En faisant une rotation de 90° de la position de l'alimentation, le mode opposé est obtenu. La figure A.9 illustre la configuration de la structure proposée. Il est important de mentionner qu'il est possible de créer des ondes OAM avec des numéros de mode plus élevés en augmentant le rayon de la cavité. Cependant, la bande passante de l'antenne est trop étroite, ce qui pourrait la rendre inadaptée aux futures communications 5G.

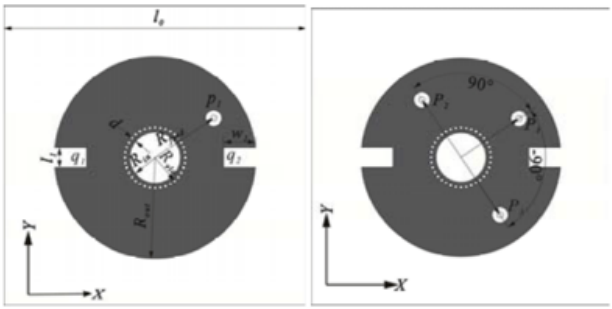

FIGURE A.9 : Configuration de la cavité SIW pour la génération de OAM [24].

A.3 Problématique et motivation

Comme mentionné précédemment, afin d'améliorer davantage la capacité des canaux dans les systèmes de communication sans fil, en particulier dans le lien de *Backhaul*, la BW et le SNR ont atteint leur potentiel maximal d'amélioration. Les antennes MIMO ont introduit un nouveau degré de liberté permettant d'améliorer les performances des systèmes sans fil en termes de débit de données et de résolution. Cependant, elles nécessitent un traitement du signal complexe lorsque le nombre d'antennes augmente. En outre, comme pour les systèmes conventionnels, différents types de schémas de multiplexage, tels que le multiplexage temporel, le multiplexage en fréquence, etc., sont requis à la fois au niveau de l'émetteur et du récepteur. Ces types de multiplexage limitent l'utilisation complète de la bande de fréquence ainsi que l'allocation temporelle.

Les antennes OAM sont capables de propager plusieurs faisceaux orthogonaux à partir d'une ouverture partagée. Étant donné que ces faisceaux orthogonaux ne s'interfèrent pas entre eux, une nouvelle méthode de multiplexage appelée multiplexage en modes spatiaux peut être introduite dans les futurs systèmes sans fil. Ainsi, l'intégralité de la bande de fréquence et de l'intervalle temporel peut être allouée à un seul lien de communication. D'autres liens peuvent être activés simultanément et à la même fréquence en utilisant différents numéros de mode OAM. De plus, les systèmes utilisant des antennes OAM ne nécessitent pas de traitement du signal complexe. Tout cela souligne la supériorité des antennes OAM par rapport aux systèmes MIMO et aux antennes conventionnelles à élément unique.

Dans ce contexte, afin de permettre la conception de systèmes sans fil intelligents capables de contrôler de manière autonome leurs modes OAM, leur fréquence et leur polarisation, nous proposerons de nouvelles architectures.

A.4 Objectifs de recherche

Après avoir mis en évidence l'importance des antennes OAM dans les systèmes sans fil avancés, l'objectif de notre recherche est défini. L'accent est principalement mis sur les antennes OAM reconfigurables. La reconfigurabilité permet de concevoir des systèmes intelligents. En d'autres termes, une fois l'antenne fabriquée, celle-ci est capable de modifier ses caractéristiques afin de s'adapter à un nouvel environnement ou à de nouvelles conditions. La reconfigurabilité sera étudiée en fonction du nombre de modes, de la polarisation et de la fréquence. Par ailleurs, les objectifs visés comprennent un gain supérieur à 6 dBi, une BW de 100 MHz et une pureté de mode supérieure à 70 %.

À titre d'exemple d'application pratique, dans un système d'imagerie micro-ondes tel que la détection d'objets enfouis, l'intégration de la reconfigurabilité en fréquence dans la partie antennaire permettrait d'éliminer les interférences potentielles en modifiant la fréquence de fonctionnement. De même, dans un lien de communication sans fil point-à-point, les conditions environnementales ou un brouillage peuvent dégrader la qualité du lien assuré par un mode OAM donné. Ainsi, le changement du numéro de mode permettrait d'obtenir une nouvelle caractéristique de propagation, capable de surmonter les conditions défavorables affectant la liaison.

En parallèle avec notre objectif de recherche portant sur la conception d'antennes OAM reconfigurables, des antennes OAM à gain élevé seront également étudiées. Un gain élevé permet d'étendre la distance de communication. En effet, en concevant une structure OAM à gain élevé, la divergence des faisceaux propagés est réduite, ce qui se traduit par une portée de communication accrue. Nous concevrons un réseau de transmission (*transmit array*) présentant un gain supérieur à 16 dBi pour générer des modes OAM mixtes.

A.5 Méthodologie

Nous avons considéré la technique UCA, présentée dans la sous-section A.2.1, pour la conception d'antennes OAM reconfigurables. À cet effet, nous avons utilisé des réseaux d'alimentation à base de phase-shifters afin de modifier la phase d'excitation de chaque élément dans l'UCA. Cette méthode nous a permis de changer le mode de propagation. Par la suite, pour concevoir des structures ajustables en fréquence, nous avons proposé de nouvelles conceptions d'antennes basées sur des cavités SIW. La tunabilité en fréquence a été introduite au niveau des éléments d'antenne de l'UCA. De plus, l'utilisation de deux antennes à polarisations orthogonales intégrées dans une cavité SIW nous a permis de rendre nos structures sélectives en polarisation.

Les détails de chaque conception sont brièvement expliqués comme suit :

A.5.1 Un système d'antenne à faible profil pour la génération de faisceaux transportant un OAM reconfigurable

Un feeding network 1×4 est proposé avec la capacité de générer la distribution de phase nécessaire à l'excitation des modes OAM ± 1. La structure proposée comprend un equal power divider ainsi que quatre 1-bit phase shifters. En commutant l'état des phase shifters entre $\pm 45°$, une distribution de phase de $[0, 90, 0, 90]$ est obtenue dans les directions horaire et antihoraire. Dans

le cas où un UCA avec une configuration en image miroir est utilisé, une distribution de phase de $[0, 180, 180, 0]$ est automatiquement produite entre les éléments de l'antenne. Ainsi, la combinaison du feeding network et du UCA permet de créer les conditions nécessaires pour exciter les modes OAM $+1$ et -1. De plus, il est expliqué qu'en ajoutant un autre phase shifter en cascade à chacun des phase shifters existants, la génération du mode OAM 0 devient possible. Un prototype de la structure proposée, fonctionnant à $2.45\,\mathrm{GHz}$, est conçu, fabriqué et mesuré. Après évaluation des caractéristiques de rayonnement du système, des faisceaux reconfigurables avec des fronts de phase hélicoïdaux et présentant un nul dans la direction de l'axe sont observés.

A.5.2 Antenne OAM à fréquence ajustable avec faisceaux co-divergents pour les applications Internet of Things (IoT)

Un système d'array d'antenne générant de l'OAM et accordable en fréquence est introduit pour la première fois afin d'assurer une communication à haut débit et sécurisée pour les infrastructures et dispositifs de l'Internet of Things (IoT). La propagation simultanée de modes OAM permet un haut débit, tandis que la réglabilité en fréquence permet la suppression des interférences pour une communication sécurisée. En ce qui concerne l'évolution de la conception de la structure proposée, la nouvelle antenne MIMO composée de deux ports d'entrée forme une UCA 2 $\times$ 2, donnant lieu à deux sous-UCA 2 $\times$ 2. L'alimentation de chaque sous-array 2 $\times$ 2 avec des gradients de phase [0°, 90°, 180°, 270°] dans les sens horaire et antihoraire génère des ondes à double mode portant de l'OAM, avec une capacité d'excitation simultanée. Il convient de mentionner que chaque élément MIMO est accordable en fréquence, ce qui conduit à un array d'antenne à double mode OAM ajustable en fréquence. Un prototype de l'antenne MIMO suggérée ainsi que de l'array OAM est fabriqué et mesuré. La modification de la tension continue appliquée aux diodes varactor intégrées dans les extensions capacitives des éléments d'antenne déplace la fréquence de fonctionnement dans l'antenne MIMO, et par conséquent dans l'array OAM. En ce qui concerne les caractéristiques de rayonnement uniques de l'antenne OAM, des faisceaux vortex présentant des fronts de phase hélicoïdaux sont observés, confirmant la génération des ondes OAM attendues. Par conséquent, il est affirmé que la structure introduite propose pour la première fois de nouvelles fonctionnalités d'accordabilité en fréquence et de propagation simultanée co-divergente de modes OAM en utilisant la technique MIMO-UCA, afin d'assurer une communication à haut débit et sécurisée dans les applications IoT.

A.5.3 Antenne OAM reconfigurable avec flexibilité sur les nombres de mode, la polarisation et la fréquence

Étant donné que les antennes OAM existantes n'ont aucun contrôle sur la fréquence de fonctionnement après leur fabrication et ne peuvent pas manipuler simultanément la polarisation et le nombre de modes, la conception de systèmes de communication sans fil OAM intelligents semble hors de portée. Cependant, un nouveau système d'antenne OAM est proposé, capable de surmonter efficacement les limitations susmentionnées. L'antenne suggérée utilise un UCA 2 $\times$ 2 composé d'antennes MIMO pour introduire la technique MIMO-UCA pour la génération simultanée des nombres de mode OAM +1 et 1. La flexibilité de la polarisation de chaque mode découle du fait que chaque antenne MIMO est constituée d'éléments polarisés à ±45, ce qui permet l'utilisation de sondes accordables pour assigner simultanément les modes à la polarisation souhaitée.

La flexibilité de la fréquence de fonctionnement est également due à la reconfigurabilité en fréquence des antennes MIMO. Le prototype fabriqué de la structure proposée vérifie les résultats simulés. La fréquence de fonctionnement peut être accordée de 3.8 à 4.4 GHz. Sur cette bande, le gain maximal est maintenu au-dessus de 6 dBi. Le couplage mutuel entre les ports est inférieur à 20 dB.

A.5.4 Système d'antenne OAM à modes accordables avec caractéristique de sélectivité de polarisation

Un nouveau système d'antenne OAM avec un réseau d'alimentation reconfigurable innovant et des antennes à double polarisation est présenté. Le réseau d'alimentation 2 $\times$ 4 génère des gradients de phase de 0°, 90° et -90° à ses sorties, permettant la génération des modes OAM 0, -1 et +1. En intégrant un UCA 2 $\times$ 2 avec des antennes à double polarisation et deux copies du réseau d'alimentation proposé, le système prend en charge six types de propagation reconfigurables, idéaux pour les communications OAM intelligentes. Fonctionnant à 2.4 GHz, il atteint des gradients de phase avec un déséquilibre maximal de 4° et des coefficients de réflexion des ports d'entrée inférieurs à -15 dB. En résumé, la configuration novatrice du réseau d'alimentation, le concept de combinaison de la polarisation et des modes OAM, ainsi que la capacité à générer des faisceaux orthogonaux reconfigurables supplémentaires sont les parties novatrices.

En plus de notre objectif principal, nous avons introduit une nouvelle méthode pour augmenter le nombre de modes générés à partir d'un UCA. De plus, nous avons travaillé sur la conception de transmitarray avec la capacité de générer des modes OAM mixtes à fort gain.

TABLE DES MATIÈRES

ACKNOWLEDGMENT ..... **iii**

RÉSUMÉ ..... **v**

ABSTRACT ..... **vii**

SOMMAIRE RECAPITULATIF ..... **ix**

A.1 TITRE DE LA THÈSE EN FRANÇAIS ix

A.2 INTRODUCTION ix

A.2.1 Génération de OAM utilisant des array circulaire x

A.2.2 Génération de modes OAM avec des métamatériaux xii

A.2.3 Génération de modes OAM à l'aide de single antenna elements xiv

A.3 PROBLÉMATIQUE ET MOTIVATION xv

A.4 OBJECTIFS DE RECHERCHE xvi

A.5 MÉTHODOLOGIE xvi

A.5.1 Un système d'antenne à faible profil pour la génération de faisceaux transportant un OAM reconfigurable xvi

A.5.2 Antenne OAM à fréquence ajustable avec faisceaux co-divergents pour les applications IoT xvii

A.5.3 Antenne OAM reconfigurable avec flexibilité sur les nombres de mode, la polarisation et la fréquence xvii

A.5.4 Système d'antenne OAM à modes accordables avec caractéristique de sélectivité de polarisation xviii

TABLE DES MATIÈRES ..... **xix**

LISTE DES FIGURES ..... **xxi**

LISTE DES TABLEAUX ..... **xxvii**

LISTE DES ABREVIATIONS ..... **xxix**

LISTE DES ABRÉVIATIONS ..... **xxix**

1 INTRODUCTION AND BACKGROUND **1**

1.1 INTRODUCTION 1

1.2 BACKGROUND 2

1.2.1 Generation of OAM Using Circular Arrays 2

1.2.2 Generation of OAM Modes with Metamaterials 5

1.2.3 Generation of OAM Modes Using Single Antenna Elements 8

1.3 Problem Statement and Motivation 11
1.4 Research Objectives 11
1.5 Thesis organization 12
1.6 Published works in OAM 13
1.7 Other published works 14
1.8 Achievements 18
2 MODE-TUNABLE OAM ANTENNA 20
2.1 Introduction 20
2.2 Design Process 21
2.2.1 UCA tunable feeding network 21
2.2.2 Phase and amplitude response evaluation 23
2.3 Experimental Results 24
2.4 Discussion 25
2.5 Acknowledgment 27
2.6 Conclusion 27
3 FREQUENCY-ADJUSTABLE OAM ANTENNA 29
3.1 Introduction 29
3.2 Tunable MIMO Antenna Design 32
3.2.1 Design process 32
3.2.2 Experimental results for MIMO antenna 36
3.3 Frequency-Adjustable MIMO-UCA Antenna Design 38
3.3.1 Experimental results for frequency-adjustable MIMO-UCA 41
3.4 Discussion 45
3.5 Acknowledgment 48
3.6 Conclusion 48
4 FREQUENCY AND MODE-TUNABLE OAM ANTENNA WITH POLARIZATION SELECTIVITY 51
4.1 Introduction 51
4.2 Tunable Dual-Polarized MIMO Antenna Design 52
4.2.1 Process of designing 52
4.2.2 The MIMO antenna's experimental findings 53
4.3 Proposed OAM antenna design 54
4.4 Experimental Validation 55
4.5 Discussion 58

4.6 ACKNOWLEDGMENT 59
4.7 CONCLUSION 59
5 TRIPLE-MODE TUNABLE DUAL-POLARIZED OAM ANTENNA 61
5.1 INTRODUCTION 61
5.2 TRIPLE-MODE POLARIZATION-SELECTIVE OAM ANTENNA 62
5.2.1 OAM antenna feed design 62
5.2.2 Dual-polarized Bow-tie dipole antenna 64
5.2.3 Proposed OAM antenna system 65
5.3 DISCUSSION 66
5.4 ACKNOWLEDGMENT 68
5.5 CONCLUSION 68
6 METASURFACE-BASED OAM ANTENNAS 69
6.1 INTRODUCTION 69
6.2 UNIT CELL CHARACTERISTICS 72
6.3 MIXED-OAM GENERATING TA DESIGN 72
6.4 EXPERIMENTAL VERIFICATION 75
6.5 DISCUSSION 76
6.6 CONCLUSIONS 78
7 CONCLUSION AND FUTURE WORK 81
7.1 CONCLUSION 81
7.2 FUTURE WORKS 82
7.2.1 Mode augmentation technique in generating OAM modes 82
7.2.2 OAM mode with beam-steering capabilities 83
7.2.3 Multi-mode OAM generation 84
7.2.4 Limitations of OAM communication 84
BIBLIOGRAPHIE 86

LISTE DES FIGURES

FIGURE A.1 GÉOMÉTRIE DE L'ARRAY D'ANTENNES HORN : (A) VUE ARRIÈRE. (B) VUE AVANT x

FIGURE A.2 (A) LES STRUCTURES DE L'ARRAY RADIAL, (B) DE L'ARRAY TANGENTIEL ET (C) DE L'UNIFORM CIRCULAR ARRAY xi

FIGURE A.3 MESURE DE LA DISTRIBUTION DE PHASE DU NEAR-FIELD POUR L'ANTENNE 4-D ARRAY xi

FIGURE A.4 L'ANTENNE OAM À TROIS MODES MÉLANGÉS xiii

FIGURE A.5 STRUCTURE FSS À DOUBLE COUCHE : (A) VUE DE DESSUS ; (B) VUE EN COUPE xiii

FIGURE A.6 VUE ÉCLATÉE D'UNE UNIT CELL PSS MULTICOUCHE xiii

FIGURE A.7 CONFIGURATION DE LA SINGLE PATCH ANTENNA ET DE SON RÉSEAU D'ALIMENTATION POUR LA GÉNÉRATION D'UNE ONDE PORTEUSE DE OAM xiv

FIGURE A.8 FIELD DISTRIBUTION DES MODES SUPÉRIEURS SOUS LE CIRCULAR PATCH xiv

FIGURE A.9 CONFIGURATION DE LA CAVITÉ SIW POUR LA GÉNÉRATION DE OAM xv

FIGURE 1.1 HORN ANTENNA ARRAY GEOMETRY : (A) REAR VIEW. (B) FRONT VIEW 3

FIGURE 1.2 (A) STRUCTURES OF THE RADIAL ARRAY, (B) TANGENTIAL ARRAY, AND (C) UNIFORM CIRCULAR ARRAY 3

FIGURE 1.3 NEAR-FIELD PHASE DISTRIBUTION MEASUREMENT SETUP FOR THE 4-D ARRAY ANTENNA 4

FIGURE 1.4 THE PROPOSED SEQUENTIALLY ROTATES STRUCTURE FOR FULL-DUPLEX APPLICATION USING DIFFERENT OAM MODES 6

FIGURE 1.5 THE THREE-MODE MIXED OAM ANTENNA 7

FIGURE 1.6 DOUBLE LAYER FSS STRUCTURE : (A) TOP VIEW; (B) CROSS-SECTIONAL VIEW . 7

FIGURE 1.7 EXPLOSIVE VIEW OF A MULTILAYER PSS UNIT CELL 8

FIGURE 1.8 A CIRCULAR ARRAY WITH CIRCULAR BOUNDARY FOR GENERATING OAM MODE . 9

FIGURE 1.9 CONFIGURATION OF THE SINGLE PATCH ANTENNA AND ITS FEEDING NETWORK FOR GENERATING AN OAM WAVE 9

FIGURE 1.10 FIELD DISTRIBUTION OF HIGHER-ORDER MODES UNDER THE CIRCULAR PATCH 9

FIGURE 1.11 CONFIGURATION OF THE SIW CAVITY FOR OAM GENERATION 10

FIGURE 1.12 THE CONFIGURATION OF THE FEEDING NETWORK ENGENDERING OAM MODES 10

Figure 2.1 The block diagram of the proposed tunable UCA feeding (P.D.=Power divider, PH.=Phase shifter, P=port and Ant.=Antenna). 22

Figure 2.2 The configuration of the utilized 1-bit phase shifter. 22

Figure 2.3 Phase response of the OAM-generating feeding network (a) mode +1, and (b) mode -1. 23

Figure 2.4 Amplitude response of the OAM-generating feeding network (a) mode +1, and (b) mode -1. 23

Figure 2.5 Configuration of the fabricated structure. 24

Figure 2.6 Reflection coefficient related to the input port when (a) OAM mode +1, and (b) OAM mode -1 are excited. 24

Figure 2.7 Normalized gain in the E-plane for OAM mode (a) +1, and (b) -1. 26

Figure 2.8 Normalized gain in the H-plane for OAM mode(a) +1, and (b) -1. 26

Figure 2.9 Simulated and measured phase front for OAM mode (a) +1, (b) -1. 26

Figure 3.1 textcolorblack Potential application for high-data-rate and secure OAM-based IoT communication. 32

Figure 3.2 Electric field distribution in a (a) full-mode, (b) half-mode, (c) quarter-mode SIW cavity, and (d) the reflection coefficients associated with each one. 33

Figure 3.3 (a) Full-mode SIW cavity, (b) half-mode SIW cavity, (c) the proposed non-tunable MIMO antenna, and (d) frequency adjustable MIMO antenna. 33

Figure 3.4 The configuration of the radiator of the proposed MIMO antenna and its equivalent circuit model. (Ls=24mm, s=0.7mm, p=1.5mm). 34

Figure 3.5 The configuration of the radiator of the proposed MIMO antennas and its equivalent circuit. 34

Figure 3.6 (a) Front side, (b) backside of the fabricated tunabe MIMO antenna, and (c) the measurement setup. 36

Figure 3.7 The simulated and measured reflection coefficients associated with Port 1, as well as the mutual coupling among them. 36

Figure 3.8 The current distribution at the resonance frequencies of 3.8, 4, and 4.15 GHz. 38

Figure 3.9 The normalized E-plane and H-plane radiation patterns associated with Port 1 at (a) 3.8 GHz, (c) 4 GHz, (e) 4.15 GHz, and with Port 2 at (b) 3.8 GHz, (d) 4 GHz, (f) 4.15 GHz. 39

Figure 3.10 The configuration of antenna feeds for generating OAM modes (P=Port). 40

Figure 3.11 Amplitude response and reflection coefficient when (a) Port 1 is excited, and (b) Port 6 is fed. 40

Figure 3.12 Phase response when (a) Port 1 is excited, and (b) Port 6 is fed. 40

Figure 3.13 The prototype of the proposed frequency adjustable MIMO-UCA OAM antennas array. 41

Figure 3.14 Simulated and measured reflection coefficients associated with Port 1, and the mutual coupling among the input ports of the OAM array. 42

Figure 3.15 The proposed setup for measuring the near filed characteristics of the OAM array (wires have connected the DC-pads together and have no effect on the radiation pattern due to being behind the structure). 42

Figure 3.16 The electric field amplitude at different frequencies for OAM (a) mode +1 associated with Port 6, and (b) mode -1 related to Port 1. 43

Figure 3.17 The phase front at different frequencies for OAM (a) mode +1 associated with Port 6, and (b) mode -1 related to Port 1. 44

Figure 3.18 The mode purity for OAM (a) mode -1, and (b) mode +1. 45

Figure 3.19 2D radiation patterns for OAM mode -1 at (a) 3.8 GHz, (b) 4 GHz, (c) 4.15 GHz, and OAM mode +1 at (d) 3.8 GHz, (e) 4 GHz, (cf) 4.15 GHz (E=E-plane, and H=H-plane). 46

Figure 3.20 The proposed setup for a communication link using the OAM antenna arrays. 46

Figure 3.21 The received amplitude values at different frequencies and distances for (a) OAM mode +1, and (b) OAM mode -1. 47

Figure 4.1 (a) Full-mode SIW cavity, (b) half-mode cavity, (c) the proposed non-adjustable MIMO antenna, and (d) frequency variable MIMO antenna. (l=27mm, S=19.25mm, p=9mm, t=1.5mm) 52

Figure 4.2 The reflection coefficients of Port 1, both simulated and measured, and their mutual coupling. 53

Figure 4.3 Configuration of the proposed double-layer OAM antenna; (a) front view, (b) back view, and (c) side view. (P.D.=Power Divider and PH.=Phase Shifter) and (m=10.4mm, n=10.4mm, d=2.2mm). 55

Figure 4.4 The model of the suggested array of MIMO-UCA OAM antennas with adjustable frequency; (a) viewed from the front, and (b) viewed from the back. 56

Figure 4.5 Reflection coefficients for Port 1 (mode -1 with +45° polarization condition), and (b) Port 2 (mode +1 with -45° polarization condition). 56

Figure 4.6 The phase front at different frequencies for OAM (a) mode -1 associated with Port 1 (+45° polarization), and (b) mode +1 related to Port 2 (-45° polarization). 57

Figure 4.7 2D radiation patterns for OAM mode -1 +45° Polarization at (a) 3.8 GHz, (b) 4.1 GHz, (c) 4.4 GHz, and OAM mode +1 -45° Polarization at (d) 3.8 GHz, (e) 4.1 GHz, (cf) 4.4 GHz (E=E-plane, and H=H-plane). 57

FIGURE 5.1 SCHEMATIC OF THE PROPOSED FEEDING NETWORK FOR GENERATING OAM MODES. (P.H.=PHASE SHIFTER) 63

FIGURE 5.2 THE FABRICATED PROTOTYPE OF THE PROPOSED OAM ANTENNA FEED. 64

FIGURE 5.3 THE CONFIGURATION OF THE DUAL-POLARIZED ANTENNA FROM (A) TOP VIEW, (C) SIDE VIEW. 65

FIGURE 5.4 REFLECTION COEFFICIENTS RELATED TO HORIZONTAL (S11), AND (B) VERTICAL BOW-TIE (S22). 65

FIGURE 5.5 RADIATION PATTERNS ASSOCIATED WITH (A) HORIZONTAL BOW-TIE, AND VERTICAL BOW-TIE. 65

FIGURE 5.6 SIMULATED PHASE FRONTS FOR (A) OAM MODE 0, (B) MODE -1, (C) MODE +1 AT HORIZONTAL POLARIZATION, AND (D) MODE 0, (E) MODE -1, (F) MODE +1 AT VERTICAL POLARIZATION. 67

FIGURE 5.7 E-PLANE AND H-PLANE CUTS FOR OAM MODES (A) 0, (B) -1, (C) +1 IN CASE OF HORIZONTAL POLARIZATION, AND (D) 0, (E) -1, (F) +1 IN CASE OF VERTICAL POLARIZATION. 67

FIGURE 6.1 THE CONFIGURATION OF THE HUYGENS' METASURFACE, (A) FRONT VIEW, (B) BACK VIEW, (C) SIMULATION SETUP, AND (D) THE PARAMETER VALUES. 73

FIGURE 6.2 (A) PHASE RESPONSE, AND (B) AMPLITUDE RESPONSE OF THE MENTIONED UNIT CELL ACCORDING TO DIFFERENT VALUES FOR l (l+g=4.4 MM). 73

FIGURE 6.3 THE SCHEMATIC OF A SIMPLIFIED TA INCLUDING M×N=6×6 ELEMENTS TO DEMONSTRATE THE VARIABLES OF EQUATION (6.1). 74

FIGURE 6.4 CONFIGURATION OF THE FABRICATED STRUCTURE : (A) FRONT SIDE, AND (B) BACK SIDE. 75

FIGURE 6.5 AMPLITUDE AND PHASE RESPONSE FOR (A) X-POLARIZATION, AND (B) Y-POLARIZATION. 76

FIGURE 6.6 THE FAR-FIELD MEASURED PATTERNS FOR SUGGESTED TA. 77

FIGURE 6.7 THE MODE PURITY ANALYSIS FOR X-POLARIZATION ONCE (A) R=4λ, (B) R=8λ, AND (C) R=12λ 78

FIGURE 7.1 SCHEMATIC OF THE UCA INCLUDING TUNABLE OAM GENERATING ANTENNA ELEMENTS. 82

LISTE DES TABLEAUX

TABLEAU 2.1 MAXIMUM GAINS AND EFFICIENCIES ASSOCIATED WITH OAM MODES. 25
TABLEAU 2.2 COMPARISON BETWEEN THIS WORK AND EXISTING ONES. 25

TABLEAU 3.1 INFORMATION REGARDING THE VALUES OF VOLTAGES AND CAPACITANCES AT THE DESIRED RESONANCE FREQUENCIES. 38
TABLEAU 3.2 THE SIMULATED AND MEASURED GAINS RELATED TO OAM MODES ALONGSIDE THE RADIATION EFFICIENCIES. 41
TABLEAU 3.3 THE COMPARISON BETWEEN THE PROPOSED WORK AND SOME RECENTLY PUBLISHED ONES 48

TABLEAU 4.1 REQUIRED DC-VOLTAGES AND THE CORRESPONDING CAPACITANCE VALUES FOR THE SPECIFIED OPERATING FREQUENCIES. 54
TABLEAU 4.2 THE SIMULATED AND MEASURED GAINS OF OAM MODES IN CONJUNCTION WITH RADIATION EFFICIENCIES. 58
TABLEAU 4.3 A COMPARISON BETWEEN THE PROPOSED STUDY AND SOME RECENTLY PUBLISHED RESEARCH. 58

TABLEAU 5.1 S-PARAMETER RESULTS RELATED TO THE PROPOSED OAM *antenne* FEED FOR BOTH SIMULATION AND MEASUREMENT SCENARIOS. 64
TABLEAU 5.2 THE SIMULATED GAINS RELATED TO OAM MODES ALONGSIDE THE RADIATION EFFICIENCIES. 65
TABLEAU 5.3 COMPARISON BETWEEN THE PROPOSED WORK AND RECENTLY PUBLISHED DESIGNS 66

LISTE DES ABREVIATIONS

BW Bandwidth
SNR Signal to Noise Ratio
AR Axial Ratio
OAM Orbital Angular Momentum
UCA Uniform Circular Array
MIMO Multiple-Input Multiple-Output
DFT Discrete Fourier Transform
SPST Single-Pole Single-Throw
SPDT Single-Pole Double-Throw
VNA Vector Network Analyzer
PSPP Planar-Spiral Phase Plate
FSS Frequency Selective Surfaces
SIW Substrate Integrated Waveguide
IoT Internet of Things
TA Transmitarray
CDR cylindrical Dielectric Resonator
RHCP Left-Hand Circular Polarization
LHCP Left-Hand Circular Polarization
SAM Spin Angular Momentum
ADS Advanced Design System

1 INTRODUCTION AND BACKGROUND

This chapter begins with an introduction explaining the necessity of Orbital Angular Momentum (OAM) antennas and highlighting their advantages over conventional systems. It is followed by a comprehensive literature review, where three primary techniques for exciting OAM modes are discussed in detail. The subsequent section outlines the problem statement and motivation, along with the research objectives. Finally, the chapter concludes with an overview of the thesis structure and a summary of the related published works.

1.1 Introduction

When discussing advanced wireless systems, high-speed communication and high-resolution imaging come to mind. These features cannot be achieved with traditional antennas because they are limited by BW and SNR. Specifically, impedance BW is sometimes constrained by the BW of gain or AR, and SNR decreases due to changes in environmental conditions or other uncontrollable parameters. One solution is to use MIMO antennas, which can introduce an additional degree of freedom to enhance data throughput in communication systems and improve results in imaging devices [1, 2]. However, beamforming systems are required for this purpose [3]. These systems require considerable effort during the design and implementation phases. Furthermore, they make the systems more complex. Moreover, we need separate RF chains including power amplifiers, mixers, filters and so on for each antenna element, resulting in costly and bulky systems.

The best alternative to the antennas mentioned above are Orbital Angular Momentum (OAM) antennas. OAM antennas can generate multiple orthogonal donut-shaped beams from a shared aperture, with orthogonality arising from helical phase fronts. Thus, it is possible to transfer multiple data streams at the same frequency simultaneously. To demonstrate this, let us assume the goal is to transmit three video streams from a conventional antenna. For this, the BW should be divided into three distinct parts, each assigned to a stream of data. As it is evident, the BW becomes limited, resulting in a lower data rate. Moreover, three carriers would need to be generated for modulation and multiplexing, requiring external circuits. In the case where the antenna is replaced with one carrying three OAM beams, each data stream could be transferred by an OAM beam simultaneously at the same frequency. On the receiver side, they could be separated by their corresponding OAM modes, without the need for sophisticated demultiplexing processes. As another example, traditional imaging systems process signals based on the waves scattered from the imaged objects. It is clear that the more information the scattered waves carry, the better the image quality after signal processing. Thus, to provide more information to the scattered waves, multimode OAM antennas can be very useful [4, 5]. In fact, each mode carries its own information.

Having acquired a general understanding of the capabilities of OAM modes, it is now appropriate to explain how they can be generated. Consider a loop antenna with a current distribution $I = I_0.e^{jl\phi}$; the calculation of the antenna's radiation pattern reveals the term $e^{jl\phi}$ in the electric field on the plane perpendicular to the propagation axis. This indicates the presence of a helical phase front in the beam, where l represents the OAM mode number and ϕ is the transverse azimuthal angle. This phase front indeed represents a vortex-type wave propagation. In some cases, multiple orthogonal OAM mode numbers can be generated from a shared aperture. For this purpose, a circular array of antennas is used. By introducing a progressive phase difference $\Delta\phi = \frac{2\pi l}{N}$ — where N is the number of antennas in the circular array — the desired OAM mode is generated [6]. For example, to produce the OAM mode $+2$ using an array of 12 antennas, the phase difference between adjacent elements must be $2\pi(+2)/12 = \pi/3$.

1.2 Background

Regarding the literature, three main methods exist for generating OAM modes. It is attempted to explain each category in detail.

1.2.1 Generation of OAM Using Circular Arrays

In [7], an efficient solution for generating radio beams carrying OAM with three polarizations is proposed. Ten horn antennas are arranged in a circular manner as shown in figure 1.1. Each antenna has the capacity to produce three polarizations : linear, left-handed circular, and right-handed circular. By exciting the elements with successive phase differences of 0, ±1, ±2, ±3, and ±4, OAM modes are generated. Equation (1.1) shows the required successive phase differences.

$$\Delta\varphi = \frac{2\pi l}{N} \tag{1.1}$$

Where N indicates the number of elements and shows the OAM mode. For example, to obtain mode -1, the elements need to be excited with a phase difference of -36°. Clearly, +36° gives mode +1. In theory, a large number of OAM modes can be generated using equation (1.1), but the radiation diagram deteriorates as the number of modes increases. This is due to the number of elements; the number of modes is less than half the number of radiation elements. Therefore, to obtain higher-order modes, the number of horn antennas needs to be increased. It is also worth mentioning that the larger the diameter of the array, the higher the maximum gain, and the wider its directional angle becomes.

In [6], three different circular array arrangements are studied to determine which is the best for generating OAM modes. It is concluded that a UCA provides the desired results. Figure 1.2 shows the proposed arrangements.

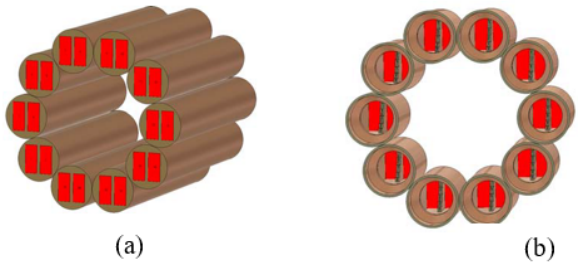

FIGURE 1.1 : Horn antenna array geometry : (a) Rear view. (b) Front view [7].

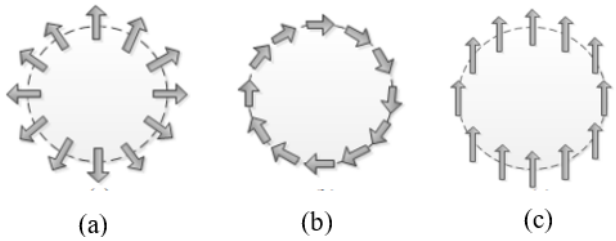

FIGURE 1.2 : (a) Structures of the radial array, (b) tangential array, and (c) uniform circular array [6].

Furthermore, in this reference, the conditions for multiplexing and demultiplexing are studied, and it is concluded that each OAM mode carrying information can be easily extracted by the receiver using DFT. This is valid because OAM modes are orthogonal to each other, and each pattern with a specific mode can be multiplied by a separate signal and transmitted simultaneously.

In [8], the realization of multiple OAM modes simultaneously through a four-dimensional UCA is discussed. The fourth dimension is related to switches : SPST and SPDT. The performance of the structure depends on the switches placed before a $1\times N$ power divider exciting the antennas. In fact, the switches induce a delay in the excitation of each antenna. If the SPST is used, since the N-1 switches are "deactivated," a large amount of power is absorbed by them, which is inefficient in terms of energy. On the other hand, using the SPDT, there is no "deactivated" state, and all the divided signals can reach the antennas with a phase difference of 180° relative to one signal, which is our preferred state. This is valid because the other state of the SPDT induces such a phase difference instead of deactivating.

Another important point in [8] is related to a new setup for measuring the phase front. Figure 1.3 shows the setup.

The waves carrying OAM generated simultaneously by the 4-D circular array are distributed over multiple harmonic frequencies, not just at the central frequency. Therefore, the traditional experimental platform in an anechoic chamber, where the transmitting antenna and the probe antenna operate at the same frequency, is not applicable for this measurement. In the experiment, the sampling plane is located 200 mm above the circular array with a scanning range of 500 mm $\times$ 500 mm. To obtain the near-field distribution, an open rectangular waveguide is used as the probe. Here, the key issue is to solve the difficulty of measuring the phase distribution. Since the phase of the fields is a relative value and not an absolute value, a reference antenna is added to provide a

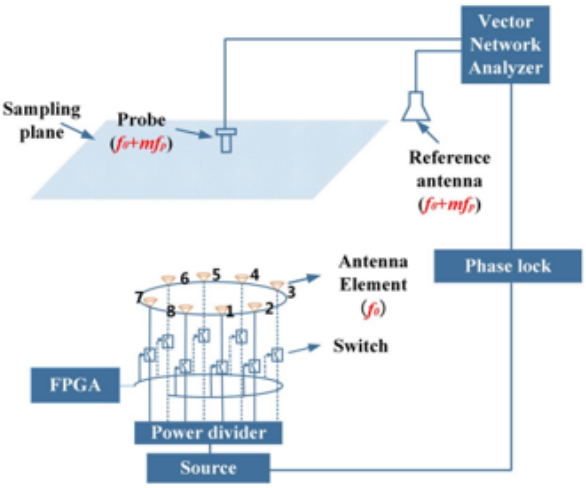

FIGURE 1.3 : Near-field phase distribution measurement setup for the 4-D array antenna [8].

reference phase. The reference antenna is fixed while the probe antenna scans the sampling plane. At the same time, both terminals of the open rectangular waveguide and the reference antenna are connected to a two-port VNA. The VNA performs the function of comparing the two signals from the open rectangular waveguide and the reference antenna. Thus, the phase distribution of the near field can be directly extracted from the $\angle$S21 measured by the VNA. Furthermore, a phase-locked loop is used to ensure that the VNA and the signal source are synchronized.

A dual-channel 60 GHz communication link is enabled by means of stacked circular arrays in [9]. QPSK and 16-QAM are used for modulation schemes to measure Bit Error Rate (BER) and SNR. The effect of mutual coupling among radiation elements, the obstruction effect along the axis of the lower layers caused by the upper layers, and the influence of non-ideal patches are discussed in this paper.

Two concentric circular arrays including eight radiators are designed to excite OAM modes of $+1$ and $+2$ [10]. The feeding network of one array is printed on top of the first layer, while the other is etched on the bottom of the third layer. In order to excite the antennas of the second array, plated holes are drilled to connect the outputs of the feeding network to the patches. The elements of the first array are fed with the aid of simple transmission lines. The operating frequency of each array is 2.4 GHz and by properly applying the progressive phase shifts of 45° and 90°, the aforementioned OAM modes are generated.

It is worth mentioning that in the proposed reference, all the measurement setups are thoroughly explained. Also, two video streams are considered to validate simultaneous transmission and reception at the same operating frequency.

To obtain different OAM modes with the same divergence angle, several concentric circular arrays are used in [11]. The central element is a simple patch antenna to excite OAM mode 0. Two arrays with different radii, each including eight elements, are placed in a configuration to generate

OAM modes -1 and -2. Another concentric array with sixteen elements is assigned for generating mode -3. The key contribution of this work lies in the feeding networks that produce the necessary phase shifts. To design such structures, stacked substrates are utilized.

For full-duplex applications, it is crucial to have low self-interference leakage from the transmitter to the local receiver. Although designing antennas with different polarizations for transmission and reception can help reduce interference, using OAM modes provides a more effective solution. This idea is explored in [12]. It is first demonstrated that in the well-known phase difference equation for generating OAM-carrying waves, equation (1.1), l represents the mode number when the array polarization is linear. When the polarization is Left-Hand Circular Polarization (RHCP) or Left-Hand Circular Polarization (LHCP), the variable l indicates the total angular momentum, which is the sum of Spin Angular Momentum (SAM) and OAM. For RHCP, SAM is -1, and for LHCP, it is $+1$. Thus, an RHCP array with an OAM mode of -1 has $l = -2$. This holds true only if the antenna array elements are sequentially rotated. As no rotation exists in the element positions in this case, l solely represents the OAM mode number.

An array with eight elements is designed, where each element is composed of sequentially rotated patches to generate RHCP. As shown, the subarrays are excited using H-shaped slots and transmission lines. The feeding network produces anticlockwise phases of $0°$, $-90°$, $-180°$, and $-270°$, resulting in RHCP. Note that the blue and red lines are separately connected to different feeding networks, each corresponding to a distinct input port, which results in the creation of two different OAM modes. Thus, low self-interference between transmitting and receiving scenarios is achieved. In the cited reference, it is also proven that under the condition :

$$l_A + l_B \neq 0 \tag{1.2}$$

the self-interference is minimized. Here, l_A and l_B denote the angular momentum of antennas A and B, respectively, as shown in figure 1.4.

Based on the results in [12], it is feasible to feed the antennas with a common phase and amplitude to generate OAM modes, provided sequential rotation is applied. By rotating the antennas, RHCP or LHCP is obtained, corresponding to SAM modes -1 or $+1$, respectively. If the antennas are excited in-phase, $l = 0$. Therefore, as the total angular momentum l is the sum of SAM and OAM, OAM modes of $+1$ or -1 are created. Such a structure operating at mm-wave frequencies is implemented in [13].

1.2.2 Generation of OAM Modes with Metamaterials

In [14], a PSPP is designed to create mixed OAM modes. To this end, a large number of unit cells, consisting of 4 holes in a square substrate, are used. To convert the incoming spherical wave (from an open waveguide) into a spiral-type wave with different modes, each unit in the PSPP

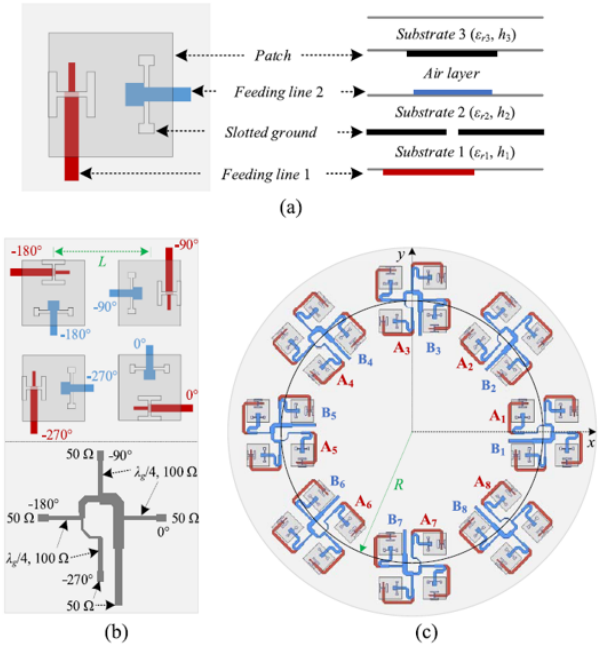

FIGURE 1.4 : The proposed sequentially rotates structure for full-duplex application using different OAM modes [12].

transforms the incoming phase into the required output phase. In fact, the unit cells compensate for the phase difference between the required phase and the incoming phase. Equations (1.3) to (1.5) clarify the above statement.

$$\text{outphase}(\phi) = \phi l \tag{1.3}$$

$$\text{inphase}(\theta) = \frac{2\pi F}{\lambda_0}\left(1 - \cos(\theta)\right) / \cos(\theta) \tag{1.4}$$

$$\text{Phase}(\theta, \phi) = \text{outphase}(\phi) - \text{inphase}(\theta) \tag{1.5}$$

Equation (1.3) shows the required output phase. Equation (1.4), which calculates the incoming phase, is determined using a geometric optics approximation [15] under the assumption that the spherical wave originates from the phase center of the antenna. Finally, equation (1.5) generates the required compensation phase, which must be obtained by each unit cell based on its position.

Figure 1.5 shows the structure of the PSPP capable of generating the 3 modes mentioned in the figure.

In [16], a Split-Ring Frequency Selective Surface(FSS) Spiral Phase Plate is used to create the first order of an OAM-carrying wave. It is designed from two-layer unit cells, consisting of two orthogonal split-rings. Regarding the angle between the rings, θ_r, a specific phase shift is achieved.

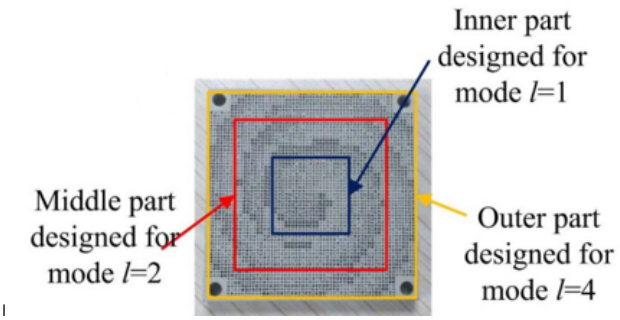

FIGURE 1.5 : The three-mode mixed OAM antenna [14].

For instance, if the rings are orthogonal to each other, a phase shift of $180°$, or twice the angle between the rings, is achieved. Thus, a left-handed circularly polarized wave is transformed into its right-handed counterpart. Figure 1.6 illustrates the unit cells.

To use such a structure for an OAM carrying wave, a 10×10 array is designed. Each element of the array must generate a phase shift based on its angular coordinate.

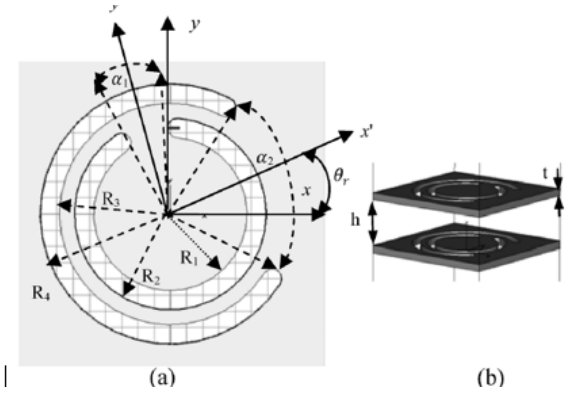

FIGURE 1.6 : Double layer FSS structure : (a) top view; (b) cross-sectional view [16].

A flat-lensed Spiral Phase Plate (SPP) based on a phase-shifting surface for generating an OAM beam at millimeter waves is investigated in [17]. The unit cell, shown in figure 1.7, consists of four stacked substrates with five metallic patches. By adjusting the width and length of the slot, a spatial phase shift is achieved. By determining the required phase for each unit cell based on its angular position within the array, an OAM mode is generated. It is worth mentioning that the rectangular patches act as a flat lens, enabling the two separated beams of the OAM mode to be redirected toward the axis by compensating the phase difference of a spherical incident wave. This effectively produces a focusing effect within the array.

In [18], a metasurface antenna is responsible for generating arbitrary OAM modes with arbitrary main beam angles. To achieve this, an array of unit cells (square patches), whose dimensions determine the reflection phase characteristics, is employed. Based on the superposition of aperture fields for each OAM mode, the required phase shift is obtained. Although it is possible to generate

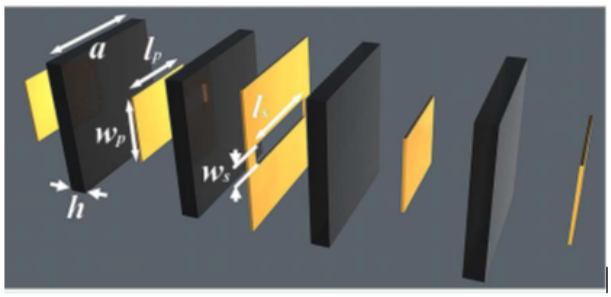

FIGURE 1.7 : Explosive view of a multilayer PSS unit cell [17].

OAM modes in different directions, exciting multiple modes in the same direction is not feasible, which limits the potential for increasing the capacity of the wireless channel.

One of the most critical factors to consider is the width of the null in the radiation pattern of OAM modes. This becomes a significant issue in long-distance communication, as the null width increases with the distance from the transmitter, requiring a larger aperture to receive the signal. To reduce this null width, various types of lenses can be employed in front of the transmitter. In [19], a 3D-printed planar graded-index lens is used in front of a circular array, and in [20], a Luneburg lens helps to reduce the divergence. However, such structures are often difficult to fabricate, expensive, and bulky.

Reference [21] evaluates the impact of the array element arrangement on mode purity, power loss, beam steering capabilities, and more. It concludes that circular arrays perform better than ring arrays. As the receiver moves away from a ring array, the null width increases more significantly compared to a circular array. Regarding beam steering, circular arrays generate purer modes; however, power loss increases at high steering angles, particularly beyond 70°. Another important advantage of circular arrays is their ability to preserve mode purity over long distances. This work also investigates the effect of lattice shape and boundary shape on the OAM spectrum. Overall, it demonstrates that the optimal configuration for generating OAM antennas consists of circular lattices with circular boundaries, as illustrated in figure 1.8.

1.2.3 Generation of OAM Modes Using Single Antenna Elements

There is also a simple method for generating OAM modes using a single element. This also helps reduce the complexity of the feeding network. In [22], it is demonstrated that by exciting a circular patch antenna with a phase difference of 90° from two specific points, OAM modes are generated in higher-order cavity modes. It is also concluded that it is possible to excite OAM modes using an elliptical patch antenna. In this case, two excitation points with a 90° phase difference are no longer necessary, and a single input port is sufficient. The problem associated with this technique is its narrow bandwidth. To solve this issue, the authors in [23] excited the circular patch antennas from four points, making the structure broadband. Figure 1.9 illustrates such a structure along with its feeding network.

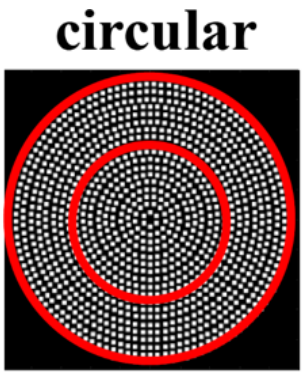

FIGURE 1.8 : A circular array with circular boundary for generating OAM mode [23].

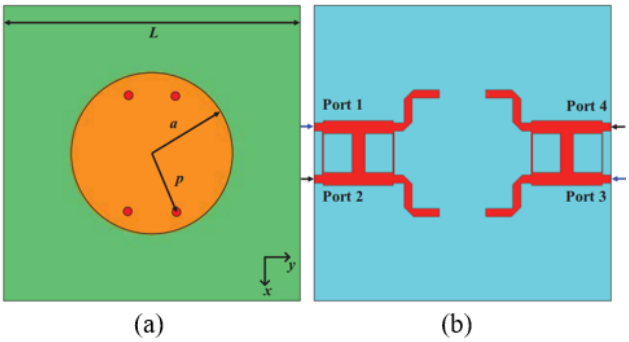

FIGURE 1.9 : Configuration of the single patch antenna and its feeding network for generating an OAM wave [22].

As is evident, two hybrid couplers excite the patch from two points independently. When the excitation port of the coupler is changed, the order of the OAM mode changes from -1 to +1 and from -2 to +2, or vice versa. It is also worth mentioning that the radial distance between the two points connected to each coupler is 135 degrees. This originates from placing the feed at the null point of the other feed. In other words, since we aim to exploit higher-order modes, depending on the number of modes, fields will form under the patch. By examining the field pattern, it can be observed that the TM_{21} mode exhibits a field distribution as illustrated in figure 1.10. Therefore, the radial distance between the two feeds should be 135 degrees. To excite other modes, the same method is used.

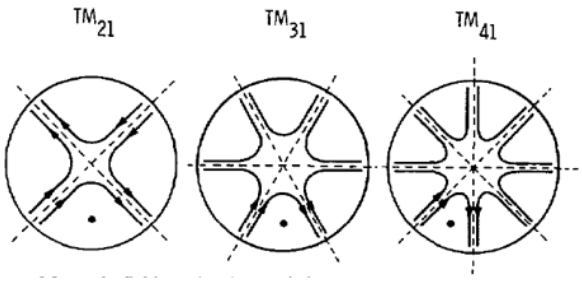

FIGURE 1.10 : Field distribution of higher-order modes under the circular patch [23].

A half-mode SIW cavity is presented with the capability to generate OAM modes using a single feed [24]. A ring cavity resonator with two rectangular slots on the metallic surface is used for this

purpose. By rotating the feed position by 90°, the opposite mode is obtained. Figure 1.11 illustrates the configuration of the proposed structure. It is important to mention that it is possible to generate OAM waves with higher mode numbers by increasing the radius of the cavity. However, the bandwidth of the antenna is too narrow, which may make it unsuitable for future 5G communications.

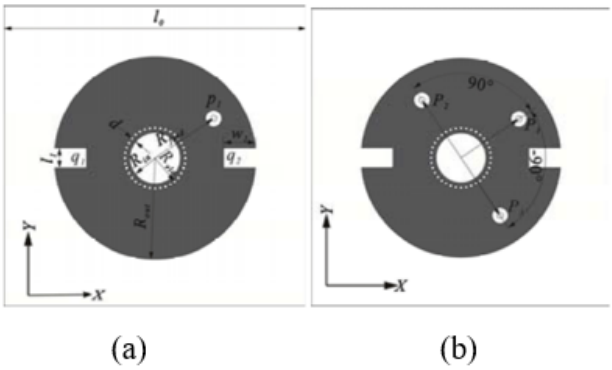

FIGURE 1.11 : Configuration of the SIW cavity for OAM generation [24].

In [25], a single square patch is employed to generate OAM modes ± 1 and 0. The patch is excited at its four edges using progressive phase shifts. When all phase shifts are zero, the OAM mode 0 is generated. When a phase shift of $\pm 90^{\circ}$ is applied, OAM modes of ± 1 are obtained, respectively. The configuration of the feeding network is illustrated in figure 1.12. Transmission lines with varying widths are implemented to achieve impedance matching.

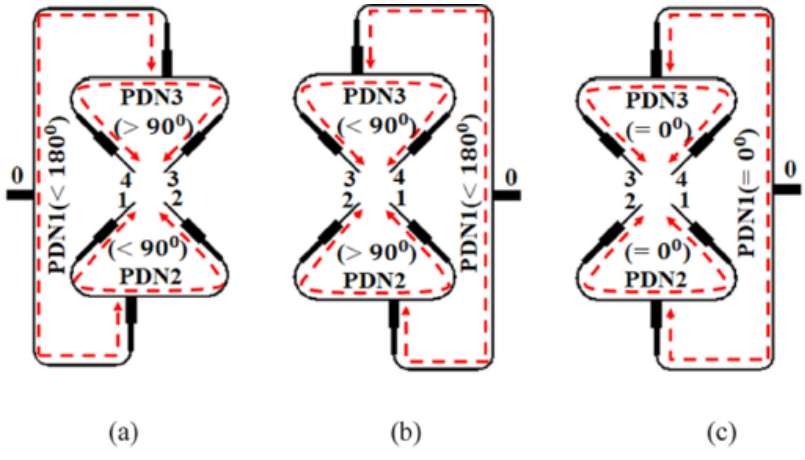

FIGURE 1.12 : The configuration of the feeding network engendering OAM modes [25].

As evident from figure 1.12, it is not feasible to use a single feeding network for generating different OAM modes. In other words, a distinct antenna must be designed and fabricated for each mode. It should also be noted that, in the proposed structure, the OAM modes ± 1 exhibit no null in the radiation pattern. This is attributed to the constructive interference of the radiating edges in the far field. Nevertheless, the simulated and measured phase fronts confirm the successful generation of the intended OAM modes.

1.3 Problem Statement and Motivation

As previously mentioned, in order to further enhance the channel capacity of wireless communication systems, Specially in Backhual link, BW and SNR have reached their maximum potential for improvement. MIMO antennas have provided another degree of freedom to improve wireless system performance in terms of data rate and resolution. However, they require complex signal processing once the number of antennas are increased. Furthermore, with conventional systems, different types of multiplexing schemes such as time division multiplexing, frequency division multiplexing, etc., are required at both the transmitter and the receiver. These types of multiplexing limit the full utilization of the frequency band as well as the time allocation.

OAM antennas are capable of propagating multiple orthogonal beams from a shared aperture. Since these orthogonal beams do not interfere with each other, a new multiplexing method called spatial mode multiplexing can be introduced in future wireless systems. As a result, the entire frequency band and time slot can be allocated to a single communication link. Other links can be activated simultaneously and at the same frequency by using different OAM mode numbers. Moreover, systems using OAM antennas do not require complicated signal processing. All of this highlights the superiority of OAM antennas conventional antennas.

In this context, to enable the design of intelligent wireless systems capable of autonomously controlling their OAM modes, frequency, and polarization, we will propose novel architectures.

1.4 Research Objectives

Having gained insights into the importance of OAM antennas in advanced wireless systems, the objective of our research is defined. The main focus is on reconfigurable OAM antennas. Reconfigurability enables intelligent systems. In other words, after fabrication, the antenna itself can modify its characteristics and adapt to a new environment or new conditions. Reconfigurability will be considered in terms of the number of modes, polarization, and frequency. According to the other characteristics, gain of more than 6 dBi, BW of 100 MHz, and mode purity of more than 70 percent are the targets.

As an example of practical application, in a microwave imaging system such as buried object detection, if frequency reconfigurability is implemented in the antenna part, potential interferences can be eliminated by changing the operating frequency. Similarly, in a point-to-point wireless communication link, due to environmental conditions or jamming, the existing OAM mode may not ensure the quality of the connection. Therefore, changing the mode number would provide a new propagation characteristic capable of overcoming the challenging conditions affecting the link.

In parallel with our research objective on design of reconfigurable OAM antenna, high-gain OAM antennas will also be considered. High-gain antennas allow for extended communication

distances. Indeed, by designing a high-gain OAM structure, the divergence of the propagated beams is reduced, resulting in a longer communication range. We will design a transmit array with the gain of more than 16 dBi to generate mixed OAM modes.

1.5 Thesis organization

This thesis aims to delve deeply into the design of reconfigurable OAM antennas. Also, in part it evaluates the design of high-gain multi-mode OAM structures. Summary of each chapter is as follow :

Chapter 2 : In this chapter, a 1×4 antenna feeding network is introduced with the capability of generating the required phase distribution for exciting orbital angular momentum (OAM) modes ±1. The proposed structure includes an equal power divider and four 1-bit phase shifters. Switching the state of phase shifters between ±45°, [0, 90, 0, 90] phase distribution is achieved in clockwise and counterclockwise directions. In case a uniform circular array (UCA) with a mirror image configuration is used, the phase distribution of [0, 180, 180, 0] is automatically produced between the antenna elements. Thus, the combination of feeding network and UCA will bring about the desired condition for exciting OAM modes +1 and -1. Furthermore, it is explained that by cascading another phase shifter to each of existing ones, the possibility of generating OAM mode 0 is obtained. A prototype of the suggested structure operating at 2.45 GHz is designed, fabricated, and measured. Upon evaluating the radiation characteristics of the system, reconfigurable beams with helical phase fronts and owing the null in the broadside are observed.

Chapter 3 : In this chapter, a frequency-tunable OAM-generating antenna array system is introduced for the first time to provide high-data-rate and secure communication for Internet of Things (IoT) infrastructures and devices. Propagation of simultaneous OAM modes brings about the high-data-rate and frequency tunability leads to interference suppression for secure communication. Regarding the design evolution of the proposed structure, the novel Multiple-Input-Multiple-Output (MIMO) antenna consisting of two input ports creates a 2×2 UCA, resulting in two 2×2 sub-UCA. Feeding each 2×2 sub-array with [0°, 90°, 180°, 270°] phase gradients in clockwise and counterclockwise states gives rise to dual-mode OAM-carrying waves with simultaneous excitation capability. It should be mentioned that each MIMO element owns frequency tunability, resulting in a frequency-adjustable dual-mode OAM antenna array. A prototypes of the suggested MIMO antenna as well as the OAM array are fabricated and measured. Changing the applied DC-voltage to the varactor diodes embedded in capacitive stubs of the antenna elements shifts the operating frequency in the MIMO antenna and consequently in the OAM array. Concerning the unique radiation characteristics of the OAM antenna, vortex beams having helical phase fronts are observed, confirming the generation of expected OAM waves.

Chapter 4 : As existing OAM antennas have no control on the operating frequency after fabrication and cannot simultaneously manipulate the polarization and mode number, designing smart

OAM wireless communication systems are out of reach. However, in this chapter, a new OAM antenna system is proposed that can efficiently overcome the aforementioned limitations. The suggested antenna utilizes a 2×2 Uniform Circular Array (UCA) composed of MIMO antennas to introduce the MIMO-UCA technique for simultaneous generation of OAM mode numbers +1 and -1. The flexibility on polarization of each mode stems from the fact that each MIMO antenna consists ±45° polarized elements, thus utilization of tunable feeds assigns the modes to the desired polarization simultaneously. The flexibility on the operating frequency is due to the frequency-reconfigurability of MIMO antennas as well. The fabricated prototype of the proposed structure verifies the simulated results. The operating frequency can be tuned from 3.8 GHz to 4.4 GHz. Over this band, the maximum gain is preserved above 6 dBi. The mutual coupling between the ports is below -20 dB.

Chapter 5 : This chapter presents a new OAM antenna system with an innovative reconfigurable feeding network and dual-polarized antennas. The 2×4 feeding network generates phase gradients of 0°, 90°, and -90° at its outputs, enabling OAM modes 0, -1, and +1. By integrating a 2×2 UCA with dual-polarized antennas and two copies of the proposed feeding network, the system supports six reconfigurable propagation types, ideal for smart OAM communications. Operating at 2.4 GHz, it achieves phase gradients with a maximum 4° imbalance, and input port reflection coefficients below -15 dB. All in all, the novel configuration of the feeding network, concept of combination of polarization and OAM modes, and ability to generate additional orthogonal reconfigurable beams can be highlighted as the novel parts of this chapter.

Chapter 6 : This study employs an ultrathin dual-polarized Huygens' metasurface to design a Transmitarray (TA) that can generate mixed-OAM modes. Two concentrically-embedded TAs are used to excite the desired modes by achieving the required phase difference according to the coordinate position of each unit cell. The prototype of the TA, which operates at 28 GHz and has a size of 11×11 cm^2, generates mixed OAM modes of -1 and -2 using dual-band Huygens' metasurfaces. This is the first time that such a low-profile and dual-polarized OAM carrying mixed vortex beams have been designed using TAs, to the best of the authors' knowledge. The maximum gain of the structure is 16 dBi.

Chapter 7 : In this chapter, a brief conclusion of the whole thesis as well as potential future works are discussed.

1.6 Published works in OAM

1. **H. Naseri**, P. PourMohammadi, N. Melouki, F. Ahmed, A. Iqbal, and T. A. Denidni, "Reconfigurable OAM Antenna With Flexibility on Mode Numbers, Polarization, and Frequency," *IEEE Antennas and Wireless Propagation Letters*, vol. 23, no. 6, pp. 1710-1714, Jun. 2024.
2. **H. Naseri**, P. Pourmohammadi, N. Melouki, F. Ahmed, A. Iqbal, and T. A. Denidni, "Frequency-adjustable OAM antenna with co-divergent beams for IoT applications," *AEU-International Journal of Electronics and Communications*, vol. 177, pp. 155188, Apr. 2024.

3. **H. Naseri**, P. Pourmohammadi, N. Melouki, F. Ahmed, A. Iqbal, and T. A. Denidni, “Generation of mixed-OAM-carrying waves using huygens’ metasurface for mm-wave applications,” *Sensors*, vol. 23, no. 5, p. 2590, Feb. 2023.
4. **H. Naseri**, P. Pourmohammadi, N. Melouki, A. Iqbal, and T. A. Denidni, “A low-profile antenna system for generating reconfigurable OAM-carrying beams,” *IEEE Antennas and Wireless Propagation Letters*, vol. 22, no. 2, pp. 402-406, Feb. 2023.
5. **H. Naseri**, P. Pourmohammadi, S. Ahmed, A. Iqbal, and T. A. Denidni, “Mode-Tunable OAM Antenna System with Polarization Selectivity characteristic," *2024 19th European Conference on Antennas and Propagation (EuCAP)*, Stockholm, Sweden, 2025, pp. 1-4.
6. **H. Naseri**, P. Pourmohammadi, N. Melouki, F. Ahmed, A. Iqbal, and T. A. Denidni, “Dual-Polarized OAM Antenna with Frequency and Mode Agility for Intelligent OAM Communications," *2024 18th European Conference on Antennas and Propagation (EuCAP)*, Glasgow, United Kingdom, 2024, pp. 1-4.
7. **H. Naseri**, P. Pourmohammadi, M. Bizan, N. Melouki, F. Ahmed, A. Iqbal, and T. A. Denidni, “Reconfigurable Dielectric Resonator OAM Antenna with Augmented Modes," *2023 IEEE International Symposium on Antennas and Propagation and USNC-URSI Radio Science Meeting (USNC-URSI)*, Portland, OR, USA, 2023, pp. 703-704.
8. **H. Naseri**, P. Pourmohammadi, M. Bizan, N. Melouki, F. Ahmed, A. Iqbal, and T. A. Denidni, “Triple-Mode OAM Generating Dielectric Resonator Antenna," *2023 URSI International Symposium on Electromagnetic Theory*, Vancouver, BC, CANADA, 2023.

1.7 Other published works

1. F. Ahmed, F. Faisal, N. Melouki, A. Ahmed, **H. Naseri**, P. Pourmohammadi, and T. A. Denidni, “A Multi-Functional Reflective Polarization Transforming Surface with In-Band and Out-Band Transmission Characteristics," *IEEE Antennas and Wireless Propagation Letters*, Jul. 2024.
2. F. Ahmed, A. Ahmed, N. Melouki, P. PourMohammadi, **H. Naseri**, N. Shoai, and T. A. Denidni, “A wideband bianisotropic FSS absorber with angular stable and polarization-insensitive properties," *Waves in Random and Complex Media*, pp. 1-16, Jun. 2024.
3. A. Butt, S. Barua, N. Safdar, **H. Naseri**, S. Ahmed, and T. A. Denidni, “Substrate integrated waveguide-based self-triplexing antenna-sensor," *AEU-International Journal of Electronics and Communications*, vol. 170, pp. 154833, May 2024.
4. N. Melouki, F. Ahmed, P. Pourmohammadi, **H. Naseri**, M. Bizan, A. Iqbal, and T. A. Denidni, “3D-Printed Conformal Meta-Lens with Multiple Beam-Shaping Functionalities for Mm-Wave Sensing Applications,” *Sensors*, vol. 24, no. 9, p. 2826, Apr. 2024.
5. N. Melouki, P. Pourmohammadi, **H. Naseri**, F. Ahmed, A. Iqbal, A. Hocini and T. A. Denidni, “Ultracompact Quarter-Mode SIW Self-Hexaplexing Antenna for C-Band and X-Band Appli-

cations," *IEEE Antennas and Wireless Propagation Letters*, vol. 23, no. 3, pp. 995-999, Mar. 2024.

6. F. Ahmed. T. Hassan, N. Meouki, **H. Naseri**, P. Pourmohammadi, A. Iqbal, and T. A. Denidni, “A Multibit and Frequency-Reconfigurable Reflecting Surface for RIS Applications," *IEEE Antennas and Wireless Propagation Letters*, vol. 23, no. 2, pp. 653-657, Feb. 2024.
7. P. PourMohammadi, **H. Naseri**, N. Melouki, F. Ahmed, Q. Zheng, A. Iqbal, and T. A. Denidni, “Highly-isolated compact self-diplexing antenna," *AEU-International Journal of Electronics and Communications*, vol. 173, pp. 155025, Jan. 2024.
8. **H. Naseri**, P. Pourmohammadi, P. Fei, N. Melouki, A. Iqbal, and T. A. Denidni, “Butler matrix-based beamforming with polarization reconfigurability for reducing electromagnetic interference," *AEU-International Journal of Electronics and Communications*, vol. 170, pp. 154833, Oct. 2023.
9. P. Pourmohammadi, **H. Naseri**, N. Melouki, F. Ahmed, M. S. Bizan, A. Iqbal, and T. A. Denidni, “A Fabry–Perot antenna using a frequency selective surface layer with wideband and Low RCS for Mm-wave applications." *AEU-International Journal of Electronics and Communications*, vol. 169, pp. 154736, Sep. 2023.
10. P. Pourmohammadi, **H. Naseri**, N. Melouki, F. Ahmed, A. Iqbal, G. A. Vandenbosch, and T. A. Denidni, “Compact SIW-Based Self-Quadruplexing Antenna for Microwave and Mm-Wave Communications," *IEEE Transactions on Circuits and Systems II : Express Briefs*, vol. 70, no. 9, pp. 3368-3372, Sept. 2023.
11. **H. Naseri**, P. PourMohammadi, N. Melouki, F. Ahmed, A. Iqbal, and T. A. Denidni, “Substrate Integrated Waveguide-Based Dual-Polarized Self-Diplexing Antenna Array," *IEEE Transactions on Circuits and Systems II : Express Briefs*, vol. 70, no. 8, pp. 2839-2843, Aug. 2023.
12. M. S. Bizan, **H. Naseri**, P. Pourmohammadi, N. Melouki, A. Iqbal, and T. A. Denidni, “Dual-Band Dielectric Resonator Antenna with Filtering Features for Microwave and Mm-Wave Applications,” *Micromachines*, vol. 14, no. 6, p. 1236, Jun. 2023.
13. P. Pourmohammadi, **H. Naseri**, N. Melouki, F. Ahmed, A. Iqbal, G. A. Vandenbosch, and T. A. Denidni, “Substrate Integrated Waveguide-Based Full-Duplex Antenna With Improved Out-of-Band Suppression," *IEEE Transactions on Circuits and Systems II : Express Briefs*, vol. 70, no. 4, pp. 1430-1434, Apr. 2023.
14. P. Pourmohammadi, P. Fei, **H. Naseri**, Q. Zheng, O. J. Babarinde, V. Volski, G. A. Vandenbosch, and T. A. Denidni, “A Single-Layer Compact Wideband Circularly Polarized Patch Array for 5G Communications," *IEEE Antennas and Wireless Propagation Letters*, vol. 22, no. 4, pp. 754-758, Apr. 2023.
15. **H. Naseri**, P. Pourmohammadi, Z. Mousavirazi, A. Iqbal, G. A. E. Vandenbosch, and T. A. Denidni, “A Low-profile Dual-band Hybrid Coupler with Flexible Frequency Band Ratio,” *Progress in Electromagnetic Research Letter*, vol. 107, pp. 119–124, Nov. 2022.

16. Z. Mousavirazi, **H. Naseri**, M. M. M. Ali, P. Rezaei, and T. A. Denidni, “A Low-Profile and Low-Cost Dual Circularly Polarized Patch Antenna,” *Progress in Electromagnetic Research Letter*, vol. 107, pp. 67–74, Oct. 2022.
17. N. Melouki, A. Hocini, F. Z.Fegriche, P. Pourmohammadi, **H. Naseri**, A. Iqbal, and T. A. Denidni, “High-Gain Wideband Circularly Polarised Fabry–Perot Resonator Array Antenna Using a Single-Layered Pixelated PRS for Millimetre-Wave Applications ,” *Micromachines*, vol. 13, no. 10, Oct. 2022.
18. Z. Mousavirazi, M. M. M. Ali, **H. Naseri**, and T. A. Denidni, “Analysis and design of ultra-wideband PRGW hybrid coupler using PEC/PMC waveguide model,” *Scientific Reports*, vol. 12, no. 1, p. 14214, Aug. 2022.
19. **H. Naseri**, P. Pourmohammadi, A. Iqbal, A. A. Kishk and T. A. Denidni, “SIW-Based Self-Quadruplexing Antenna for Microwave and mm-Wave Frequencies," *IEEE Antennas and Wireless Propagation Letters*, vol. 21, no. 7, pp. 1482-1486, Jul. 2022.
20. **H. Naseri**, P. Pourmohammadi, M. Bizan, and T. A. Denidni, “Butler Matrix-based Beam Switching with Frequency-tunable MIMO Array," *2024 IEEE International Symposium on Antennas and Propagation and USNC-URSI Radio Science Meeting (USNC-URSI)*, Florence, Italy, Jul. 2024.
21. P. Pourmohammadi, **H. Naseri**, N. Melouki, and T. A. Denidni, “A 1-Bit Wideband Electronically Beam Steering Transmitarray For 5G Communication Systems," *2024 IEEE International Symposium on Antennas and Propagation and USNC-URSI Radio Science Meeting (USNC-URSI)*, Florence, Italy, Jul. 2024.
22. P. Pourmohammadi, **H. Naseri**, F. Ahmed, and T. A. Denidni, “A Wideband Transmit Array based on Huygens’ Metasurface For Millimeter-Wave Applications," *2024 IEEE International Symposium on Antennas and Propagation and USNC-URSI Radio Science Meeting (USNC-URSI)*, Florence, Italy, Jul. 2024.
23. M. Bizan, **H. Naseri**, P. Pourmohammadi, and T. A. Denidni, “Ultra-Wideband Dielectric Resonator Antenna Fed By Printed Ridge Gap Waveguide Technology," *2024 IEEE International Symposium on Antennas and Propagation and USNC-URSI Radio Science Meeting (USNC-URSI)*, Florence, Italy, Jul. 2024.
24. M. Bizan, **H. Naseri**, P. Pourmohammadi, and T. A. Denidni, “Ultra-Wideband Dielectric Resonator Antenna Fed By Printed Ridge Gap Waveguide Technology," *2024 IEEE International Symposium on Antennas and Propagation and USNC-URSI Radio Science Meeting (USNC-URSI)*, Florence, Italy, Jul. 2024.
25. N. Melouki, F. Ahmed, **H. Naseri**, P. Pourmohammadi, A. Iqbal, and T. A. Denidni, “Multi-Bit Wideband Transmitarray Aperture with Independent Phase and Amplitude Control for High Gain with Low Sidelobe Mm-Wave Applications," *2024 18th European Conference on Antennas and Propagation (EuCAP)*, Glasgow, United Kingdom, 2024, pp. 01-04.
26. P. Pourmohammadi, **H. Naseri**, N. Melouki, F. Ahmed, G. A.E. Vandenbosch, A. Iqbal, and T. A. Denidni, “A Low-profile Self-duplexing Antenna for Millimeter-wave and Microwave

Frequency Bands," *2023 IEEE International Symposium on Antennas and Propagation and USNC-URSI Radio Science Meeting (USNC-URSI)*, Portland, OR, USA, 2023, pp. 605-606.

27. P. Pourmohammadi, **H. Naseri**, N. Melouki, F. Ahmed, M. Bizan, A. Iqbal, and T. A. Denidni, "A Wideband Fabry-Perot Antenna with a Bianisotropic FSS Layer," *2023 IEEE International Symposium on Antennas and Propagation and USNC-URSI Radio Science Meeting (USNC-URSI)*, Portland, OR, USA, 2023, pp. 649-650.
28. M. S. Bizan, **H. Naseri**, P. PourMohammadi, and T. A. Denidni, "Integrate Fabry–Perot Resonator into Dielectric Resonator Antenna for Microwave and Mm-wave Operations," *2023 IEEE International Symposium on Antennas and Propagation and USNC-URSI Radio Science Meeting (USNC-URSI)*, Portland, OR, USA, 2023, pp. 1161-1162.
29. N. Melouki, F. Ahmed, P. PourMohammadi, **H. Naseri**, A. Iqbal, and T. A. Denidni, "3D-Printed Conformal Metamaterial Lens with Multiple Beam Steering Functionalities," *2023 IEEE International Symposium on Antennas and Propagation and USNC-URSI Radio Science Meeting (USNC-URSI)*, Portland, OR, USA, 2023, pp. 791-792.
30. F. Ahmed, N. Melouki, P. PourMohammadi, **H. N. Gheisanab**, and T. A. Denidni, "A 2-Bit Reconfigurable Reflecting Metasurface for Mm-Wave Applications," *2023 IEEE International Symposium on Antennas and Propagation and USNC-URSI Radio Science Meeting (USNC-URSI)*, Portland, OR, USA, 2023, pp. 1425-1426.
31. P. Pourmohammadi, **H. Naseri**, N. Melouki, F. Ahmed, M. Bizan, A. Iqbal, and T. A. Denidni, "A Wideband Anisotropic Metasurface for Cross-Polarization Applications," *2023 URSI International Symposium on Electromagnetic Theory*, Vancouver, BC, CANADA, 2023.
32. M. Bizan, **H. Naseri**, P. Pourmohammadi, A. Iqbal, and T. A. Denidni, "Ultra-Wideband Dielectric Resonator Antenna With Integrated Fabry-Perot Cavity," *2023 URSI International Symposium on Electromagnetic Theory*, Vancouver, BC, CANADA, 2023.
33. F. Ahmed, N. Melouki, P. Pourmohammadi, **H. Naseri**, and T. A. Denidni, "4-Bit Reconfigurable Reflecting Metasurface for Sub-6 GHz Band," *2023 URSI International Symposium on Electromagnetic Theory*, Vancouver, BC, CANADA, 2023.
34. N. Melouki, F. Ahmed, P. Pourmohammadi, **H. Naseri**, and T. A. Denidni, "Low-Loss 2-Bit Reflective Intelligent Surface for mm-Wave Applications," *2023 IEEE International Symposium on Antennas and Propagation and USNC-URSI Radio Science Meeting (AP-S/URSI)*, Vancouver, BC, CANADA, 2023.
35. **H. N. Gheisanab**, P. Pourmohammadi, N. Melouki, A. Iqbal, and T. A. Denidni, "Self-diplexing Antenna Operating at Sub-6 GHz and Millimeter-wave Frequency Bands," *2023 17th European Conference on Antennas and Propagation (EuCAP)*, Florence, Italy, 2023, pp. 1-3,
36. N. Melouki, **H. Nasseri**, A. Iqbal, and T. A. Denidni, "Compact Quarter-Mode SIW Self-triplexing Antenna for C-band and X-band Applications," *2023 17th European Conference on Antennas and Propagation (EuCAP)*, Florence, Italy, 2023, pp. 1-5.
37. **H. Naseri**, P. Pourmohammadi, Z. Mousavirazi , A. Iqbal, and T. A. Denidni, "Full Azimuth Beam Steering by Means of Radiation Pattern with the Narrow Beamwidth," *2022 IEEE*

International Symposium on Antennas and Propagation and USNC-URSI Radio Science Meeting (AP-S/URSI), Denver, CO, USA, 2022, pp. 1630-1631.

38. P. Pourmohammadi, **H. Naseri**, R. Alwahishi, G. A.E. Vandenbosch, and T. A. Denidni, “A 2×3 High-Gain Coupled Patch Array for Body Area Network Applications," *2022 IEEE International Symposium on Antennas and Propagation and USNC-URSI Radio Science Meeting (AP-S/URSI)*, Denver, CO, USA, 2022, pp. 2068-2069.
39. M. M. M. Ali, Z. Mousavirazi, **H. Naseri**, and T. A. Denidni, “Design of Low-Loss Printed Ridge-Gap-Waveguide Crossover for Millimeter-Wave Applications," *2022 IEEE International Symposium on Antennas and Propagation and USNC-URSI Radio Science Meeting (AP-S/URSI)*, Denver, CO, USA, 2022, pp. 547-548.

1.8 Achievements

Alberta Innovate Recruitment Postdoc Fellowship (Sep. 2025-2027)

Fonds de Recherche du Quebec Nature and Technologies (FRQNT) scholarship (Summer 2023-2027).

Student Travel Grant from University of Quebec for the EUCAP conference held in Stockholm, Sweden (2025, April 1-5).

Student Travel Grant from IEEE organization for the AP-S conference held in Denver, U.S (2022, July 10-15).

Sensors MDPI journal editor’s choice article (August 2024)

Assistant guest editor for MDPI *Electronics* journal (September 2024)

2 MODE-TUNABLE OAM ANTENNA

This chapter contains materials extracted from the following publication. In this work, the targeted design specifications have been successfully achieved, including a gain greater than 6 dBi and a BW exceeding 100 MHz. Furthermore, in line with the main objective of our research on reconfigurable OAM antenna design, a mode-switchable antenna has been developed.

Low-Profile Antenna System for Generating Reconfigurable OAM-carrying Beams

Authors : Hassan Naseri, Peyman PourMohammadi, Noureddine Melouki, Amjad Iqbal, and Tayeb Denidni

Contribution of Authors : I am the main contributor to this work, under the supervision of Prof. Tayeb Denidni

2.1 Introduction

Traditionally, to increase the channel capacity of wireless communication systems, all attention has been on the enhancement of Bandwidth (BW) and Signal to Noise Ratio (SNR) [26,27]. In fact, to achieve a high-data transfer rate, systems with wide impedance BW and providing acceptable SNR level (high gain) are required [28, 29]. However, nowadays, current systems are not able to satisfy user's growing demand for high-speed communications due to the fact that there are limitations regarding BW and SNR; the BW sometimes is restricted by gain or axial ratio (AR) BWs, and SNR drops as a result of a change in environmental conditions or other uncontrollable parameters.

Orbital angular momentum (OAM) antennas have been one of the best candidates for increasing the channel capacity of a wireless communication network [30–32]. This holds true because in theory, it is possible to create an infinite number of orthogonal modes from a common aperture, providing the possibility of high-data-rate communications. One way to generate OAM-carrying waves is to use a UCA having a specific phase difference between elements [33, 34]. In [35], authors have utilized a circular phase shifter and array of patches to produce OAM mode 1. In order to excite several OAM modes, either the feeding network should be able to create the necessary phase differences associated with each mode [36], or the concentric and stacked UCAs must be taken into consideration [37, 38]. The problem with the latter one is related to the complexity of the feeding network, and with the former one is about the size of the whole system when different feeds should be designed for each UCA. To solve the mentioned issues, reconfigurable OAM-generating structures can be helpful. In fact, a single feeding network has to be able to switch between modes. In this regard, some studies have been carried out. In [39], 4 PIN diodes are employed to create two separate directions for exciting the antennas. Also, a pair of UCA is considered for changing

the state of OAM modes. Authors in [40] have introduced a complicated feeding network including several PIN diodes to engender OAM mode +1 and -1. It should be mentioned that the proposed system is a three-layer structure. Another electronically mode-reconfigurable antenna has been designed in [41]. 16 PIN diodes change the path of signals feeding the antenna elements and consequently, OAM modes 0, -1 and +1 are achieved. 32 PIN diodes are responsible for generating reconfigurable OAM modes in [42], and 20 PIN diodes bring about the feeding network producing tunable OAM radio beams [43]. A simplified UCA feed owing 4 PIN diodes has been applied to present a mode reconfigurable OAM metasurface antenna array [44]. However, a large portion of power is lost in this structure due to the fact that once a diode is OFF, the received power to it returns toward the input port, disturding the performance of structure. As became evident, so far, most of the reconfigurable OAM antennas have a feeding network composed of several PIN diodes. The more the number of diodes is, the more the structure is complex. Furthermore, as we use diodes for separating the signal path, some leakage from the reverse state of diodes might disturb the purity of OAM modes. To that end, a new design is required to solve the mentioned problems.

In this chapter, a low-profile UCA feed is proposed which can enable the switching between OAM modes -1 and +1 with the aid of 1-bit phase shifters. The structure is consist of a power divider and four $\pm 45^\circ$ phase shifters. The mirror image configuration of antenna elements facilitates the generation of OAM modes due to the fact that there is no need for 180° transmission lines. All the simulated and measured results verified the desired performance of the structure at 2.45 GHz as well. It is also worth mentioning that the suggested system provides a single-layer configuration which is unique in comparison with the existing works. Cascading another phase shifter with each of existing ones provides the condition of feeding the antenna elements in-phase, thus producing OAM mode 0.

2.2 Design Process

In this section, the architecture of the suggested feeding network is evaluated. Subsequently, its phase and amplitude response is presented. The fabricated prototype of structure including the antenna elements are measured to validate the generation of desired OAM modes. In the end, a comparison between this work and those existing in the literature is discussed.

2.2.1 UCA tunable feeding network

The general approach to design the feed for OAM-generating UCAs is to utilize a $1\times N$ power divider, which N corresponds to the number of antenna elements in the UCA. Besides this, fixed phase shifters should be connected to each output of power divider to produce the required phase response for a desired OAM mode. The mentioned method can only excite one OAM mode. Thus,

in order to make a UCA to generate more than one mode, the feed should be designed in a way that it can be reconfigurable. Here one of the simplest and most efficient ways to make a reconfigurable feed is introduced. The schematic of the proposed structure is depicted in figure 2.1. To demonstrate, consider the input port is excited. In the first step, the signal is divided into two equal parts with the same phase; each of which arrives at its corresponding T-junction, resulting in another in-phase division. The key components here are the 1-bit phase shifters. Once the state of them according to the number of Antennas is [45°, -45°, 45°, -45°], the outputs of the feeding network would be equal to [0°, -90°, 0°, -90°]. As a result of the fact that Antenna 1 and 4 are the mirror image of Antenna 2 and 3, an automatic phase difference of 180° exists among them. Thus, OAM mode -1 is generated with the phase response of [0°, 90°, 180°, 270°]. To create mode +1, the state of phase shifters should be [-45°, 45°, -45°, 45°]. It should be clarified that 0° is considered as the reference for all the mentioned phases.

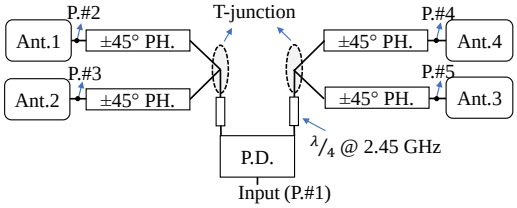

FIGURE 2.1 : The block diagram of the proposed tunable UCA feeding (P.D.=Power divider, PH.=Phase shifter, P=port and Ant.=Antenna).

To design a sample of structure, 2.45 GHz is taken into account as the operating frequency. According to [45, 46], an equal power divider is designed. The power divider includes a 50-ohm resistor for isolation purpose and transmission lines with characteristic impedance of 50-ohm. This helps to reduce the potential reflection losses due to the minimum number of discontinuities.

The 1-bit phase shifters include 2 Varactor diodes of SMV 2020 placed on both sides of a short circuit transmission line. The line behaves like an inductor. By changing the applied DC voltage to the bias pads, the required phase shifts of ±45° are obtained. The necessary information concerning the bias network of the diode can be found at its data sheet. Also, all the component values are presented in figure 2.2.

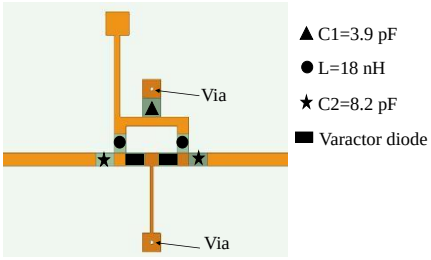

FIGURE 2.2 : The configuration of the utilized 1-bit phase shifter.

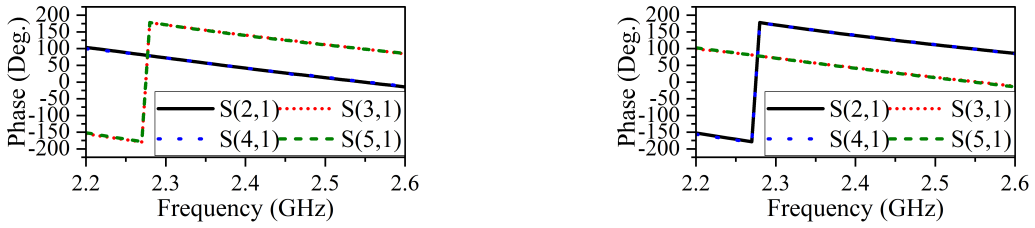

FIGURE 2.3 : Phase response of the OAM-generating feeding network (a) mode +1, and (b) mode -1.

FIGURE 2.4 : Amplitude response of the OAM-generating feeding network (a) mode +1, and (b) mode -1.

Another important parameter which should be studied is related to the impedance matching of the network. Considering the antennas as 50-ohm loads, the input impedances seen from each output of the power divider should be 50-ohm as well. As each branch of the T-junction is matched to the loads, so the equivalent impedances observed from T-junctions would be 25-ohm; it has its root in two parallel 50-ohm lines. To match 50 to 25-ohms, quarter-wavelength transmission lines are utilized. It should be mentioned that the characteristic impedance of the lines is 35.35 ohm.

2.2.2 Phase and amplitude response evaluation

It is expected that the proposed feeding network equally distributes the input signal with [0°, -90°, 0°, -90°] or [0°, +90°, 0°, +90°] phase gradients. Figure 2.3 shows the phase response of the structure for both OAM modes. The output ports connected to Antennas 1 and 3 are in-phase. Also, those associated with Antennas 2 and 4 have the same phase response. While, there is a phase difference of +90 or -90 between the mentioned couples. These characteristics confirm the achievement of required phase condition for producing OAM modes ±1.

Figure 2.4 provides the necessary information regarding the amplitude response of the structure. Over the frequency range from 2.3 GHz to 2.8 GHz, the feeding network is well matched. However, the output signals become imbalanced as we go away from the operating frequency of 2.45 GHz.

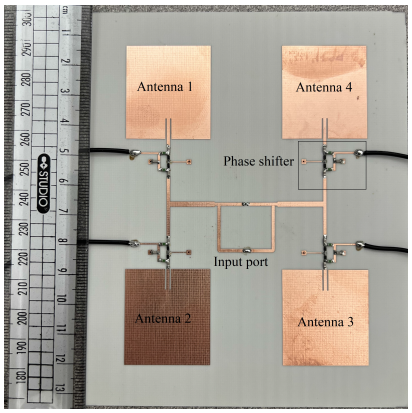

FIGURE 2.5 : Configuration of the fabricated structure.

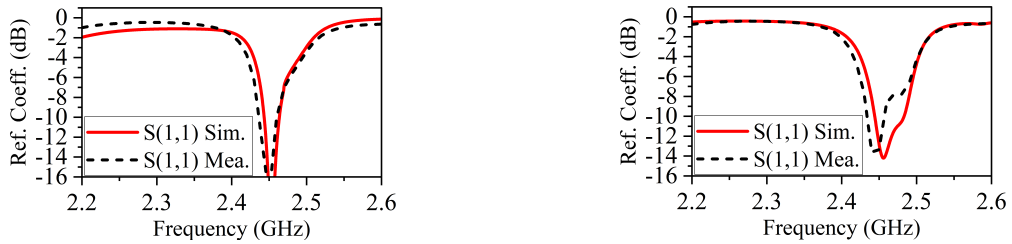

FIGURE 2.6 : Reflection coefficient related to the input port when (a) OAM mode +1, and (b) OAM mode -1 are excited.

2.3 Experimental Results

To analyze the performance of the suggested feeding network in the generation of OAM modes, four rectangular patch antennas have been designed to be connected to the outputs. The point here is to consider the mirror image configuration so as to satisfy the desired phase response for OAM modes. Figure 2.5 shows a picture of the fabricated prototype. In order to avoid any long transmission line for the input port, a coaxial probe has been utilized for exciting the structure. The applied voltage to Varactor diodes is controlled by means of soldered wires to the places determined for bias. It is also worth expressing that the substrate is Rogers 4003C with a dielectric constant of 3.55 and a thickness of 20 mils. Figure 2.6 depicts the reflection coefficients associated with the input port in both OAM modes ±1. It is evident that the impedance bandwidth is limited after connecting the antennas. This has its root in the thickness of the substrate. In this case, since the thickness of the substrate is less, the impedance bandwidth has become less as well. In order to increase the bandwidth, a thicker substrate can be helpful. However, for our purpose which is to introduce a new method for generating reconfigurable OAM modes, bandwidth increment has not been taken into consideration.

Figure 2.7 and figure 2.8show the normalized gain patterns for OAM modes. As obvious, a null exists at the broadside, confirming the generation of OAM modes. Also, it should be mentioned that the achieved maximum gains are almost 7 dBi for measured cases and 7.5 dBi for simulated

TABLE 2.1 : MAXIMUM GAINS AND EFFICIENCIES ASSOCIATED WITH OAM MODES.

Mode Number	Simulated gain (dBi)	Measured gain (dBi)	Efficiency
Mode +1 (f=2.45 GHz)	7.6	7.1	0.78
Mode -1 (f=2.45 GHz)	7.5	7	0.75

TABLE 2.2 : COMPARISON BETWEEN THIS WORK AND EXISTING ONES.

Ref.	[40]	[41]	[42]	[43]	[44]	[47]	This work
Freq. (GHz)	2.5	5.7	2.5	2.5	6.2	3	2.45
Size ($\lambda \times \lambda \times \lambda$)	1.28×1.28×0.07	2.3×2.3×0.069	2.6×2.6×0.06	2.6×2.6×0.06	1.98×1.98×0.07	*Not mentioned*	1.7×2×0.007
Number of layers (Sub.)	3	4	3	3	2	1	1
Number of PIN Diodes	16	32	32	20	4	50 V.D.	8 V.D.
Number R, L, C	7, 4, 4	0, 0, 8	7, 40, 0	0, 22, 4	0, 4, 2	0, 0, 24	1, 8, 12
Current Leakage in R.B.	Yes	Yes	Yes	Yes	Yes	*N/A*	*N/A*
Design complexity	high	high	high	high	medium	high	low
Gain (dBi)	5.3, 5.3	15.9, 11.17, 11.05	*Not mentioned*	5.2, 5.2	9.4, 9.4	*Not mentioned*	7.1, 7
Mode	±1	0, ±1	±1	±1	±1	0, ±1	±1

R.B. = Reverse Bias (for PIN diodes), V.D. = Varactor diode, N/A = Not applicable, Sub. = Substrate, R = resistor, L = inductor, C = capacitor

cases. The simulated efficiency values for OAM modes +1 and -1 are 0.78 and 0.75, respectively. All the values are listed in TABLE 2.1 as well. It is worth expressing that we used spline curve fitting option from MATLAB to make our measured results smooth for better comparison with simulated ones. Applying this technique did not have any effect on the dips.

As well-known, paramount characteristic of OAM modes is them having helical phase fronts. To evaluate this feature, a square area at 5λ away from the structure is scanned by using a standard waveguide antenna. The results have been provided in figure 2.9. From the figure, it is observed that on any circle on the plane, the phase alters from 0 to 360°; Clockwise or anti-clockwise rotation distinguishes the mode numbers. All in all, referring to radiation patterns and phase fronts, it is concluded that the tunable OAM modes are obtained.

2.4 Discussion

To compare the proposed tunable OAM structure with existing ones, TABLE 2.2 is presented. As mentioned before, the suggested structure utilizes 1-bit phase shifters each having 2 Varactor diodes, while other works have used PIN diodes. Thus, the problems regarding the leakage of current (signal) once diodes are in their reverse states are avoided, and consequently we will have pure modes. Furthermore, the size of the proposed structure is smaller than the mentioned works. Moreover, it should be pointed out that however [44] uses less diodes, it is a lossy structure; when a diode is OFF, the received signal to it is reflected, leading to a large portion of loss. The achieved higher gains in [41,44] is related to the use of a metasurface layer on top of the structure. However, it comes without saying that 32 pin diodes utilized in [41] will bring about much higher loss in comparison with 8 varactor diodes used in our structure.

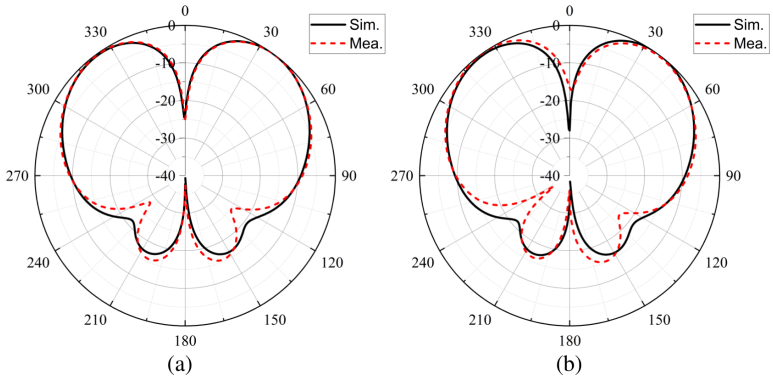

FIGURE 2.7 : Normalized gain in the E-plane for OAM mode (a) +1, and (b) -1.

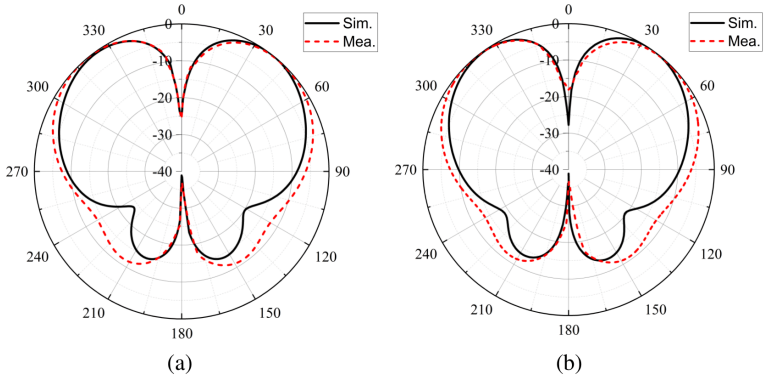

FIGURE 2.8 : Normalized gain in the H-plane for OAM mode(a) +1, and (b) -1.

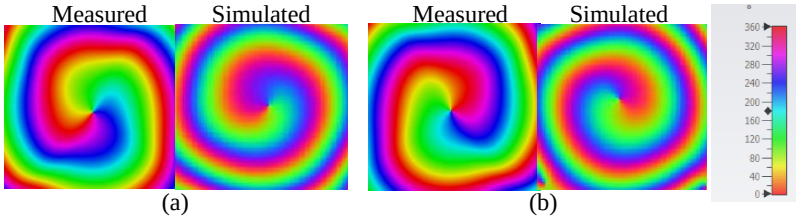

FIGURE 2.9 : Simulated and measured phase front for OAM mode (a) +1, (b) -1.

The tunable OAM-generating system owns a single-layer architecture, while other structures have not been able to achieve such a characteristic. Specially in [42, 43] that the existence of final PIN diodes does not allow the fabrication possibility on one layer.

As mentioned, the suggested structure is able to create OAM mode 0 as well. This feature is obtained easily by adding another similar phase shifter to each end of the existing ones. By doing so, it is possible to excite the antenna elements in-phase, resulting in generation of OAM mode 0. If all the cascaded phase shifters are adjusted to operate at the same state, OAM mode +1 and -1 are achieved.

2.5 Acknowledgment

This work has been funded by Fonds de Recherche du Québec Nature et technologies (FRQNT) under the file number of 333948.

2.6 Conclusion

In this chapter, a low-profile tunable feeding network has been introduced which can produce required phase and amplitude response for generating OAM-carrying waves with modes ±1. The structure consists of an equal power divider and four 1-bit phase shifters. Changing the state of phase shifters between +45° and -45° in a specific order, [0°, 90°, 0°, 90°] or [0°, -90°, 0°, -90°] phase gradients are created. In case, antennas with mirror image configuration are connected to the feeding network, the necessary condition is provided to engender OAM modes ±1. Moreover, it has been explained that the proposed structure enables the generation of OAM mode 0, adding another phase shifter to each end of existing ones. It is also worth mentioning that the proposed structure has the lowest-profile and design complexity in the literature.

3 FREQUENCY-ADJUSTABLE OAM ANTENNA

This chapter contains materials extracted from the following publication. In this work, we maintained the achievement of the general design targets, including a gain greater than 6 dBi and a BW exceeding 100 MHz. In addition, we achieved a mode purity higher than 70 %. Unlike the previous chapter, we successfully obtained simultaneous mode generation combined with frequency tunability.

Frequency-adjustable OAM Antenna with Co-divergent Beams for IoT applications

Authors : Hassan Naseri, Peyman PourMohammadi, Noureddine Melouki, Amjad Iqbal, Fahad Ahmed, and Tayeb Denidni

Contribution of Authors : I am the main contributor to this work, under the supervision of Prof. Tayeb Denidni

3.1 Introduction

Internet of Things (IoT) aims at providing the connectivity between devices and internet [48,49]. Health monitoring [50], autonomous cars [51], smart cities [52], and smart buildings [53] are some examples of IoT.

Antennas play the key role in IoT devices and infrastructures as the signals and data are transmitted and received by them [54, 55]. To achieve high-data-rate communication which is essential for real-time connections, MIMO antennas are utilized for IoT applications as well [56, 57]. Such antennas need beamformers, and this makes the systems sophisticated.

Orbital Angular Momentum (OAM) antennas are one of the best options to achieve high-data-rate in so many applications like IoT [58–60]. This has its root in OAM antennas ability to generate orthogonal radiation patterns at the same time and frequency. Therefore, each signal can be transmitted using the specific OAM mode, resulting in multiple signal propagation at once. It should also be emphasized that the orthogonality of OAM modes does allow the signals become combined with each other, and consequently in the receiving side, they can be separated easily. However, in MIMO antennas it is not the case.

As the foundation for exciting the OAM modes, if, in theory, we have a loop antenna with the current distribution of $I = I_0 e^{jl\phi}$, upon calculating the radiation pattern of the antenna, $e^{jl\phi}$ component would appear in the electric field on the plane perpendicular to the propagation axis. This indicates the helical phase front of the beam in which *l* shows the OAM mode number and ϕ presents the transverse azimuth angle. In particular, the mentioned phase front illustrates the vortex-like propagation wave. If we can excite multiple modes from one antenna, due to the orthogonality of these

modes, they can carry signals independently. In the other words, each OAM mode is used for data transfer while there is no overlap between the modes. This has its root in orthogonality of OAM modes. Spatial multiplexing is the name selected for this kind of communication.

In practice, inspired by this principle, some single antenna elements can enable the propagation of OAM modes [22, 25, 61, 62]. However, since exciting such a current distribution in single antenna elements is a challenging task, and because the possibility of generating simultaneous OAM modes is not possible in this way, the discrete current is replaced with the continuous one. In addition, the circular array antennas are replaced with single antennas as well.

Putting aside the single antenna elements due to their limitation in propagating simultaneous OAM modes, and according to the literature, OAM antennas are divided into two main categories : uniform circular array (UCA)-based and metasuraface-based. It should be noted that the metasurface-based OAM antennas are transmitarrays and reflectarrays. Most importantly, in both of the categories, with regard to the desired OAM mode number and angular position of each unit cell or single element, the discrete current having the amplitude of 1 and phase of Φ is applied.

As some examples for the first category, ten horn antennas are arranged in a circular manner to produce multiple OAM modes [31]. In [36], realization of multiple OAM modes simultaneously through a four-dimensional UCA is discussed. Generating and steering the OAM modes by means of delay lines are suggested in [63]. However, passive delay lines make the structure non-planar, lossy and expensive, thus difficult for practical applications. A dual-channel 60GHz communication link is enabled with the aid of stacked circular arrays in [38]. Dipole antennas can also be placed in a circular array and generate OAM modes in both side : back and front [64]. Recently, authors in [37], have used sequentially rotation technique in a UCA to produce OAM modes with different polarizations. Furthermore, there exist some works that can generate multiple OAM modes either by designing multiple input feeding networks producing the required phase gradients associated with each OAM mode [65–67] or by stacked and concentrically embedded UCAs having individual feeds [34, 68, 69].

All the mentioned works in the first category produce OAM modes in a fixed manner. However, there have been recent introductions of structures that allow for mode adjustments. A recent advancement includes an array in [40, 42, 70] that can reconfigure both the CP and OAM modes. If the ability to reconfigure polarization is not a priority, the works in [39, 41, 44, 47, 71–73] should be taken into consideration. A multi-gigabit OAM beam with tunable modes is proposed in [74]. Authors in [75] designed a mm-wave tunable OAM antenna with the capability of steering the beam. An Archimedean spiral antenna has also been used for generating OAM beams [76]. Digital control method is the base for exciting vortex beams in [77]. Very recently, in [78], the authors developed a compact and adaptable antenna system for OAM generation, using 1-bit phase shifters to resolve issues found in earlier designs with PIN diodes.

Regarding the second category, in [79], a Miniaturized Element Frequency Selective Surface (MEFSS) is investigated to produce the first order of OAM-carrying waves. A split-ring FSS Spi-

ral Phase Plate (SPP) is used to create the OAM mode +1 in [80]. A flat-lensed SPP based on phase-shifting surface for generation of millimeter-wave OAM beam (l=+1) is investigated in [81]. A combined OAM modes are achieved according to the contributions in [82,83] as well; former one utilizes concentrically embedded spatially divided technique, and the latter one uses cascaded transmitarrays each creating one OAM mode. Authors in [84], have introduced a reflectarray with the capability of creating different OAM modes. However, in this structure it is not possible to excite simultaneous OAM modes. Further, the frequency-tunability cannot be achieved after fabrication since unit cells can only control the reflective phase and not operating frequency. Generation of mixed-OAM modes using huygens' metasurface is carried out by authors in [85].

Among the existing OAM antennas, the suitable structures for IoT applications are those with the capability of simultaneous OAM mode generation so as to achieve high-data-rate. In fact, each stream of data should be transmitted by one OAM mode at the same time and frequency. With all this in mind, UCA-based structures belonging to the first category are appropriate. Stacked UCAs or concentrically embedded ones which have individual feeds for each mode are the best candidates from first category [37, 38, 68, 69]. Theses kind of UCA-based OAM antennas own three main limitations : (a) they lead to designing multi-layer architectures and thus being costly, (b) they need separate UCAs which requires mutual coupling reduction between them, and (c) the propagating OAM beams do not have the same divergent angle due to the different UCA radii. Being co-divergent is very important feature as in the receiving side, the maximum power should be captured from different modes at the same position [86]. We will take advantage of MIMO antennas to introduce MIMO-UCA concept for solving these restrictions.

Another important factor in IoT applications is related to the security of communication [87,88]. In the other words, the interferences coming from the other sources should be suppressed so as to have a secure connection. In general, researchers use the frequency tunable antennas for multi functional purposes. For instance, when one wants to use the antenna for other applications, instead of designing a new antenna, they can adjust the operating frequency to the desired value [89–93]. Beside this feature, it is possible to use frequency-tunable antennas for suppressing the interferences. When one unwanted signal tries to disturb the communication, changing the operating frequency can readily eliminate the effect of jamming. This feature is also obtained using the proposed structure.

Figure 3.1 depicts how the recommended OAM antenna might be utilized within IoT setups. In the context of a hospital, the suggested OAM antennas can be installed atop structures to facilitate secure and high-speed communication. To exemplify, vital signs data of a patient can be transmitted securely and in real-time to a doctor situated in a separate building.

In this chapter, a frequency-adjustable OAM antenna structure is proposed that can produce co-divergent simultaneous modes to help design high-data-rate and secure IoT infrastructure and devices. MIMO-UCA technique has been taken into consideration to obtain the above-mentioned characteristics. Since each MIMO has two input ports, we come up with two 2×2 sub-arrays. Fee-

FIGURE 3.1 : textcolorblack Potential application for high-data-rate and secure OAM-based IoT communication.

ding the sub-arrays with [0°, 90°, 180°, 270°] phase gradients in clockwise and counterclockwise states provides the necessary phase distribution for OAM generation. It should be mentioned that the frequency tunability is enabled by changing the DC-voltage level applied to embedded varactor diodes in each stub of antenna elements. Regarding the validation of desired OAM mode generation, the vortex beams with helical phase fronts are observed during the measurement process.

3.2 Tunable MIMO Antenna Design

In this section, the design evolution of the proposed frequency-tunable MIMO antenna is discussed. In addition, the reflection coefficients associated with each input port under different values of capacitance for varactor diode as well as mutual coupling among the ports are explained. Finally, the radiation patterns of the antenna are evaluated.

3.2.1 Design process

Before delving into the explanation of the design process for the frequency-tunable MIMO antenna, it is necessary to examine a phenomenon related to Substrate Integrated Waveguide (SIW) cavities. Consider a scenario where there is a square SIW cavity (shown as a full-mode cavity in figure 3.2a) where the fundamental mode of TE_{110} occurs at 4.2 GHz. If this cavity is divided into two halves, the fundamental mode and resonance frequency remain preserved. Each of these halves is referred to as a half-mode cavity, as illustrated in figure 3.2b. Further division of a half-mode cavity leads to a quarter-mode cavity, without causing significant alterations in the fundamental mode or resonance frequency, as depicted in figure 3.2c. Additionally, it is important to note that the reflection coefficients shown in figure 3.2d validate the stability of the resonance frequency during the transition from a full-mode cavity to a quarter-mode one.

The unique characteristic of a SIW cavity mentioned above paves the way for designing a miniaturized antenna structure. For our purpose, we explore this feature further so as to introduce a MIMO antenna with the frequency tunability inside a half-mode cavity. To that end, at the first step, a full-mode SIW cavity with the resonance frequency at 4.2 GHz is designed. Equations (3.1)

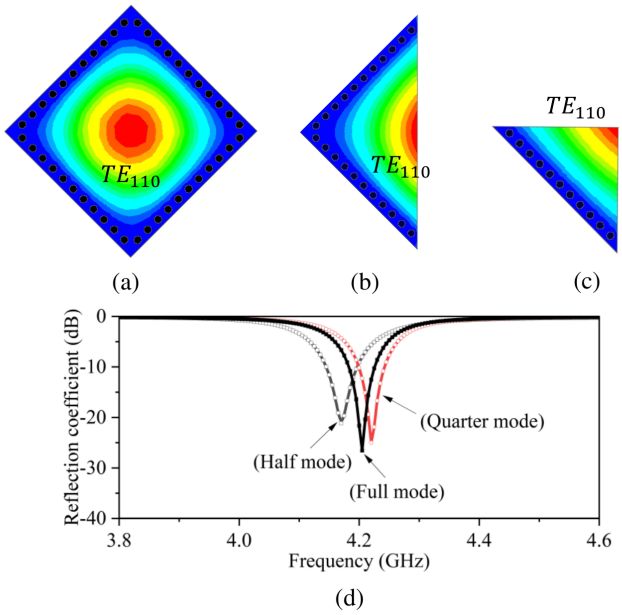

FIGURE 3.2 : Electric field distribution in a (a) full-mode, (b) half-mode, (c) quarter-mode SIW cavity, and (d) the reflection coefficients associated with each one.

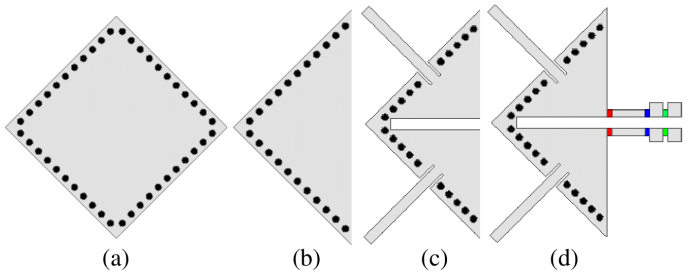

FIGURE 3.3 : (a) Full-mode SIW cavity, (b) half-mode SIW cavity, (c) the proposed non-tunable MIMO antenna, and (d) frequency adjustable MIMO antenna.

and (3.2) are used to obtain the dimensions of the square cavity [94].

$$f_r = \frac{c}{\sqrt{2} l_e \sqrt{\epsilon_r}}, \tag{3.1}$$

where

$$l_e = l - \frac{p^2}{0.95s}. \tag{3.2}$$

In the equations, f_r presents the dominant resonance frequency, which is initially taken as 4.2 GHz. *c*, *l*, l_e, *s*, and *p* are light velocity in free space, length and width of square cavity, effective length and width of cavity, diameter of vias, and distance between vias, respectively. It should be mentioned that the dielectric constant of the substrate is ϵ_r=2.2. The configuration of the full-mode cavity is presented in figure 3.3a.

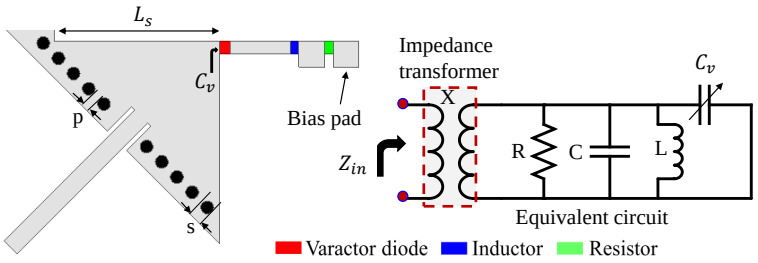

FIGURE 3.4 : The configuration of the radiator of the proposed MIMO antenna and its equivalent circuit model. (Ls=24mm, s=0.7mm, p=1.5mm).

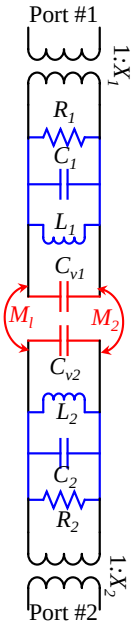

(a)

Components	Values at 4.15 GHz	Values at 4 GHz	Values at 3.8 GHz
X1	0.16	0.16	0.16
X2	0.16	0.16	0.16
R1	1650 Ω	1650 Ω	1650 Ω
R2	1650 Ω	1650 Ω	1650 Ω
C1	1.01 pF	1.01 pF	1.01 pF
C2	1.01 pF	1.01 pF	1.01 pF
L1	1.08 nH	1.08 nH	1.08 nH
L2	1.08 nH	1.08 nH	1.08 nH
Cv1	0.35 pF	0.455 pF	0.61 pF
Cv2	0.35 pF	0.455 pF	0.61 pF
M1	0.11	0.11	0.11
M2	0.11	0.11	0.11

(b)

FIGURE 3.5 : The configuration of the radiator of the proposed MIMO antennas and its equivalent circuit.

In the second step, the designed full-mode cavity is divided into two parts, figure 3.3b, and one part is selected for antenna design. A slot can divide the existing half-mode cavity into two sections, each assigned for one antenna. It is worth pointing out that this does not change the resonance frequency that much as well, figure 3.3c. In the final step, in order to adjust the resonance frequencies, open-circuit stubs cascaded with varactor diodes are introduced, figure 3.3d. The varactor diodes embedded inside the stubs are responsible for altering the operating frequencies. To further illustrate the role of stubs, a circuit model of one antenna is depicted in Fig. 4. To demonstrate, since a cavity is modeled as a parallel RLC tank, and the stub behaves like another parallel capacitor, the circuit model of each antenna would be the one presented in figure 3.4.

By calculating the input impedance of the circuit as follow,

$$Z_{in} = \frac{1}{\frac{1}{R} + \frac{1}{jL\omega} + j\left(C + C_v\right)\omega} \tag{3.3}$$

and with this knowledge that at the resonance frequency, the input impedance should be *R*,

$$Z_{in}(f_r) = R \tag{3.4}$$

Equation (3.5) must be solved.

$$\frac{1}{jL\omega_0} + j\left(C + C_v\right)\omega_0 = 0 \tag{3.5}$$

By doing so, the resonance frequency is calculated.

$$\omega_0 = \frac{1}{\sqrt{L(C + C_v)}}. \tag{3.6}$$

Referring to Equation (3.6), due to the fact that *L* and *C* are constant values, the only parameter which can change the resonance frequency is C_v.

The parallel capacitor, C_v, shown in figure 3.4. includes one tunable capacitor related to the varactor diode (SMV 1247) and a fixed capacitor regarding the short-circuit stub, both series to each other. Therefore, only the value of diode determines the resonance frequency. It should also be noted that the inductor and resistor depicted in the figure are for the bias circuit of the diode; *R*=10 k-ohm is for limiting the current from DC source, and *L*=47 nH is used as an RF choke.

To go deeply inside the equivalent circuit, the value of each component is calculated using Advanced Design System (ADS) software. More specifically, the complete circuit model of the proposed tunable MIMO antenna is depicted in ADS, and then by considering three different resonance frequencies, the values of the components of the circuit are calculated. This is performed by importing the S-parameters of the antenna achieved from a full wave simulation, as an S2P file, to ADS simulator, and by tuning the value of C_v, the resonant frequencies regarding the full wave simulation and ADS are corresponded to each other. Figure 3.5 expresses the complete circuit model taking into account the mutual coupling among the ports (M_1 and M_2) and impedance transformers (X_1 and X_2). The impedance transformers are due to the transition from microstrip line to the SIW cavity.

Getting back to figure 3.5, once the operating frequency alters, all the components remain unchanged except C_v, which consists of a variable capacitance related to the varactor diode and a fixed one concerning the stub at each resonance frequency. In the following section, from full wave simulations, the value of the capacitance of varactor diodes will be determined, and one can readily calculate the capacitance of stub at each operating frequency by considering the available equation for two series capacitors.

Among the parenthesis, for further completeness, it should be pointed out that the proposed MIMO structure can easily be changed to a dual-band antenna if each part of the antenna is tuned independently. In fact, by independently controlling the varactor diodes of the MIMO structure, a

dual-band antennas with the possibility of altering the bands is designed. Such a characteristic is unique in its kind.

3.2.2 Experimental results for MIMO antenna

A prototype of the proposed MIMO antenna was fabricated on Rogers 5880 with the thickness of 30 mils and a dielectric constant of 2.2, figure 3.6. The bias pads shown in Fig. 4 are connected to the lines on backside of the structure assigned for applying the necessary DC voltages, Fig. 6b. The negative part of the power supply is connected to the ground of the antenna.

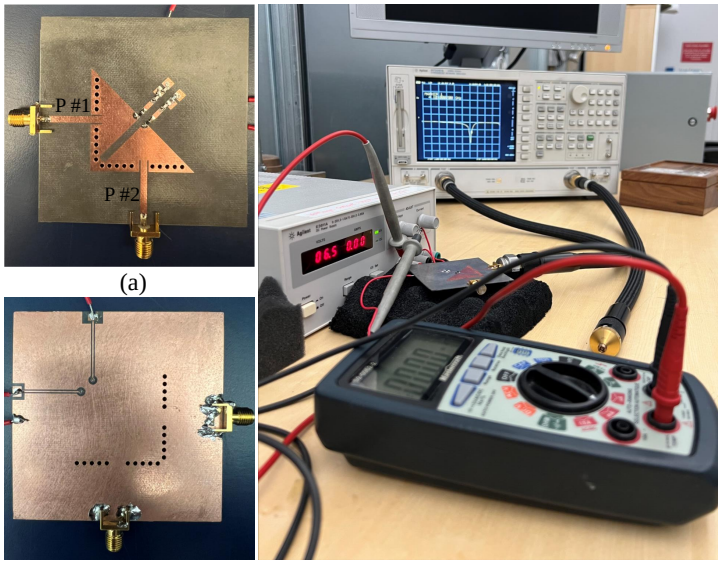

FIGURE 3.6 : (a) Front side, (b) backside of the fabricated tunabe MIMO antenna, and (c) the measurement setup.

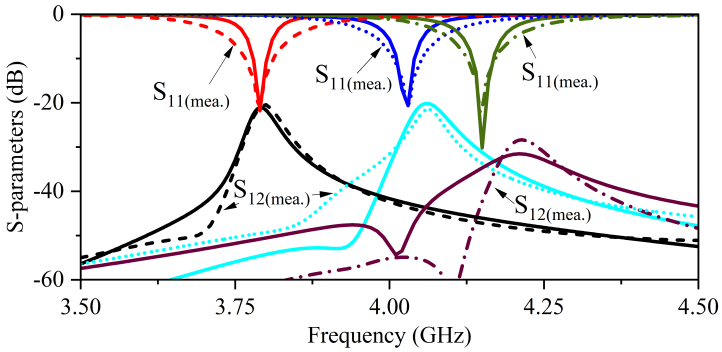

FIGURE 3.7 : The simulated and measured reflection coefficients associated with Port 1, as well as the mutual coupling among them.

Figure 3.7 shows the reflection coefficients for Port 1 and mutual coupling between the ports with different capacitance for diodes. As evident, increasing the capacitive values, the resonance

frequency shifts toward the lower bands. A good agreement between the simulated results achieved from HFSS software and measured ones can be observed from the figure. Furthermore, due to the fact that the structure is symmetric, reflection coefficients for Port 1 and 2 are almost the same, and because of this, we did not present S_{22} in figure 3.7. It is also worth expressing that other resonance frequencies between the depicted ones in Fig. 7 can be obtained. However, for the sake of making the plots more clear and not busy, we just considered three stages of voltages.

The required DC voltages for diodes are presented in TABLE 3.1. Once the value of capacitance is set to be 0.64 pF, the resonance frequency is at 4.15 GHz, and the mutual coupling between the ports is less than -30 dB. When the DC voltage decreases to 3 V, the operating frequency of MIMO antenna becomes 4 GHz and the isolation between the ports is higher than 25 dB. Finally, by putting the DC voltage level at 1 V, the resonance frequency comes to 3.8 GHz. The mutual coupling in this situation is below -20 dB.

According to the mutual coupling between the ports, it is seen from figure 3.7 that in all scenarios, it is below -20 dB, which is sufficient for most of the IoT applications. To further illustrate the MIMO performance of the proposed antenna element and well present the obtained high isolation between the input ports, figure 3.8 should be taken into account. As obvious, there is a minimum of current leakage from Port 1 to 2 and vice versa, confirming the achievement of defined condition for MIMO performance. The mutual coupling among the ports is due to the introduction of slot in the half-mode cavity. Width of the slot has an important role in controlling the isolation level as it is in the place that normal magnetic field is equal to zero. In fact, this place is considered as a magnetic wall and by making the slot bigger and bigger, the leakage from one port to the other one decreases.

Another important characteristic of a MIMO structure is related to ECC [1], given by Equation (3.7). By evaluating the simulated values for this parameter, it has been concluded that at the mentioned operating frequencies in figure 3.7, all well satisfy the required value : 0.0045, 0.00279, 0.00095 for 3.8, 4, and 4.15 GHz, respectively.

$$\rho_e(\mathrm{ECC}) = \frac{\left| \iint\limits_{4\pi} [E_1(\theta,\phi).E_2(\theta,\phi)] d\Omega) \right|^2}{\iint\limits_{4\pi} |E_1(\theta,\phi)|^2 d\Omega \iint\limits_{4\pi} |E_2(\theta,\phi)|^2 d\Omega}. \tag{3.7}$$

In Equation (3.7), $E_i(\theta,\phi)$ is the electric field of antenna *i*, and $d\Omega$ expresses the spatial angle. As it comes to the radiation patterns of the proposed MIMO antenna, the plots presented in figure 3.9 provide useful information. The normalized E-plane and H-plane patterns for Port 1 and Port 2 at different frequencies are almost the same. Therefore, according to the characteristics of the proposed MIMO antenna, it is concluded that the structure is a good candidate for introducing the MIMO-UCA concept for coming up with simultaneous OAM-generating antenna structure having only one layer.

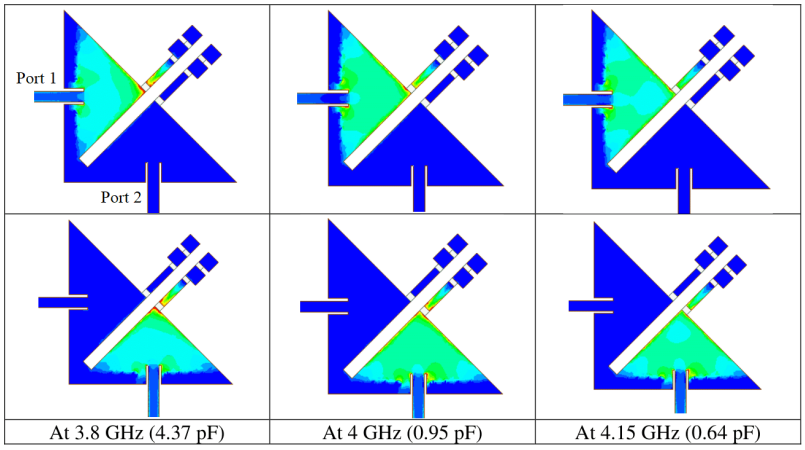

FIGURE 3.8 : The current distribution at the resonance frequencies of 3.8, 4, and 4.15 GHz.

TABLE 3.1 : INFORMATION REGARDING THE VALUES OF VOLTAGES AND CAPACITANCES AT THE DESIRED RESONANCE FREQUENCIES.

Voltage	8 V	3 V	1 V
Capacitance value	0.64 pF	0.95 pF	4.37 pF
Resonance freq.	4.15 GHz	4 GHz	3.8 GHz
ECC	0.00095	0.00279	0.0045

ECC=Envelope Correlation Coefficient.

3.3 Frequency-Adjustable MIMO-UCA Antenna Design

As a proof of concept, having designed the tunable MIMO antenna element, it is time to utilize it for designing MIMO-UCA to generate co-divergent simultaneous OAM modes. To that end, a 2×2 array is considered. The distance between the antenna elements is selected to be $0.7\lambda_0$ at 4.2 GHz. In the next step, two antenna feeds should be designed to excite each 2×2 sub-array in a way that one generates OAM mode -1 and the other creates mode +1. It should also be noted that the required condition for exciting the mentioned OAM modes is that the antennas are fed with [0°, 90°, 180°, 270°] phase gradients in clockwise and counterclockwise states. The configuration of the proposed feeding network is depicted in figure 3.10.

To demonstrate, consider the first signal is applied to Port 1 (P $\#1$). Then, it is divided into two parts in the first T-junction, and owing to the fact that one arm of the T-junction is longer than the other one, 180° phase difference exists between the divided signals when they arrive at their corresponding T-junctions. Later, once again, the signals are divided into two parts and flow toward P $\#2$ to P $\#5$. Because of longer transmission lines connected to Port 3 and Port 5, they obtain -90° phase difference, and consequently [0°, 90°, 180°, 270°] phase gradients are achieved in clockwise direction. The same scenario happens as Port 6 is exited. However, this time, [0°, 90°, 180°, 270°] are achieved in counterclockwise direction.

As obvious, the inputs of T-junctions consist of wider transmission lines. This is for impedance matching purpose. In fact, since in each T-junction, there are two parallel arms with 50-ohm cha-

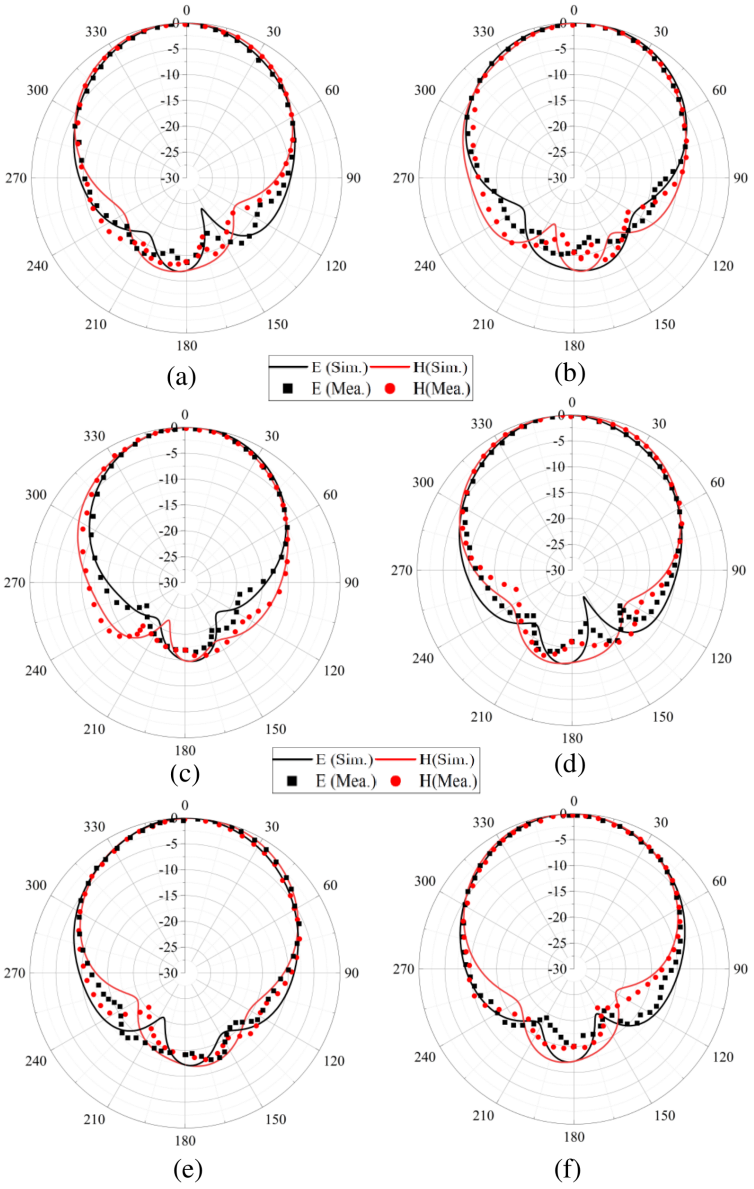

FIGURE 3.9 : The normalized E-plane and H-plane radiation patterns associated with Port 1 at (a) 3.8 GHz, (c) 4 GHz, (e) 4.15 GHz, and with Port 2 at (b) 3.8 GHz, (d) 4 GHz, (f) 4.15 GHz.

racteristic impedances, the equal impedance becomes 25-ohm. Therefore, to match 50-ohms to 25-ohms, 35.35-ohm lines are taken into account [78].

Reflection coefficients, the output amplitudes and phase responses associated with each input port of the feed networks (Port 1 and Port 6), are presented in figure 3.11 and 3.12. From figure 3.11, beside the fact that the reflection coefficient (S_{11}) is below -10 dB on the whole band, it is seen that the amplitude of output signals are almost the same at 3.8 GHz. The imbalance between them increases by 4 GHz, and then they become converged going to the higher frequencies. The same scenario happens for outputs as Port 6 is excited. Over the presented impedance bandwidth (3.5 to 4.5 GHz), the maximum imbalance is around 2 dB, and this does not affect the

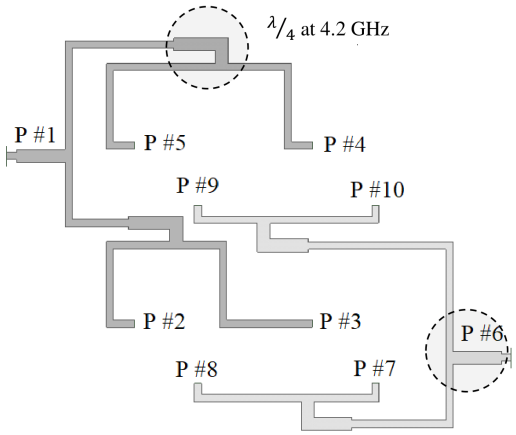

FIGURE 3.10 : The configuration of antenna feeds for generating OAM modes (P=Port).

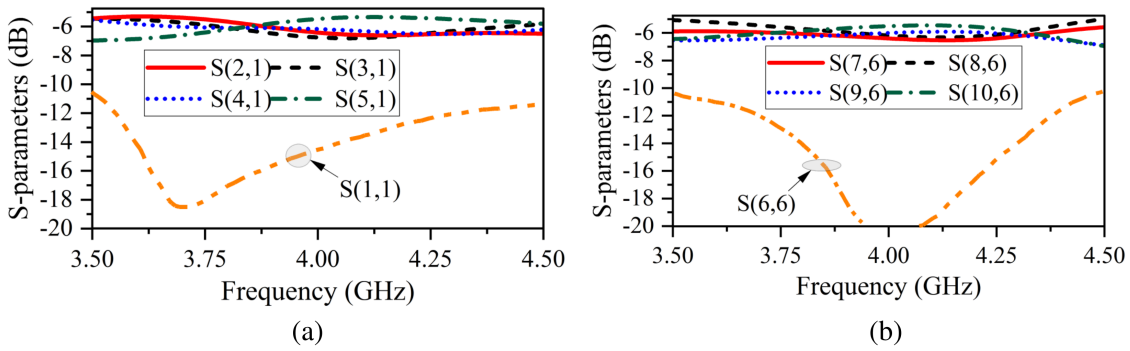

FIGURE 3.11 : Amplitude response and reflection coefficient when (a) Port 1 is excited, and (b) Port 6 is fed.

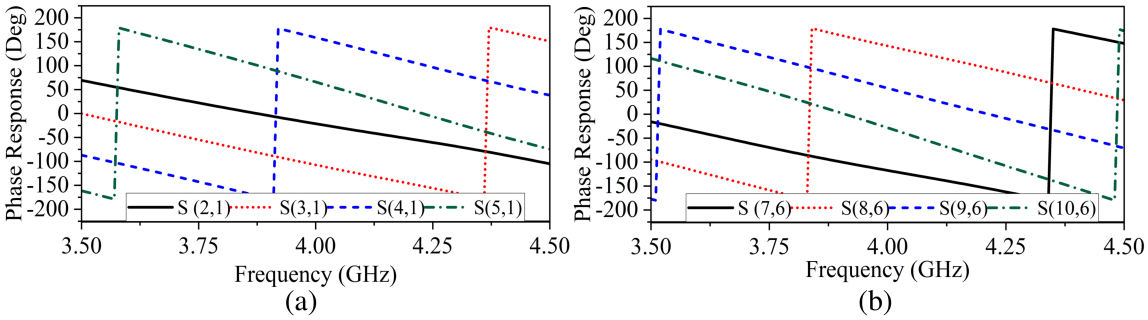

FIGURE 3.12 : Phase response when (a) Port 1 is excited, and (b) Port 6 is fed.

generation of OAM modes. This assertion will be observed once the radiation patterns and phase fronts of the OAM modes are explained. According to figure 3.12, the phase difference between two consequent output ports is almost 90° in a clockwise and counterclockwise states over 3.8 to 4.2 GHz. The maximum phase imbalance from 90° is around 10° over the mentioned frequency range, guaranteeing the generation of desired OAM modes.

With the available information concerning the amplitude and phase responses of the antenna feeds, and having the tunable MIMO structures in hand, it is possible to generate dual-mode OAM-carrying waves at different resonance frequencies. The configuration of the prototype of the propo-

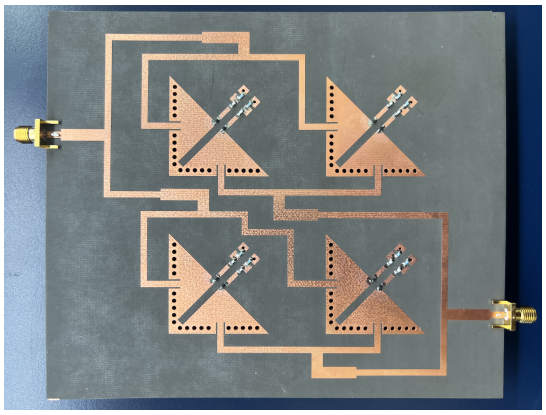

FIGURE 3.13 : The prototype of the proposed frequency adjustable MIMO-UCA OAM antennas array.

TABLE 3.2 : THE SIMULATED AND MEASURED GAINS RELATED TO OAM MODES ALONGSIDE THE RADIATION EFFICIENCIES.

Mode Number	Simulated gain (dBi)	Measured gain (dBi)	Efficiency
Mode +1 (f=3.8 GHz)	8.3	7.8	0.78
Mode -1 (f=3.8 GHz)	8.5	8	0.8
Mode +1 (f=4 GHz)	8.4	8	0.78
Mode -1 (f=4 GHz)	7.8	7.4	0.72
Mode +1 (f=4.15 GHz)	8	7.6	0.77
Mode -1 (f=4.15 GHz)	8.2	7.9	0.78

sed antenna system in rendered in figure 3.13. The same substrate utilized for fabrication of MIMO elements (Rogers 5880 with the thickness of 30 mils and a dielectric constant of 2.2) has also been considered for the array one.

3.3.1 Experimental results for frequency-adjustable MIMO-UCA

First of all, the matching of the array at each operating frequency should be verified. Also, the mutual coupling between the input ports must be taken into consideration. To that end, the dispersion parameters of the structure have been measured by using a Network Analyzer, and the achieved results have been compared with those obtained from simulations. Figure 3.14 depicts the outcome of the comparisons. Due to the fact that the reflection coefficient associated with Port 6 is almost the same with Port 1, for making the figure well readable, we avoided presenting the S_{66} result. It is worth expressing that the similarity of reflection coefficients stem from the MIMO antenna elements which are composed of 2 similar radiators.

Referring to figure 3.14, in all the scenarios, the reflection coefficients are below -20 dB, and the isolation between the ports is better than 20 dB. Concerning the applied DC voltages, the same voltage levels presented in TABLE 3.2 are selected to feed the varactor diodes of arrays, and as evident, the resonance frequencies did not confront any big change compared with those related to the single antenna element.

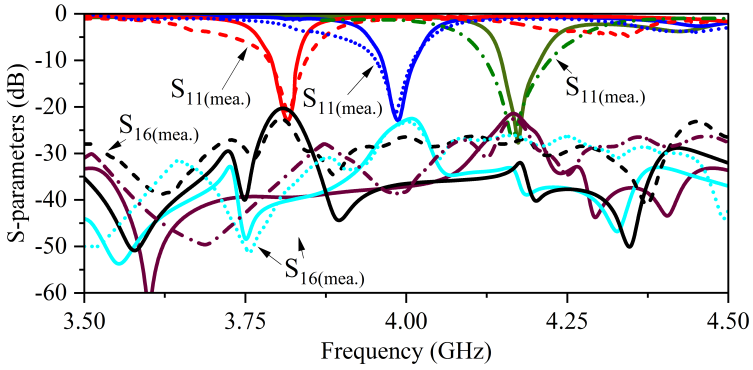

FIGURE 3.14 : Simulated and measured reflection coefficients associated with Port 1, and the mutual coupling among the input ports of the OAM array.

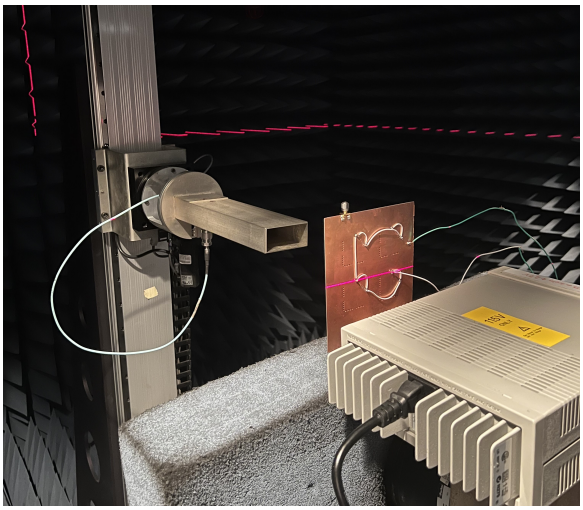

FIGURE 3.15 : The proposed setup for measuring the near filed characteristics of the OAM array (wires have connected the DC-pads together and have no effect on the radiation pattern due to being behind the structure).

The paramount characteristic of OAM carrying waves is to introduce helical phase fronts with radiation patterns having a null in the center. To measure the mentioned features, a setup shown in figure 3.15 is considered. To explain, the antenna is put in 32 cm away from the feed antenna (waveguide). A square planar area with dimensions of 25×25 cm^2 is scanned by the feed, and consequently the phase and amplitude distribution are achieved on the planar area. The similar measurement process is carried out for both of the ports at three different resonance frequencies corresponding to those presented in figure 3.14. All the results are rendered in figure 3.16 and 3.4. According to figure 3.16, the minimum obtained electric field amplitude is in the center of the scanned square area, validating the existence of null in the broadside of the radiation patterns. Regarding figure 3.17, the phase of electric filed alters from -180 to 180 degree in counterclockwise and clockwise directions, showing the generation of OAM mode +1 and -1, respectively. Moreover, there is a little bit impurity in the helical phase front at the frequency of 3.8 GHz. This has its root in the imbalance of phase differences between the array elements. However, this impurity will not bring about any big issue in the IoT applications.

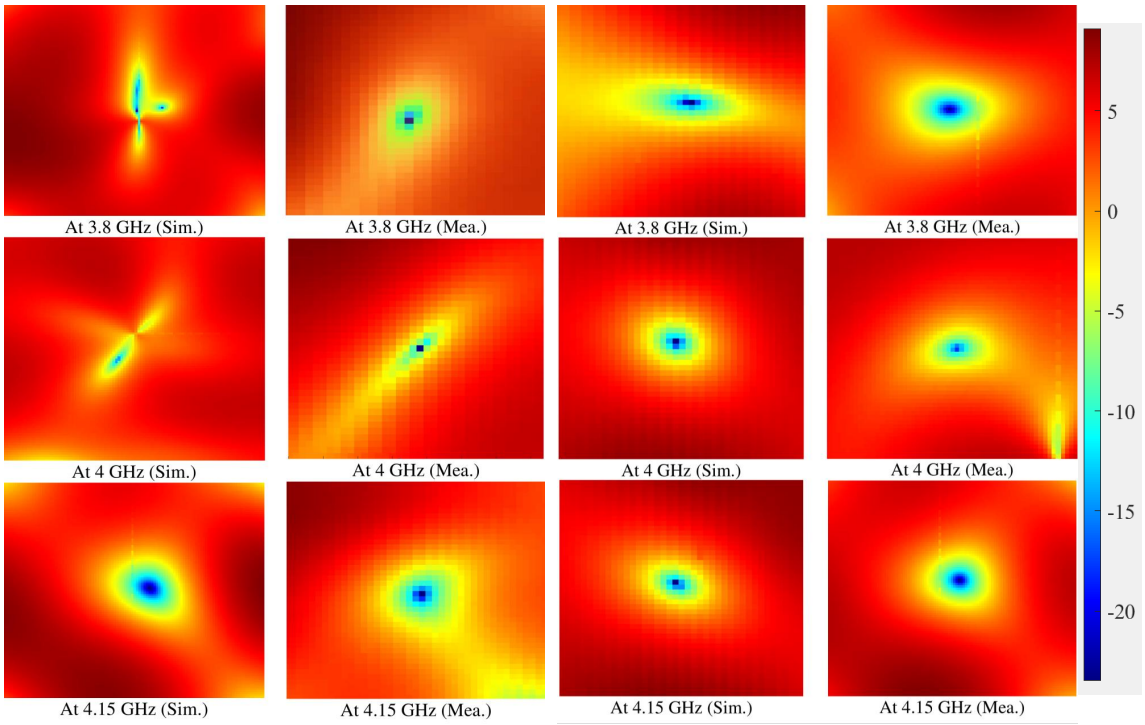

FIGURE 3.16 : The electric field amplitude at different frequencies for OAM (a) mode +1 associated with Port 6, and (b) mode -1 related to Port 1.

To go deeply inside the purity level of OAM modes at different frequencies, Equation (3.8) is used to calculate this value (mode purity).

$$S_n = \frac{P_{l=n}}{\sum_{l=-\infty}^{l=+\infty} P_l}, \tag{3.8}$$

where P_l presents the amount of average energy produced by each OAM mode, which is captured on the perpendicular observation plane. This value can be calculated as follow,

$$P_l = \int_0^{+\infty} |A_l(r,z)|^2 r dr. \tag{3.9}$$

and,

$$A_l(r,z) = \frac{1}{2\pi} \int_0^{2\pi} E(r,\varphi,\mathrm{z}) e^{-il\varphi} d\varphi, \tag{3.10}$$

In which A_l indicates the amplitude of each individual mode.

Taking into account the above mentioned equations, and by defining a circle with the radius of r=4λ_0, the mode purities are calculated inside the circle and presented in figure 3.18. It is seen

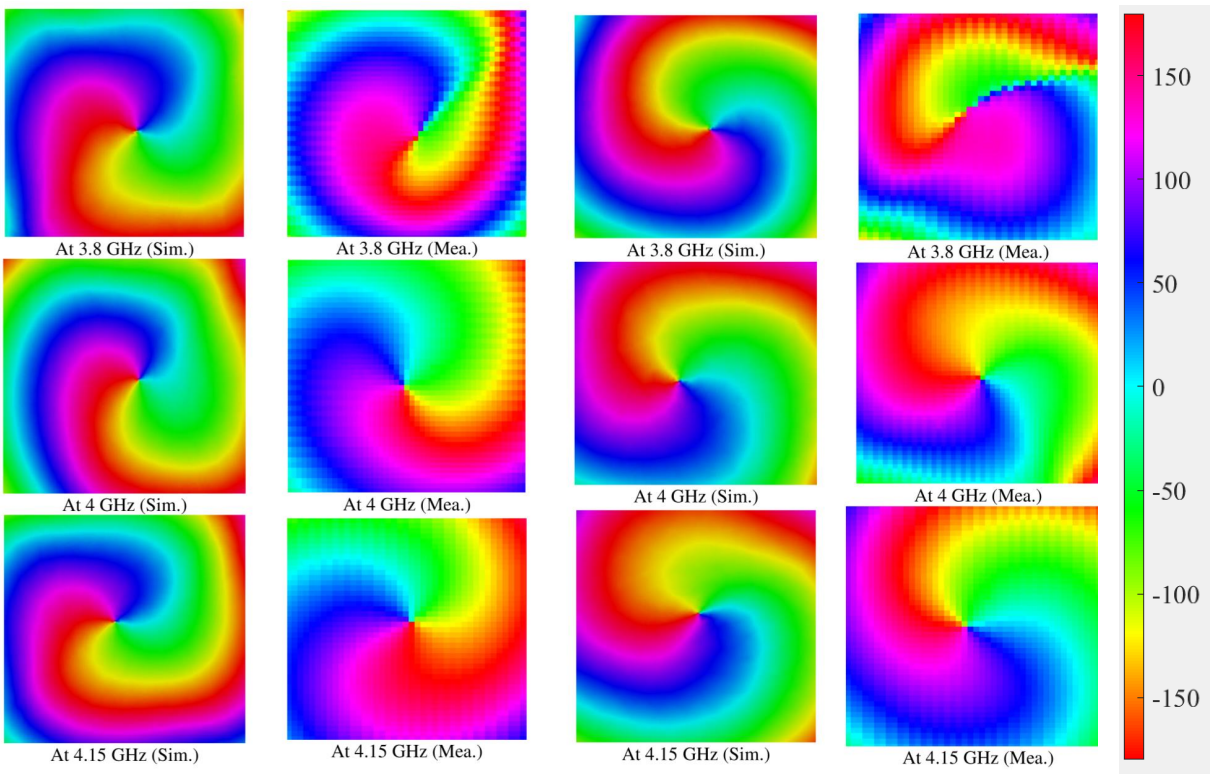

FIGURE 3.17 : The phase front at different frequencies for OAM (a) mode +1 associated with Port 6, and (b) mode -1 related to Port 1.

that at 4 and 4.15 GHz, the highest purities are achieved and this can be verified getting back to figure 3.17. At 3.8 GHz there is a little drop in mode purity. However, the purity around 0.7 is considered as a high value in comparison with those obtained for structures in literature.

To better evaluate the radiation patterns associated with the OAM antennas, the normalized beams at E and H-planes are presented in figure 3.19. In all the cases, at broadside, there exists a null with a depth of minimum 15 dB less than the maximum value of the beam which is zero due to the normalization. Furthermore, it is obvious that the peak gains, more or less, are at θ=+30 and -30. Therefore, for both OAM modes, we have the same divergent angle. However, for concentrically embedded or stacked UCAs, such a characteristic can barely be achieved because the radii of UCAs cannot be the same. In our structure the radii of UCAs are the same owing to MIMO-UCA technique. It should also be mentioned that being co-divergent is essential for OAM beams as a result of the fact that in the receiving end, the maximum power should be obtained from incident OAM modes at the same position. The value of the maximum gains is listed in TABLE 3.2 as well.

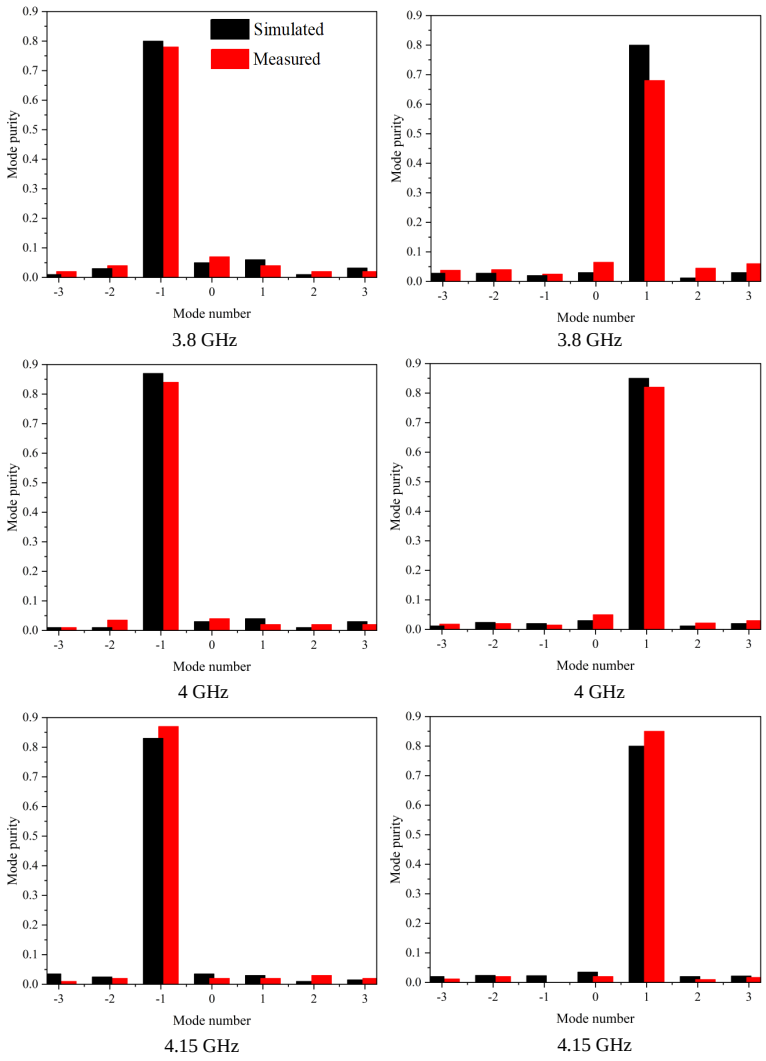

FIGURE 3.18 : The mode purity for OAM (a) mode -1, and (b) mode +1.

3.4 Discussion

As asserted, the proposed structure is capable of generating co-divergent simultaneous OAM modes by taking advantage of MIMO-UCA concept. To further explore this characteristic, a setup intended to transmit and receive two different signals at the same time and frequency is taken into consideration, see figure 3.20. More specifically, two copies of the proposed OAM array are considered to create a wireless channel for data sharing. Thus, one of the fabricated antennas is held in the transmitter side and the other one is selected to serve as a receiver. Using the signal generators and spectrum analyzers, at the operating frequencies, a communication link is achieved between the antennas. As our antennas are able to generate OAM modes, it is possible to send two signals each using one input port of the array and detect them using spectrum analyzers. It should be pointed out that, however, the frequency of signals is the same and they are transmitted

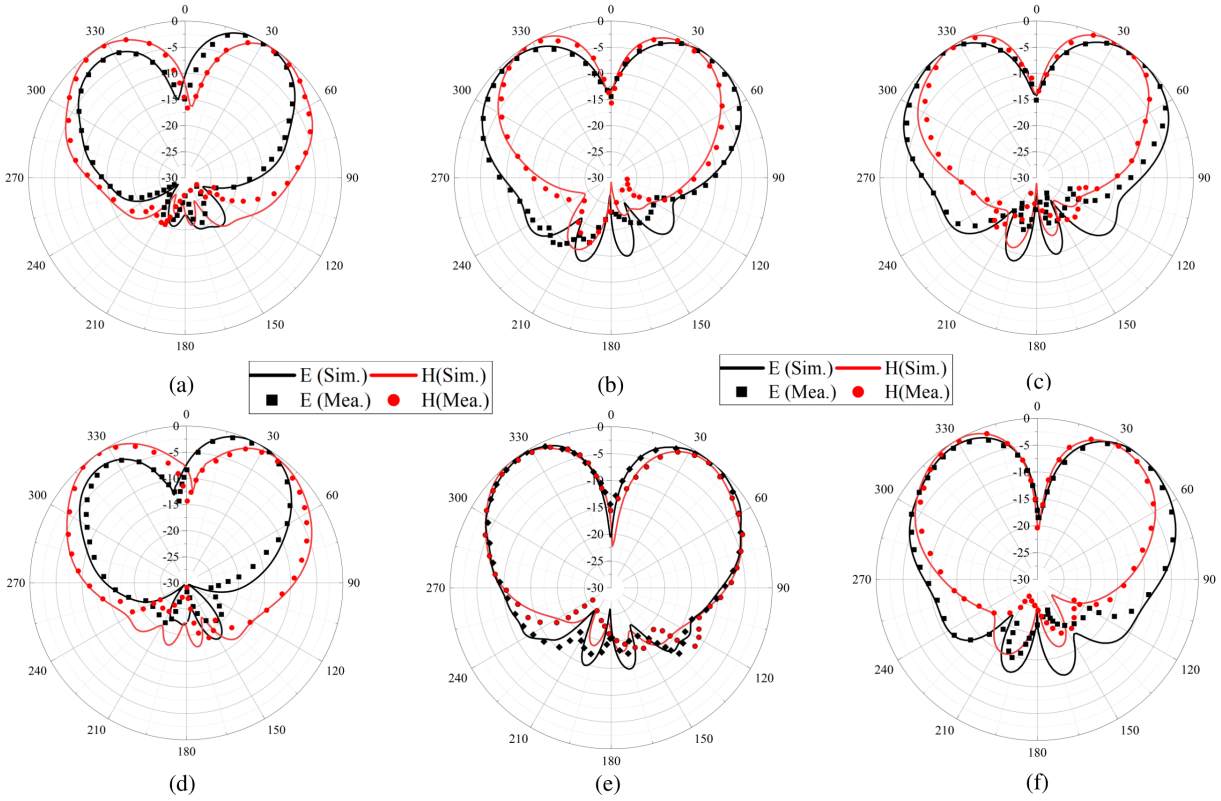

FIGURE 3.19 : 2D radiation patterns for OAM mode -1 at (a) 3.8 GHz, (b) 4 GHz, (c) 4.15 GHz, and OAM mode +1 at (d) 3.8 GHz, (e) 4 GHz, (cf) 4.15 GHz (E=E-plane, and H=H-plane).

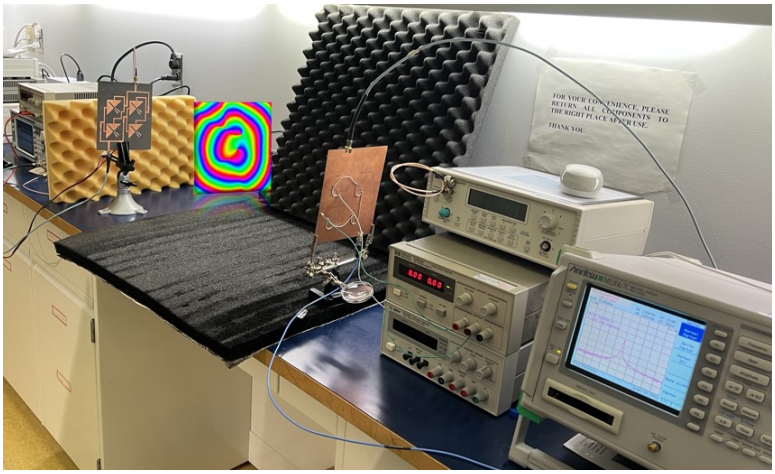

FIGURE 3.20 : The proposed setup for a communication link using the OAM antenna arrays.

at the same time, they do not get mixed together due to the orthogonality of the radiation patterns. Figure 3.21, expresses the detected amplitude values using the spectrum analyzer versus the various distances; almost the same powers are detected by spectrum analyzer for both OAM modes, showing them having co-divergent beams. It is worth pointing out that the amplitude of transmitted signal is set to be 10 dBm.

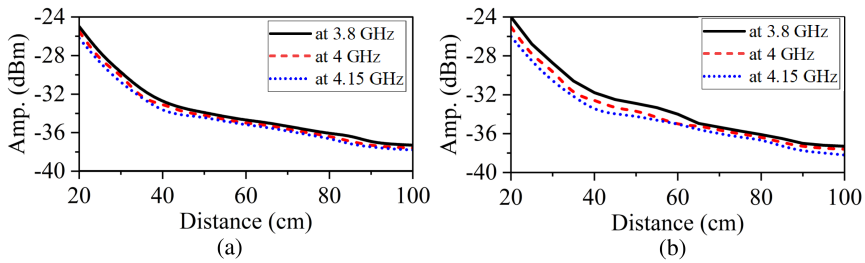

FIGURE 3.21 : The received amplitude values at different frequencies and distances for (a) OAM mode +1, and (b) OAM mode -1.

Upon validating the generation of simultaneous OAM modes with the proposed MIMO-UCA array, it is concluded that in the IoT applications, more information will be transmitted at a time, resulting in high-speed communications. Again, it is worth mentioning that the existing UCA-based OAM antennas can reach the simultaneous mode propagation by stacking different UCAs or arranging them in a concentrically embedded configuration. Both of the techniques bring about multi-layer structures (costly). Further, controlling the mutual coupling between the separate UCAs is another issue. Moreover, due to different radii of UCAs, the main beam directions (divergent angles) are not the same for OAM modes. Our MIMO-UCA method solves these limitations in an efficient way.

However, by far, there is no report regarding the frequency-tunable OAM generating antennas as well as MIMO-UCA technique, we compared the proposed antenna structure with some recently published works in terms of important characteristics. In fact, the OAM structures with the capability of generating modes +1 and -1 are taken into account for comparison. TABLE 3.3 shows the comparison table. As evident, the suggested OAM array is the first structure which has taken advantage of MIMO elements for OAM generation. Above all, the proposed antenna system presents frequency tunability for the first time as well, thus paving the way for secure communications in IoT infrastructures. Regarding the other features, the higher peak gain is obtained owing to different type of antenna elements. More specifically, in most of the existing works, the simple rectangular or circular patch antennas are chosen as the elements of 2×2 array, leading to a lower peak gain. However, in this work, SIW cavity antennas are utilized for OAM generations. Beside this, since the number of varactor diodes in our structure is less than the presented references, such high gains are achieved.

Talking about the number of layers, size and design complexity, the introduced frequency-adjustable OAM generating antenna array owns minimum number of layers (one layer), the similar size compared with the mentioned references, and a low design complexity. It is worth notifying the reader that when the proposed structure is labeled as a low complex, in fact, it refers to the utilization of MIMO-UCA technique, which brings about a single-layer structure with simultaneous OAM mode generation capability. In the existing works, to obtain this feature, a multi-layer structure with a lot of attention required to be paid for mutual coupling reduction between the different UCAs is essential. It should also be noted that all the dimensions are calculated based on the guided

TABLE 3.3 : THE COMPARISON BETWEEN THE PROPOSED WORK AND SOME RECENTLY PUBLISHED ONES

Ref.	[40]	[70]	[47]	[78]	This work
Freq (GHz)	2.5	2.5	3	2.45	3.8–4.2
MIMO-based?	No	No	No	No	Yes
Freq. Adjustable?	No	No	No	No	Yes
Number of layers	3	3	1	1	1
Number of PIN diodes	16	20	50	8	0
Number of varactor diodes	0	0	0	0	8
Modes	±1	±1	0, ±1	±1	±1
Gain (dBi)	5.3/5.3	5.2/5.2	N/A	7.1/7	7.8–8.5
Size ($\lambda_g \times \lambda_g$)	2.38×2.38	2.6×2.6	N/A	1.7×2	2.4×2.8
Design complexity	high	high	high	low	low

wavelength. In [40], the size has been reported considering the free space wavelength, and it is changed to guided one.

As the last point, the number of generated OAM modes should be discussed. According to the fact that the number of elements utilized in the UCA or in our case MIMO-UCA determines the number of possible OAM modes, in all the structures owing four elements, the maximum number of generated OAM modes can be -1 and +1. Therefore, it goes without saying that to increase the number of modes, the number of antenna elements in the array should be increased. This will need an extended power dividers (feeding networks) as well.

3.5 Acknowledgment

This work has been funded by Fonds de Recherche du Québec Nature et technologies (FRQNT) under the file number of 333948.

3.6 Conclusion

In this chapter, a frequency-tunable OAM generating antenna array has been introduced to provide interference suppression capability as well as high-data-rate communication in IoT applications. The elements of the proposed array consist of MIMO antennas to present MIMO-UCA concept for coming up with a single-layer co-divergent simultaneous OAM-generating antenna. Concerning the design process, since each MIMO element has two input ports, two 2×2 sub-arrays provide the primary condition for exciting OAM-carrying waves. In the next step, two feeding networks have been designed to feed the sub-arrays with [0°, 90°, 180°, 270°] phase gradients in clockwise and counterclockwise states, thus satisfying the necessary condition for OAM mode generation. The tunability of the operating frequencies come from the tunability of MIMO antennas. As each antenna has stubs consisting of varactor diodes, the equivalent capacitance of the circuit

model of the antenna alters, and consequently the resonance frequency changes. In addition, the suggested structure has the highest gain among 2×2 UCAs due to the utilization of quarter-mode SIW cavities as the radiating elements .With all this in mind, it can be concluded that the suggested MIMO-UCA array with the capability of frequency-tunability introduces several unique characteristics such as interference suppression, co-divergent simultaneous OAM propagation, and low cost fabrication for IoT applications.

4 FREQUENCY AND MODE-TUNABLE OAM ANTENNA WITH POLARIZATION SELECTIVITY

This chapter contains materials extracted from the following publications. In this work, besides achieving the required characteristics in terms of gain, BW, and mode purity, we obtained not only mode tunability similar to the initial design but also the capability to adjust the operating frequency. Additionally, polarization selectivity was successfully achieved.

Reconfigurable OAM Antenna With Flexibility on Mode Numbers, Polarization and Frequency

Dual-Polarized OAM Antenna with Frequency and Mode Agility for Intelligent OAM Communications

Authors : Hassan Naseri, Peyman PourMohammadi, Noureddine Melouki, Amjad Iqbal, and Tayeb Denidni

Contribution of Authors : I am the main contributor to this work, under the supervision of Prof. Tayeb Denidni

4.1 Introduction

Orbital Angular Momentum (OAM) antennas have shown a great potential to provide the upcoming wireless systems a degree of freedom for achieving high data-rate and better performance [95, 96]. This unprecedented characteristic has its root in OAM antennas being able to propagate multiple orthogonal beams at the same time and frequency [58, 97]. In fact, from a shared aperture, several orthogonal beams can be excited, and as these beams do not combine while propagating (due to orthogonality), each one can carry one stream of data independently. Thus, for communication systems, larger channel capacity [98], and for radar and imaging systems, high resolution results are obtained [4].

To provide smart OAM communications such as intelligent microwave imaging, reconfigurable antennas are in demand. The tunability can be in terms of OAM mode number, frequency and polarization. Among the existing works, recently some mode-tunable OAM structures have been introduced. An array with the capability of CP and OAM mode reconfigurability is introduced in [40, 42, 43]. In case, polarization of the OAM antenna is not important, contributions in [39, 41, 44, 47, 62, 71–73] should be considered, which has only control on mode number. Very recently, authors in [78] have introduced a low-profile reconfigurable antenna system for OAM generation with 1-bit phase shifters, solving the problems associated with PIN diodes in existing structures.

In this chapter, an advanced OAM antenna is introduced that has agility on mode numbers, polarization of each mode and operating frequency. The mentioned three characteristics are necessary as smart OAM communication systems such as intelligent imaging devices are in demand. The technique of utilizing MIMO antennas with ±45° polarized elements in a 2×2 UCA paves the way for controlling the polarization of OAM modes. To propagate reconfigurable OAM modes of +1 and -1, two independent tunable feeding networks including 1-bit phase shifters excite the elements of UCA as well. It should be mentioned that frequency-adjustability has its roots in the frequency-tunability of MIMO antennas. Upon fabricating the prototype of the proposed structure, a good agreement between simulated results and measured ones have been observed. The novelty of this work is the ability of the proposed MIMO-UCA technique in providing frequency-adjustable mode-tunable OAM modes. This feature is achieved for the first time and paves the way for more-secure Internet of Thing (IoT) communication and high-precise microwave imaging devices by having the ability of frequency-tunability. Moreover, the proposed work can be altered in a way to work at two different frequency bands with mode-tunability which is unique in its turn.

4.2 Tunable Dual-Polarized MIMO Antenna Design

4.2.1 Process of designing

Prior to starting the explanation regarding the design process of the dual-polarized frequency-tunable MIMO antenna, one phenomenon about the Substrate Integrated Waveguide (SIW) cavities should be analyzed. In case there exists a square SIW cavity with the fundamental mode of TE_{110}, cutting the cavity into two halves preserves the fundamental mode as well as resonance frequency. Each half is called a half-mode cavity. Another division of a half-mode cavity results in a quarter-mode cavity without any big change in the fundamental mode and resonance frequency [94, 99].

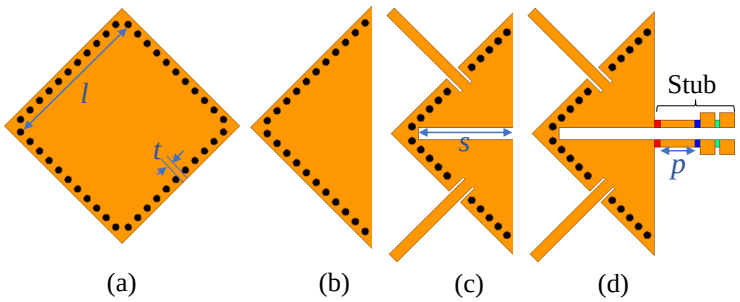

FIGURE 4.1 : (a) Full-mode SIW cavity, (b) half-mode cavity, (c) the proposed non-adjustable MIMO antenna, and (d) frequency variable MIMO antenna. (*l*=27mm, *S*=19.25mm, *p*=9mm, *t*=1.5mm)

To serve our objective, we go deeper into exploring this particular characteristic. Our aim is to introduce a dual-polarized MIMO antenna that can be tuned in frequency within a half-mode cavity. Initially, we design a full-mode SIW cavity, resonating at 4.2 GHz, as depicted in figure 4.1a.

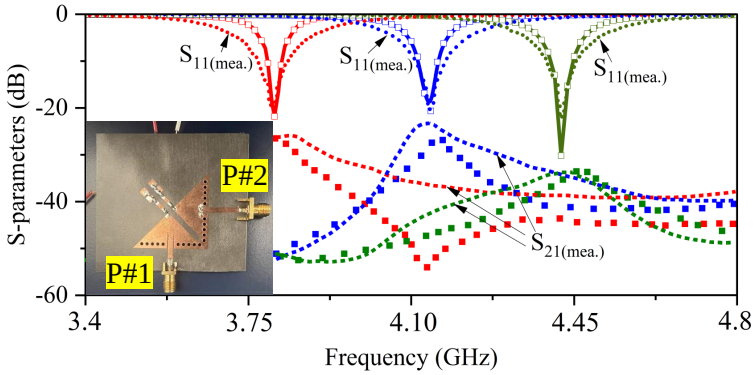

FIGURE 4.2 : The reflection coefficients of Port 1, both simulated and measured, and their mutual coupling.

Next, we split the designed full-mode cavity into two sections, as shown in figure 4.1b, selecting one part for the antenna design. A slot is used to divide the existing half-mode cavity, creating two separate sections, each allocated for an antenna with ±45° polarization. Importantly, this division has a minimal effect on the resonance frequency, as illustrated in figure 4.1c. Finally, to facilitate adjustments in the resonance frequencies, we incorporate open-circuit stubs linked with varactor diodes, as seen in figure 4.1d. The varactor diodes (specifically SMV 2020) embedded within the stubs, highlighted by red spots in figure 4.1d, are responsible for modifying the operating frequencies, given that the cavity itself is simulated as a parallel RLC tank. Additionally, it is important to emphasize that the inductor and resistor highlighted in figure 4.1d (represented by blue and green spots, respectively) serve as components of the bias circuit for the diode. The resistor (R = 10 kΩ) acts to restrict the current from the DC source, while the inductor (L = 47 nH) is utilized as an RF choke.

4.2.2 The MIMO antenna's experimental findings

A model of the suggested MIMO antenna was constructed using Rogers 5880 with a thickness of 30 mils and a dielectric constant of 2.2. To power the varactor diodes, the required DC voltage is supplied through wires linked to the bias pads on the rear of the structure.

Figure 4.2 illustrates the constructed model and displays the reflection coefficients for Port 1, as well as the mutual coupling between the ports at varying capacitance levels for the diodes. As the capacitance values increase, the resonance frequency shifts towards the lower bands. Additionally, owing to the structure's symmetry, the reflection coefficients for Port 1 and Port 2 are nearly identical, leading to the exclusion of S_{22} in figure 4.2. The necessary DC voltages for the diodes are itemized in TABLE 4.1. Furthermore, the Envelope Correlation Coefficient for the MIMO antenna is computed as per the method outlined in [1].

4.3 Proposed OAM antenna design

As a demonstration of the idea, now that the adjustable dual-polarized MIMO antenna element has been designed, the next step is to use it for constructing a MIMO-UCA. This will enable the generation of co-divergent simultaneous OAM modes, incorporating both polarization and frequency adaptability.

At the first step, a 2×2 UCA, which has dual-polarized MIMO antennas as the array elements, is taken into consideration. As well-known, to excite OAM modes +1 and -1 in such a UCA, +90° and -90° phase difference should exist between the adjacent elements [100]. In fact, [0°, 90°, 180°, 270°] phase gradients should be in clockwise and anticlockwise directions. With this in mind, the antenna feed needs to be designed in a way that some transmission lines are longer than others to create necessary phase differences. In order to avoid this and facilitate the design process, and to bring about reconfigurable feeds for switching between modes +1 and -1, mirror image configuration is utilized. In this method, a pair of antennas is in opposite direction of other pair, resulting in an automatic 180° phase difference between the pairs. Therefore, the feeding network should provide [0°, 90°, 0°, 90°] and [0°, -90°, 0°, -90°] phase gradients for mode agility. It is worth expressing that such tunable phase gradients are achieved by using 1-bit phase shifters, [101], in each branch of a 1×4 power divider.

Because of the fact that each element of the UCA has two ports (MIMO antennas), there is a need for two copies of the proposed feeding network. To that end, an architecture shown in figure 4.3 is the best choice for final design.

The signal from each port is transferred to the top layer using connecting vias. The black and white spots show the position of vias as well. For instance, once P#1 is excited, at first, the power divider, which has been presented in [102], divides the signal equally. Subsequently, the signals are transferred to the top layer by connecting vias (white spots). Then, each signal itself is divided into two equal parts. In the end, the antennas labeled by white color numbers and arrows are excited once the signals pass through the 1-bit phase shifters. It should be mentioned that the direction of arrows presents the mirror image configuration. The same scenario happens when P#2 is excited. This time black-labeled elements of the MIMO are fed.

Due to the tunability of the feeding networks, [0°, 90°, 0°, 90°] and [0°, -90°, 0°, -90°] phase gradients can be achieved, resulting in OAM modes -1 and +1, respectively. According to the polarization of each mode, the orthogonality of arrows (blacks in comparison with whites) verifies

TABLE 4.1 : REQUIRED DC-VOLTAGES AND THE CORRESPONDING CAPACITANCE VALUES FOR THE SPECIFIED OPERATING FREQUENCIES.

DC-Voltage	15 V	8 V	0.5 V
Capacitance	0.41 pF	0.75 pF	2.59 pF
Operating freq.	4.4 GHz	4.1 GHz	3.8 GHz
ECC value	0.00065	0.0032	0.0058

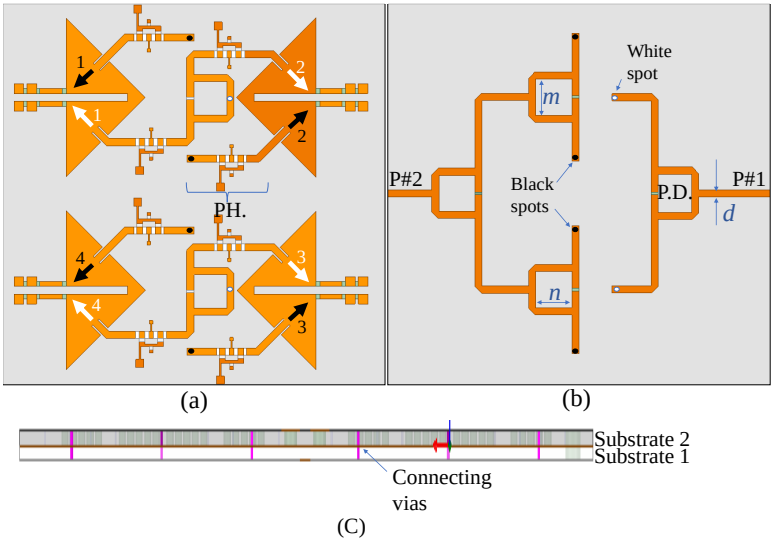

FIGURE 4.3 : Configuration of the proposed double-layer OAM antenna; (a) front view, (b) back view, and (c) side view. (P.D.=Power Divider and PH.=Phase Shifter) and (*m*=10.4mm, *n*=10.4mm, *d*=2.2mm).

±45° polarized. We call white labeled antennas +45° and black labeled one -45° polarization. All in all, four different propagations which are orthogonal to each other can be excited using the proposed OAM antenna as following :

I) OAM mode -1 with +45° polarization

II) OAM mode -1 with -45° polarization

III) OAM mode +1 with +45° polarization

IV) OAM mode +1 with -45° polarization

As obvious, simultaneous control on polarization and mode is achieved by means of the suggested structure. In fact, at the same time, it is possible to select two of the four mentioned propagations, each using one of the input ports. This feature is unique in its kind and paves th way for designing smart OAM devices; more specifically, intelligent imaging systems.

4.4 Experimental Validation

A sample of the introduced structure has been fabricated on two substrates, Rogers 5880, both with the thickness of 30 mils and dielectric constant of 2.2. Figure 4.4 shows the photo of the fabricated structure from back and front views. The ground plane of the structure is sandwiched between the substrates. There are some circular etches to avoid the connection of connecting vias to the ground plane as well. Further, there exist two holes for aligning the substrates while being glued to each other.

When it comes to measuring the reflection coefficients, it was observed that four of the states (OAM mode +1 with +45° polarization, OAM +1 with -45° polarization, OAM -1 with +45° pola-

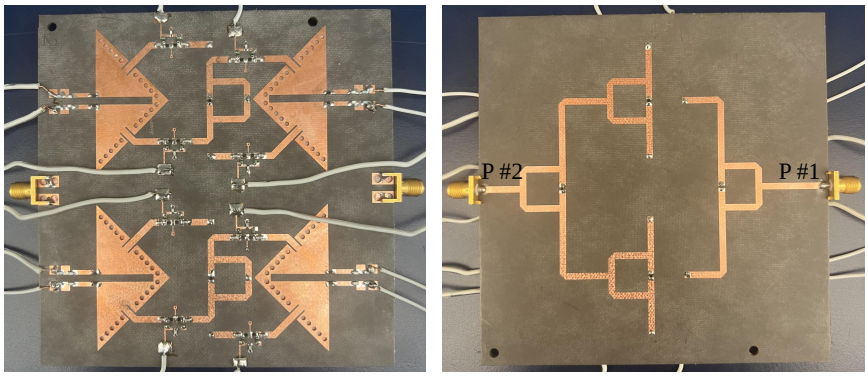

(a) (b)

FIGURE 4.4 : The model of the suggested array of MIMO-UCA OAM antennas with adjustable frequency; (a) viewed from the front, and (b) viewed from the back.

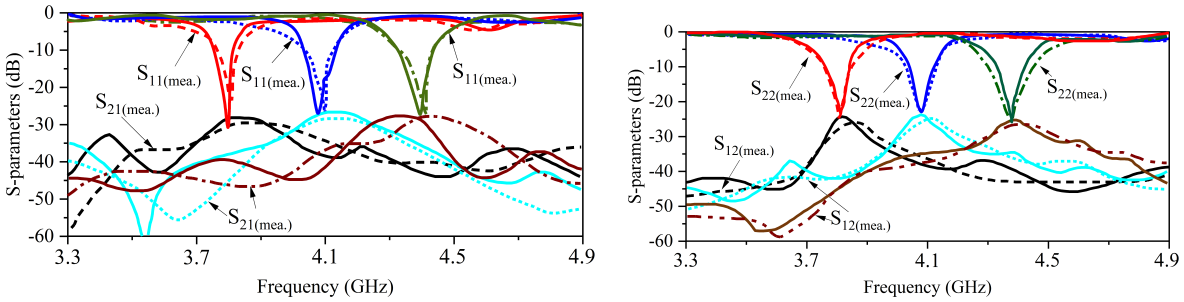

(a) **(b)**

FIGURE 4.5 : Reflection coefficients for Port 1 (mode -1 with +45° polarization condition), and (b) Port 2 (mode +1 with -45° polarization condition).

rization and OAM -1 with -45° polarization) have very similar responses at different frequencies. Therefore, in order not to repeat the results, only two of them have been presented in Figure 4.5.

The crucial feature of waves carrying OAM is the induction of helical phase fronts, resulting in radiation patterns with a void at the center. The antenna is positioned 30 cm away from the feed antenna (waveguide). A square planar region measuring 20×20 cm^2 is scanned by the feed, thereby enabling the acquisition of phase distributions across the planar area. The identical measuring procedure is conducted for four scenarios across three distinct resonance frequencies. The findings for all cases are illustrated in figure 4.6. Again, due to the similarity of results for four of the states only two of them (OAM -1 with +45° and OAM +1 with -45° polarization) are taken into account for the sake of brevity.

To assess the radiation patterns linked with the OAM antennas, the normalized beams at E and H-planes are depicted in figure 4.7. In all scenarios, a null exists at the broadside, with a minimum depth of 15 dB less than the beam's maximum normalized value, which is set at zero. Moreover, it is evident that the peak gains are approximately at θ=+30 and -30. As a result, both OAM modes have the same divergent angle. This characteristic is challenging to achieve for concentrically embedded or stacked UCAs, as their radii cannot be equal. In our setup, the radii of the UCAs are

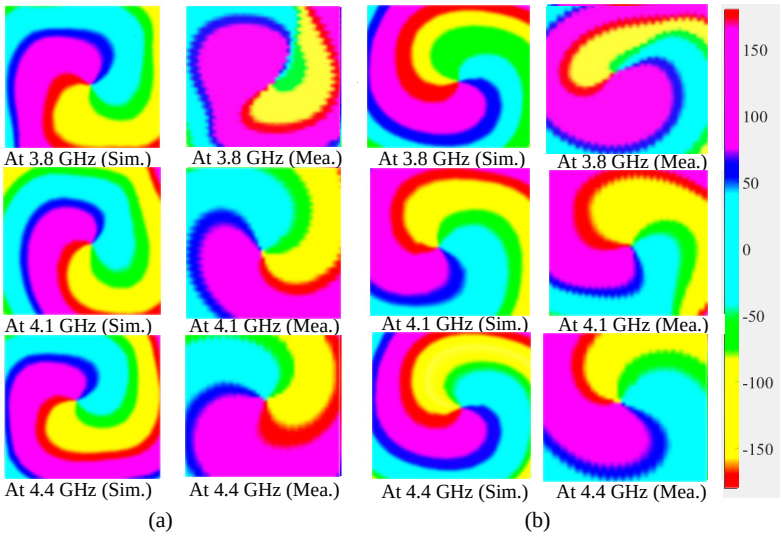

FIGURE 4.6 : The phase front at different frequencies for OAM (a) mode -1 associated with Port 1 (+45° polarization), and (b) mode +1 related to Port 2 (-45° polarization).

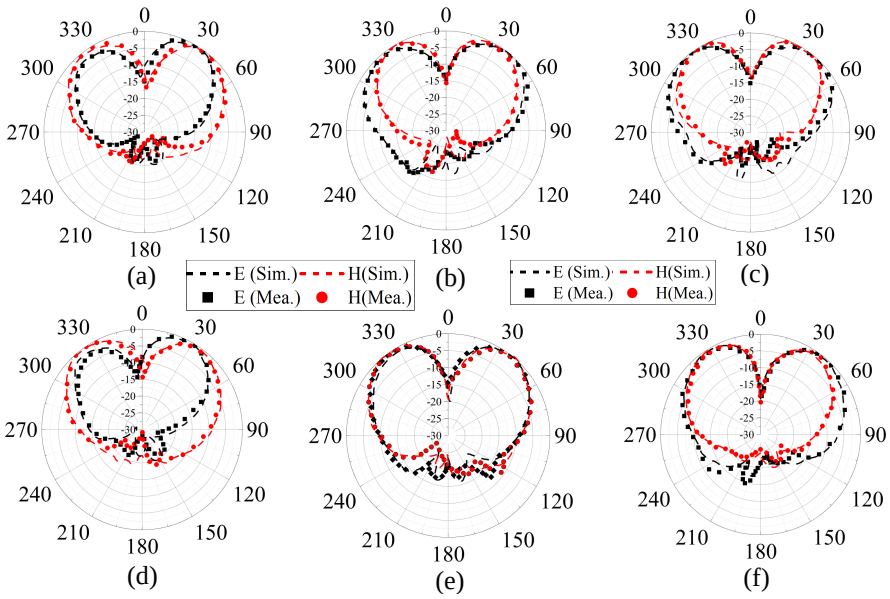

FIGURE 4.7 : 2D radiation patterns for OAM mode -1 +45° Polarization at (a) 3.8 GHz, (b) 4.1 GHz, (c) 4.4 GHz, and OAM mode +1 -45° Polarization at (d) 3.8 GHz, (e) 4.1 GHz, (cf) 4.4 GHz (E=E-plane, and H=H-plane).

identical, thanks to the utilization of the MIMO-UCA technique. It is crucial to note that achieving co-divergence is vital for OAM beams, ensuring that the maximum power is obtained from incident OAM modes at the same position during the reception phase. Additionally, for imaging applications, co-divergence aids in obtaining radar echoes [86]. The values of the maximum gains and efficiencies are also itemized in TABLE 4.2. Moreover, according to the equations mentioned in [103], the mode purity (for measured data) inside a circle with the radius of r=4λ_0 is calculated and listed in the table.

TABLE 4.2 : THE SIMULATED AND MEASURED GAINS OF OAM MODES IN CONJUNCTION WITH RADIATION EFFICIENCIES.

Mode Number	Simulated gain (dBi)	Measured gain (dBi)	Efficiency	Purity
Mode +1 +45° Pol. ($f = 3.8$ GHz)	6.75	6.5	0.66	0.83
Mode -1 +45° Pol. ($f = 3.8$ GHz)	6.8	6.5	0.68	0.78
Mode +1 -45° Pol. ($f = 3.8$ GHz)	7	6.7	0.68	0.80
Mode -1 -45° Pol. ($f = 3.8$ GHz)	6.9	6.7	0.70	0.85
Mode +1 +45° Pol. ($f = 4.1$ GHz)	6.9	6.4	0.70	0.85
Mode -1 +45° Pol. ($f = 4.1$ GHz)	6.9	6.6	0.70	0.88
Mode +1 -45° Pol. ($f = 4.1$ GHz)	7.15	6.8	0.75	0.79
Mode -1 -45° Pol. ($f = 4.1$ GHz)	7.1	6.7	0.73	0.82
Mode +1 +45° Pol. ($f = 4.4$ GHz)	7	6.5	0.71	0.88
Mode -1 +45° Pol. ($f = 4.4$ GHz)	7.1	6.9	0.73	0.85
Mode +1 -45° Pol. ($f = 4.4$ GHz)	6.9	6.4	0.70	0.79
Mode -1 -45° Pol. ($f = 4.4$ GHz)	6.8	6.5	0.68	0.82

4.5 Discussion

Upon evaluating the generation of OAM modes with the flexibility on modes, polarization and frequency, it is time to compare the proposed structure with existing works, TABLE 4.3. First of all, it should be mentioned that the introduced OAM antenna is the first one which provides the control on polarization and mode. In fact, in the current works, only one input port exists and and at a time only one mode with one polarization can be excited. However, in our system, it is possible to simultaneously control mode number and polarization due to having two independent input ports. Achieving two independent input ports, each having different polarizations, is related to the utilization of MIMO-UCA technique. Secondly, the suggested work provides frequency tuning. This feature makes the OAM communication more secure. For instance, in microwave imaging systems, in order to eliminate the unwanted interference, operating frequency can be altered. Furthermore, doing imaging in different frequencies bring about high resolution images since in one frequency the quality can be better than others. The possibility of dual-band operation is another important characteristic of the proposed advanced OAM antenna. It has its root in the independent tunability of input ports. According to the other properties of the antenna, high gain, low design complexity

TABLE 4.3 : A COMPARISON BETWEEN THE PROPOSED STUDY AND SOME RECENTLY PUBLISHED RESEARCH.

Ref.	[40]	[43]	[47]	This work
Freq (GHz)	2.5	2.5	3	3.8–4.4
MIMO-UCA?	No	No	No	Yes
Freq. Tunable?	No	No	No	Yes
Dual-band operation possibility	No	No	No	Yes
Modes	±1	±1	0, ±1	±1
Polarization	Single Pol.	Single Pol.	Single Pol.	Dual-pol.
Gain (dBi)	5.3 / 5.3	5.2 / 5.2	N/A	6.4–6.9
Size ($\lambda_g \times \lambda_g$)	2.38 $\times$ 2.38	2.6 $\times$ 2.6	N/A	1.9 $\times$ 1.9
Design complexity	High	High	High	Low

Pol. = Polarization

and compact size can be taken into consideration.

4.6 Acknowledgment

This work has been funded by Fonds de Recherche du Québec Nature et technologies (FRQNT) under the file number of 333948.

4.7 Conclusion

In this chapter, an advanced OAM antenna with the agility on polarization, mode numbers and frequency has been introduced for the first time. MIMO-UCA technique as well as tunable feeding networks play the key role in achieving the mentioned characteristics. The proposed structure can be operated among 3.8 to 4.4 GHz with preserving the OAM mode features. The maximum gain of above 6 dBi has been measured over the mentioned frequency bands as well. All in all, the suggested antenna paves the way for designing smart OAM systems such as intelligent microwave imaging devices.

5 TRIPLE-MODE TUNABLE DUAL-POLARIZED OAM ANTENNA

This chapter contains materials extracted from the following publications. In this work, despite the previous design, we are also able to obtain the fundamental mode. All other features, including gain, BW, and mode purity, are maintained.

Mode-Tunable OAM Antenna System with Polarization Selectivity characteristic

Authors : Hassan Naseri, Peyman PourMohammadi, Sarosh Ahmed, Amjad Iqbal, and Tayeb Denidni

Contribution of Authors : I am the main contributor to this work, under the supervision of Prof. Tayeb Denidni

5.1 Introduction

OAM antennas have recently taken more attention due to their unique feature. The possibility of simultaneously transmitting different data streams at the same frequency is such antennas' main characteristic. This has its root in the orthogonality of OAM modes [59, 104]. Particularly, OAM-carrying antennas can generate radiation patterns with helical phase fronts, making vortex-like propagation. In theory, it is possible to generate an infinite number of orthogonal vortex beams, allowing for an unlimited amount of data transmission within the same frequency band [97]. It is worth mentioning that each vortex-beam is identified by specific OAM mode number. Designing structures having mode-reconfigurable features are very important in this domain as altering the mode numbers results in smart OAM communications. There have been several works in this regard. Authors in [105] have presented an OAM antenna system that can switch modes between -1 and +1. The feeding network proposed in this research utilizes PIN diodes. In each state, desired transmission line branches are activated to provide the necessary phase distribution for OAM mode generation. OAM modes +1 and +2 have been excited with water antennas in [106]. Two ring water antennas are fed by a feeding network including T-junction and wilkinson power dividers. Again, PIN diodes have been used to alter the output phase gradients of the antenna feeds. RF switches have been taken into consideration for OAM mode propagation in [107]. Even though this structure has a simple configuration, high power consumption by the switches will degrade the efficiency of the whole system. In the mentioned works, there was no control over the polarization of the antennas. However, taking advantage of polarization selectivity brings about another degree of freedom for reconfigurable OAM structures. In fact, both mode and polarization agility increases the degree of reconfigurability. For example, in [108], an OAM structure has been introduced with mode +1 assigned for left-hand circular polarization and mode -1 for righ-hand counterpart. A 2×2 uniform circular array composed of circular patch antennas alongside a tunable feeding network have

provided OAM modes +1 and -1 excitation with polarization switching capability in [109]. This characteristic is equivalent to generating four switchable orthogonal beams. In these two structures, it is not possible to simultaneously generate different modes from one shared aperture due to having only one input port. Also, they suffer from sophisticated feeding networks including various PIN diodes, which will degrade the purity of OAM modes due to leakage of signal when one diode is in OFF state. A suitable structure later has been provided by authors in [110]. Two concentrically-embedded circular arrays have been introduced which can excite fixed linear polarized OAM mode of +1 by the inner array and circularly polarized tunable +2 and -2 mode numbers by outer array. Although, the number of utilized PIN diodes have been reduced, there are still some which can lower the mode purity. Furthermore, the possibility of simultaneous mode generation by inner and outer arrays has been achieved in this paper. However, the vortex beam would not be co-divergent because the arrays have different radii. This will not guarantee proper reception of signals in the receiving side. Very recently, in [111], a dual-polarized OAM antenna system has been provided which can assign modes +1 and -1 to the horizontal and vertical polarization. This structure does not include PIN diodes, and the beams can be generated co-divergently. The number of reconfigurable states is main draw back of this structure. It can only generate modes -1 and +1. With all this in mind, it is concluded that an OAM antenna system with more degree of reconfigurable states, simultaneous generation of co-divergent beams, and highly pure modes are necessary.

In this chapter, an innovative feeding network is proposed which can make the condition for generating three OAM modes (0, +1 and -1). The combination of this antenna feed and a circular array composed of dual-polarized antennas leads to generation of six different orthogonal beams. At any given time, two of the beams can be excited. Therefore, beside taking advantage of channel capacity increment of OAM antennas, this structure paves the way for highly-intelligent OAM communication with its unique reconfigurability feature.

5.2 Triple-mode polarization-selective OAM antenna

In this section, at first, the proposed OAM antenna feed is evaluated. Subsequently, the antenna utilized for the generation of OAM modes is explained. Then, the whole system alongside the achieved results are presented. Finally, a brief discussion with the focus on the potential application of the suggested antenna system and comparison table is provided.

5.2.1 OAM antenna feed design

Figure 5.1 shows the schematic of the suggested OAM antenna feeding network. It is composed of a rat-race coupler, two balanced power dividers and four 1-bit phase shifters. Once Port #1 is excited, the input signal is equally divided with the phase difference of 0°. One more time, the signals are divided by the power dividers. Therefore, the main signal from Port #1 is divided equally

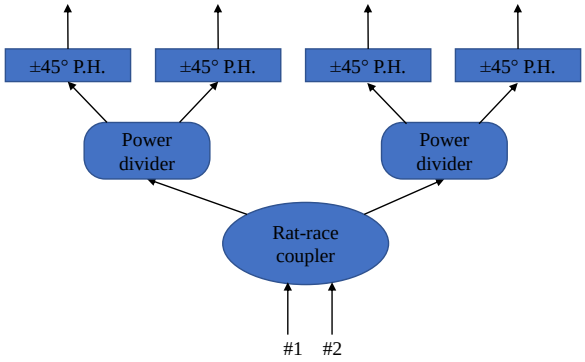

FIGURE 5.1 : Schematic of the proposed feeding network for generating OAM modes. (P.H.=Phase Shifter)

into four parts. If we set all the phase shifters at similar states, for example +45°, the outputs of the feeding network would be in-phase, resulting in generation of OAM mode 0. For exciting OAM mode -1, the phase difference between the circular array elements should be -90°. To that end, Port #2 should be fed. In this case, the signal would be divided into two equal parts with -180° phase difference due to rat-race characteristic. The phase shifters are set in a way that phase gradient of -90° is achieved. In fact, the first phase shifter is set at +45°, the second one at -45°, the third one at +45° and the last one (leftmost side) at -45°. Thus, according to the primary phase difference of -180° between input ports of the phase shifters 1 and 2 with 3 and 4, the out put phases will be +45°, -45°, -135°, -225°. It guarantees the generation of OAM mode -1. For OAM mode +1, the phase gradient should be +90°. This can easily be obtained if the state of the phase shifters are changed in comparison with the states explained for phase gradient of -90°. In particular, they have to be adjusted to -45°, +45°, -45°, and -45°.

Figure 5.2 represents the fabricated prototype of the introduced OAM antenna feed. While design process, we utilized the power dividers in [101]. Regarding the phase shifter, we took into account two varactor diodes and a transmission line-based inductor. By altering the applied DC voltage to the varactor diodes, the resonance happening between the inductor and capacitors belonging to the diodes alter the operating frequency and consequently the output phase. It should be noted that changing the operating frequency does not make the phase shifters be non-matched to 50-Ohm as their bandwidth is large enough. Any other power divider or phase shifter can be used in this structure. In this research, following the schematic in figure 5.1 matters to provide the necessary phase gradient for OAM modes 0, -1 and +1. For proof of concept, the mentioned components have been considered.

Three S-parameter measurements and three simulations, each belonging to one OAM mode, have been carried out for the suggested feeding network. For the sake of brevity and to provide the necessary data in an easy way, TABLE 5.1 has been presented. All the S-parameter results including reflection coefficient and isolation between the ports, phase and amplitudes at output ports are expressed in the table. In this table, Ref. Coef. stands for Reflection coefficient, Out. for Output, Ph. presents Phase, and Amp. indicates Amplitude. The reflection coefficients and isolation between the input ports, in all the cases, are well below -15 dB. As it comes to output phases, it

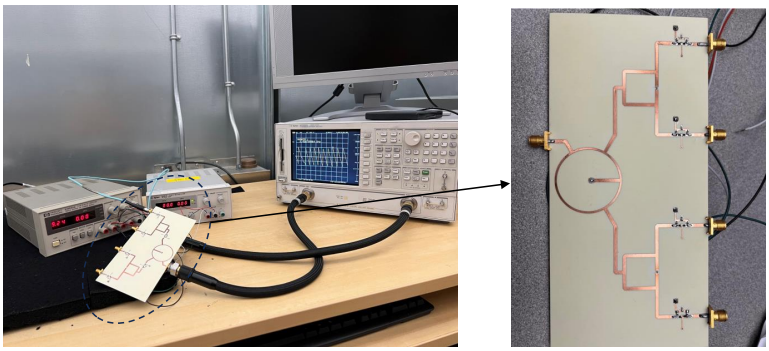

FIGURE 5.2 : The fabricated prototype of the proposed OAM antenna feed.

is evident that for OAM mode 0, the phase difference between the output ports is maximum 4°. When it goes to OAM mode -1, as predicted, the phase difference is more or less -90° with an imbalance not exceeding 4°. For OAM mode +1, the phase gradient is almost +90°. Therefore, the desired OAM modes can be generated. Concerning the output amplitudes, as obvious, they are very close to each other, showing the equal division of the input signal. It goes without saying that due to some extra losses introduced in the fabrication process, the output amplitudes are smaller than simulated values.

TABLE 5.1 : S-parameter results related to the proposed OAM *antenne* feed for both simulation and measurement scenarios.

Parameter and states		OAM 0				OAM -1				OAM +1			
Ref. Coef.	Sim.	-22 dB				-18 dB				-17 dB			
	Mea.	-20 dB				-16 dB				-17 dB			
Isolation	Sim.	-30 dB				-28 dB				-25 dB			
	Mea.	-25 dB				-24 dB				-22 dB			
Out. Ph. (deg)	Sim.	0	4	0	2	-45	+43	+132	+221	+45	+132	+223	+312
	Mea.	2	3	3	2	-46	+45	+137	+226	+44	+134	+224	+313
Out. Amp. (dB)	Sim.	-6.8	-6.2	-6.1	-6.5	-6.5	-6.7	-6.3	-6.1	-6.4	-6.6	-6.4	-6.7
	Mea.	-6.9	-6.7	-6.8	-7.0	-6.8	-7.0	-6.6	-6.5	-6.9	-7.0	-6.7	-6.6

5.2.2 Dual-polarized Bow-tie dipole antenna

In order to introduce polarization selectivity to the proposed concept, a dual-polarized antennas as shown in figure 5.3 has been considered. The antenna consists of two orthogonal bow-tie dipoles [112]. The broadband response of the antennas is evident in figure 5.4. This guarantees that if there is slight frequency shift due to the connection of the proposed OAM antenna feeds, the operating frequency will stay unchanged.

The normalized radiation patterns for both horizontal and vertical bow-tie dipoles at two main planes are presented in figure 5.5. Due to the existence of the reflector at the backside of the antennas, the back lobes are lower enough in comparison with the main beams. It should also be mentioned that the antennas are fed using coaxial probes passing through the reflector.

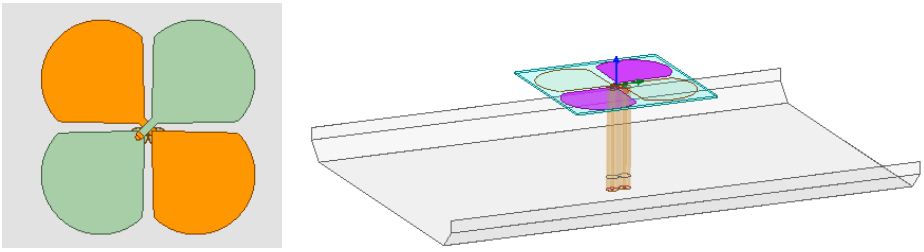

(a) (b)

FIGURE 5.3 : The configuration of the dual-polarized antenna from (a) top view, (c) side view.

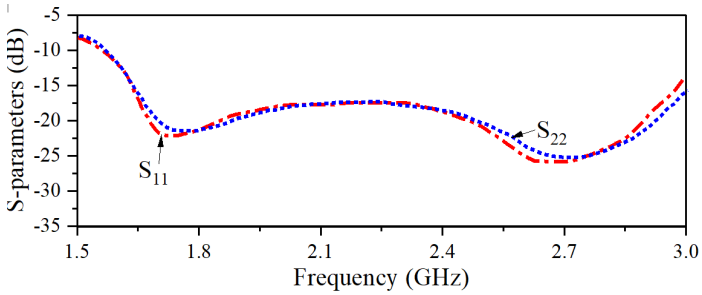

FIGURE 5.4 : Reflection coefficients related to horizontal (S11), and (b) vertical bow-tie (S22).

TABLE 5.2 : THE SIMULATED GAINS RELATED TO OAM MODES ALONGSIDE THE RADIATION EFFICIENCIES.

Mode Number	Simulated gain (dBi)	Efficiency
Mode 0 Horizontal Polarization	13	0.66
Mode -1 Horizontal Polarization	8.2	0.68
Mode +1 Horizontal Polarization	8.4	0.71
Mode 0 Vertical Polarization	13.2	0.7
Mode -1 Vertical Polarization	8.3	0.7
Mode +1 Vertical Polarization	8	0.7

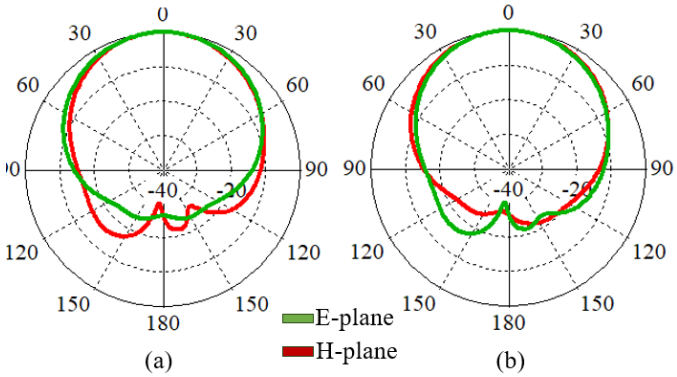

FIGURE 5.5 : Radiation patterns associated with (a) horizontal bow-tie, and vertical bow-tie.

5.2.3 Proposed OAM antenna system

Upon designing and validating the introduced feeding network and the dual-polarized antenna, it is time to setup the whole system. To that end, two copies of the proposed feeding network are considered to feed the 2×2 uniform circular array consisting the bow-tie dipole elements. The dis-

TABLE 5.3 : COMPARISON BETWEEN THE PROPOSED WORK AND RECENTLY PUBLISHED DESIGNS

Reference	[108]	[109]	[110]	[111]	This Work
Frequency (GHz)	2.45	2.5	3.28	3.8–4.4	2.4
Number of Diodes	20	16	32	24	16
OAM Modes	±1	±1	+1, ±2	±1	0, ±1
Gain (dBi)	5.2–5.3	5.2–5.3	5.9–8.4	6.4–6.9	8–8.4
Simultaneous Propagation	No	No	Yes	Yes	Yes
Number of States	4	4	5	4	6
Number of Elements	4	4	12	4	4

Note : “Sim.” = Simultaneous, “Propag.” = Propagation, “N.” = Number of.

tance between the antennas is adjusted to be free space half-lambda at 2.4 GHz. Such a setup allows the generation of OAM modes 0, -1, and +1 with horizontal polarization and vertical polarization. Therefore, six distinct orthogonal radiation patterns can be excited. Each time, two of them are propagating.

The main characteristic of the OAM-carrying waves is the existence of helical phase fronts. Also, the radiation patterns with null in the main beam direction are generated with such waves. These two features represent OAM antennas’ vortex-beam feature. To observe the existence of the mentioned characteristics in the proposed antenna system, a square plane is placed in front of the array to capture the phase front. All the simulations have been carried out in CST software. The phase responses on the plane are shown in figure 5.6. As obvious, there is no helical phase front associated with OAM mode 0 as this mode is the same as radiation patterns related to existing non-OAM antennas. For OAM mode -1 clockwise helical phase front and for OAM mode +1 the counter clockwise one is detected. For both of the polarization, more or less, the same phase fronts are observed.

Regarding the radiation patterns, figure 5.7 should be considered. As predictable, there is no null in the center of OAM mode 0 as it is generated with a regular circular array without any phase difference between the elements. For the other two modes, the null is in the center. From radiation patterns, it is seen that the gain drops once OAM modes -1 and +1 are excited. This is logical, since the null is introduced in the center. Table 5.2 provides the information about the gain and efficiency of the structure at different states. As mentioned, there is a drop of near 4.5 dBi due to generation of OAM modes.

5.3 Discussion

In this section, it is worth talking about the potential application of the proposed OAM antenna system. In terms of communication, it can be utilized in any line of sight scenario. With its polarization selectivity and mode-tunability, if there exists any unwanted signal or jamming, the states can be changed easily to avoid those interference. It should be notified that each OAM mode can only be captured by its corresponding number in the receiver side. Therefore, security of such OAM

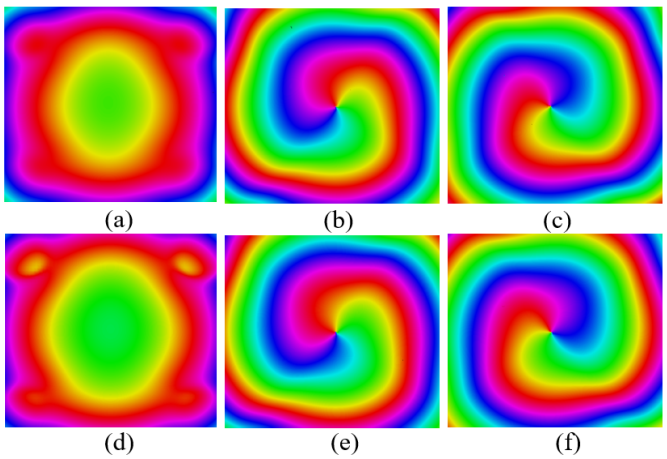

FIGURE 5.6 : Simulated phase fronts for (a) OAM mode 0, (b) mode -1, (c) mode +1 at horizontal polarization, and (d) mode 0, (e) mode -1, (f) mode +1 at vertical polarization.

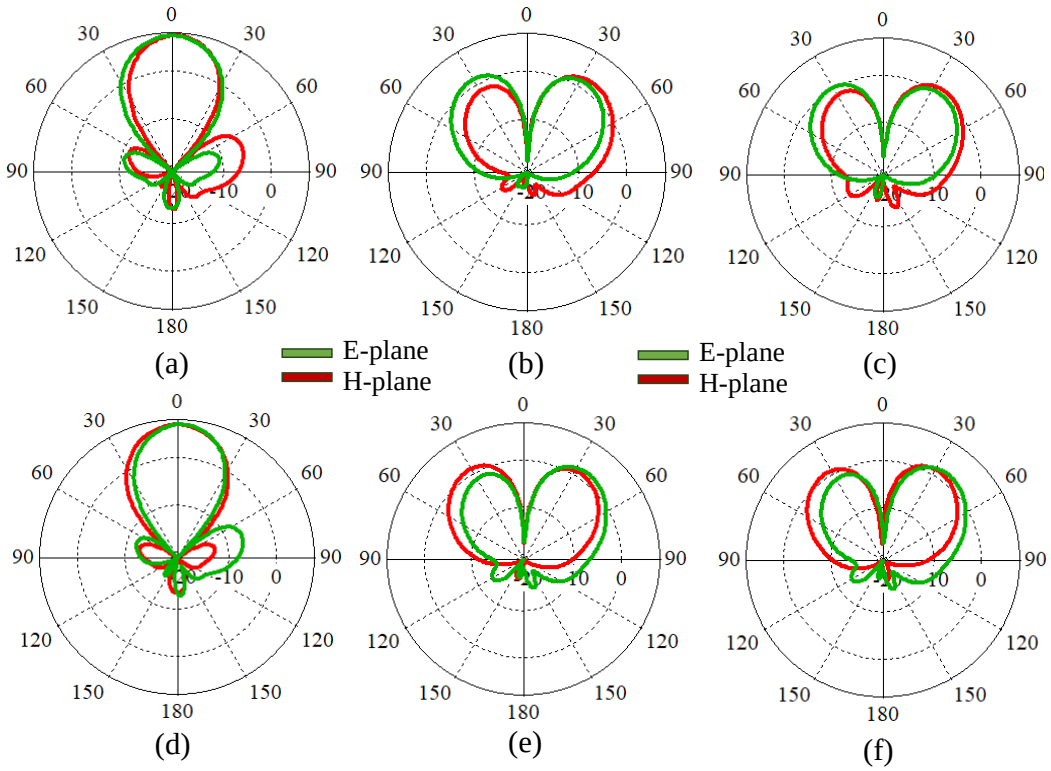

FIGURE 5.7 : E-plane and H-plane cuts for OAM modes (a) 0, (b) -1, (c) +1 in case of horizontal polarization, and (d) 0, (e) -1, (f) +1 in case of vertical polarization.

communications are improved. It goes without saying that transmitting two signals at the same time with our innovative structure will also increase the channel capacity.

In terms of imaging applications, the system will pave the way for high resolution microwave imaging devices. Capturing more back scattered data due to existence of the simultaneously propagating beams, will enhance the quality of imaging.

Table 5.3 represents the comparison between the proposed work and some works published in high-quality journals. According to the table, the proposed OAM antenna has the highest gains, maximum number of states and less amount of varactor diodes. Besides, owing to the utilization of varactor diodes, the leakage problems associated with PIN diodes deteriorating the mode purity is eliminated.

5.4 Acknowledgment

This work has been funded by Fonds de Recherche du Québec Nature et technologies (FRQNT) under the file number of 333948.

5.5 Conclusion

An innovative architecture is introduced with the aid of new OAM antenna feed configuration and utilization of dual-polarized antennas as the uniform circular array elements. The antenna feed consists of a rat-race coupler, two power dividers and four 1-bit phase shifters. The antenna element is made of two orthogonal bow-tie dipoles. The results verified the generation of predicted OAM modes. The possibility of simultaneously exciting two out of six orthogonal beams will increase channel capacity and pave the way for intelligent OAM communication.

6 METASURFACE-BASED OAM ANTENNAS

This chapter contains materials extracted from the following publications. Unlike previous works, this study aims to employ metasurface structures to achieve a high gain exceeding 16 dBi. This chapter diverges from the preceding ones and introduces new design goals and objectives.

Generation of Mixed-OAM-carrying Waves Using Huygens' Metasurface for Mm-wave Applications

Authors : Hassan Naseri, Peyman PourMohammadi, Noureddine Melouki, Fahad Ahmed, Amjad Iqbal, and Tayeb Denidni

Contribution of Authors : I am the main contributor to this work, under the supervision of Prof. Tayeb Denidni

6.1 Introduction

As a result of the fact that next-generation wireless systems require high data rates, the existing antennas cannot satisfy this demand due to the limited Bandwidth (BW) and Signal to Noise Ratio (SNR). Thus, another degree of freedom should provide users with their expected communication connections. OAM antennas are good candidates to solve this issue [113, 114]. These kinds of antennas, unlike current ones, carry the signals in their phase front. In other words, each specific mode of an OAM antenna has a helical phase front which is orthogonal to other modes', and as orthogonal phase fronts are independent of each other, they can be responsible for transmitting their own data stream. However, in traditional antennas, to transmit multiple signals using an antenna, the BW should be divided into several sections, resulting in a lower channel capacity and consequently low data rate. In this regard, to take advantage of the characteristics of OAM antennas, multiple modes must be generated from one aperture.

Referring to the literature, many structures can be found with the capability of generating OAM modes. The structures can be categorized into four groups : antennas having one input port providing reconfigurable OAM modes, antennas generating multiple OAM modes by having an individual port for each mode, single antenna elements, and metamaterials. For the first case, in [109], a 2×2 array including circular patches has been utilized to bring about a uniform circular array for exciting tunable OAM modes +1 and -1. The same patch antennas with a different feeding network have been used to create the same tunable modes in [115]. Authors in [105] take advantage of changing the direction of the input signal to alter the phase value of equally divided signals feeding the antenna elements, giving rise to the generation of reconfigurable modes. Another phase-shifting reconfigurable antenna feed introduces a system having both tunable OAM modes and polarization agility [108]. Using a circular patch antenna with two arc segments in the connection bet-

ween the feed and the resonator, second-order OAM modes are generated in [116]. A wideband single fed circular polarization array enables the propagation of reconfigurable dual-mode OAM beams [117]. OAM modes -1, 0, +1 are excited by means of electrically mode-tunable metasurface antenna [118]. Authors in [119] introduce a simplified feeding network to generate multiple OAM modes in six tunable states.

A 1-bit reconfigurable reflectarray provides the condition for generating mode switching OAM waves in [120]. A similar work, this time using a transmitarray, has been proposed in [121]. In [122], vortex beams owing circular polarization are excited using a mechanically reconfigurable *antenne* array. Spoof surface plasmon ring resonators pave the way for creating adjustable-OAM modes in [47]. A water *antenne* in [123] has been designed to propagate OAM-carrying beams with the aid of a reconfigurable feeding network. It should be noted that in most of the aforementioned references, PIN diodes have been used while designing the reconfigurable feeds. However, very recently, Hassan *et al.* has presented a low-profile structure which can enable the excitation of tunable OAM modes using Varactor diodes [124]. This leads to solving the problems associated with the leakage of signal in reverse bias state of PIN diodes.

Talking about the structures owing individual ports for each mode, in [125], two separate feeding networks produce phase responses of [0, 90, 180, 270] and [0, -90, 0, -90] degree for modes +1 and -1, respectively. In [11], four OAM modes are engendered using four different *antenne* feeds. OAM modes -1 and -2 are excited using two different feeding networks plated on the same layer. OAM mode -3 owns its own feed on one layer, and OAM mode 0 is created by a centered patch *antenne*. Sequentially rotated configuration of the *antenne* elements in a UCA paves the way for simplifying the feeding networks. This feature has been considered in [12] to obtain modes +1 and +2 with low-profile *antenne* feeds. However, achieving the mentioned modes without using the sequential rotation method would lead to designing complicated and lossy feeds. Radial Line Slot Arrays (RLSA) can also be utilized in engendering OAM-carrying waves [126]; a 4×4 Butler Matrix (BM) provides the condition for propagating OAM modes of 0, -1 and +1. Uniform circular array has been suggested in [127]. In this structure, the arrays are fed by hybrid couplers connected to ring-shaped transmission lines. Some other examples of structures having multiple input ports for multiple OAM mode generations can be found in [10, 128–131].

Beside the structures belonging to the mentioned two categories, reconfigurable OAM antennas and those having individual ports for each mode, there exist a few single elements which can excite OAM modes as well. However, these structures have a low gain in comparison with the works using arrays. Among single antenna elements producing low gain OAM modes, the structures proposed in [23–25, 61, 132–137] can be taken into consideration. In [23], a circular patch antenna is fed using two hybrid couplers to provide OAM modes with high purities. It should be mentioned that the OAM modes are excited in the second resonance frequency of the patch. A square patch antenna is fed from its four sides to create OAM modes in [25]. Authors in [61] have proposed an octagonal structure to excite higher-order OAM modes. Substrate Integrated Wave-

guide (SIW) cavity is utilized in its half mode in [24] to bring about vortex beams. A traveling-wave ring-slot structure is responsible for enabling the propagation of four OAM-carrying waves in [132]. A cylindrical dielectric resonator antenna can generate several OAM beams at different frequencies, [133]. Finally, a water-immersed rectangular horn antenna and a spiral antenna can result in vortex beam generation in [134] and [135], respectively. To come up with a high gain single element structure, leaky wave antennas have been designed as well [136], [137]. Even though both low gain and high gain single element antennas are appropriate components for compact wireless systems, they suffer from the possibility of generating more than two OAM modes at a specific frequency.

Metamaterials have been used for various applications; among which filter-antennas sensors [138], all-metal metamaterials for high gain applications [139], beam-steerable Frequency Selective Surface (FSS)-based phase shifting surfaces [140], ultra wide band (UWB) and wide band FSS-based antennas and filters [141, 142]. As it comes to metamaterial-based OAM antennas, several works exist in literature. Among them it is worth referring to [143–152]. It should be noted that a full review of guided-wave metasurfaces for vortex beam generation has been reported in [152]. The mentioned metamaterial-based structures can create only one OAM beam, resulting in them being inappropriate for high data rate communications. One way to come up with the generation of various modes is to use mixed-OAM generating antennas. Mixed-OAM modes which can be used for transmitting several versions of a data stream as MIMO antennas can, are barely achieved using single port mode-reconfigurable structures. According to those having individual ports, the design complexity is a barrier for obtaining high gain antenna systems. Furthermore, it is a difficult task to design antenna feeds for the latter cases. To resolve the mentioned issues, a few works have been reported which enable the excitation of mixed-OAM modes with the aid of TAs and reflectarrays, giving rise to high gain structures without any need for sophisticated feeding networks [14, 153–156]. [14] has utilized perforated Spiral Phase Plates (SPP) requiring the state-of-art equipment for fabrication; [153] has considered two layers during the design process, [154] has taken advantage of cascaded TAs, [155] has used two feeds at off-axis positions to superimpose two OAM modes at the broadside in the reflectarray, and [156] has carried out the same technique by means of a TA.

In this chapter, mixed OAM modes of -1 and -2 are achieved using an ultrathin dual-polarized huygens' metasurface. The design evolution starts with calculating the angular position of each unit cell in a planar TA. More specifically, the TA should satisfy two conditions; change the received spherical wave to a planar one and alter it to mixed OAM modes -1 and -2 according to the angular position of each unit cell. The measured results confirm the generation of radiation patterns with a null in broadside and having helical phase fronts. The operating frequency of the TA is considered to be 28 GHz, which is a candidate for 5G networks. The maximum gains of 16 dBi are measured at both X and Y-polarization as well.

6.2 Unit cell characteristics

An ultrathin huygens' metasurface introduced in [157] owns the capability of making the phase shifts staring from 0 to 360-degree. Figure 6.1 shows the configuration of the mentioned unit cell alongside its simulation setup carried out in CST software.

The unit cell is printed on both side of the Rogers 4003C with a dielectric constant of 3.55 and a thickness of 1.524 mm. Since the unit cell has a square shape and symmetric profile, it is called dual-polarized. In fact, it does not matter what is the polarization of incident wave as a result of the fact that its horizontal and vertical components see the same configuration. It should also be pointed out that during the simulation process, the "unit cell" boundary condition is selected for the plates connected to the unit cell in figure 6.1c. For the top and bottom plates which are open (add space) boundary conditions, the feeds exist, and by changing the value of *l* and *g* in a way that always *l*+*g*=4.4 mm, all the necessary phase compensation ranging from 0 to 360-degree is achieved. However, for our case, OAM-mixed generating TA, only quantized values which will be discussed later are taken into consideration. Concerning the distance of the top and bottom boundary box from the surface of the unit cell, it should be noted that $\lambda_0/2$ has been considered and the reference planes have been selected to be on the front and bottom surface of the unit cell.

Figure 6.2 presents the variation of transmitted phase as well as the amplitude response according to the value of *l*. It is worth mentioning that *l*+*g*=4.4 mm must be regarded in each step. Concerning figure 6.2a, the phase response of the unit cell is very smooth once the value of *l* alters from 0.5 to 2.75 mm. Then, it seems there exists a sharp change starting from 3 and ending at 3.1 mm. However, this sharp change appears merely because of the periodicity of the phase. subsequently, the phase decreases by increasing the value of *l* up to *l*=3.82 mm. It should be clarified here that during the parametric study, we only take into consideration the phase values of 0, 45, 90, 135, 180, 225, 270, and 315-degree. This has its root in phase quantization technique being used in generation of OAM modes. When it comes to the amplitude response of the huygens' metasurface, it is obvious from figure 6.2b that the mentioned unit cell has a low transmission loss, perfect candidate for achieving the high gain OAM waves.

6.3 Mixed-OAM generating TA design

Upon finding the required values for *l* in a way that the unit cell satisfies the above-mentioned quantized values and has a low transmission loss, the proposed TA can be designed. To that end, two important steps should be taken into account; TA needs to transform the received spherical wave into planar one and then create the desired mixed-OAM modes, see Equation (6.1) which is the summation of the two mentioned steps [18].

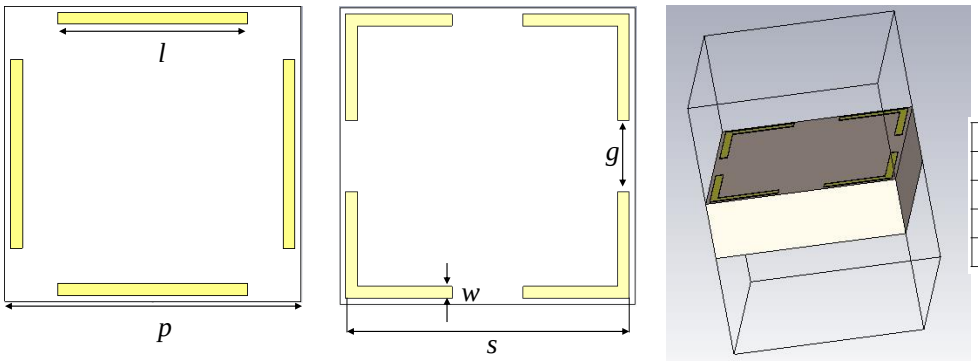

Parameter	Value (mm)
l+g	4.4
p	5
s	4.8
w	0.2

FIGURE 6.1 : The configuration of the huygens' metasurface, (a) front view, (b) back view, (c) simulation setup, and (d) the parameter values.

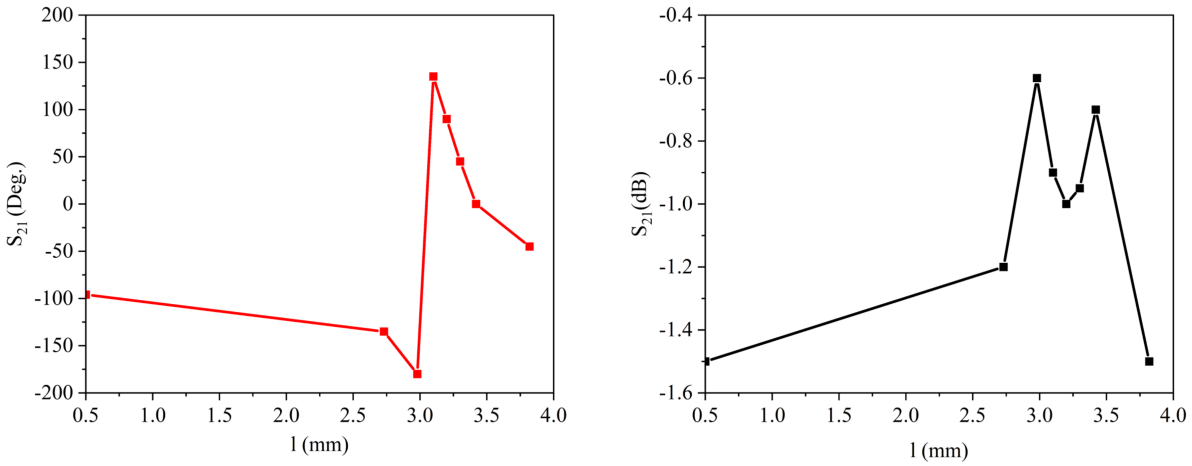

FIGURE 6.2 : (a) phase response, and (b) amplitude response of the mentioned unit cell according to different values for *l* (*l*+*g*=4.4 mm).

$$\phi^{c}_{mn} = -\frac{2\pi}{\lambda}\left|\vec{r_{mn}} - \vec{r_f}\right| + arg\left\{e^{(j)l_k.\Phi_k}\right\} \tag{6.1}$$

where ϕ^{c}_{mn} is the required phase of the *mn*th element of the TA, which is supposed to have 400 unit cells (m×n=20×20). λ, $\vec{r_{mn}}$, and $\vec{r_f}$ are the wavelength at free space considering 28 GHz as the operating frequency, vector position of each unit cell, and vector position of feed antenna (horn), respectively. Further, l_k is the OAM mode number, and Φ_k is the azimuth angle of each unit cell in the normal plane of TA. In order to have a better imagination about the components of the equation, figure 6.3 can be useful. In this figure, a simplified TA including m×n=6×6 elements is considered for illustration.

The first sentence of the Equation (6.1) is related to transforming spherical wave to planar wave. In order to have a planar wave, all the wave passing through the unit cells making the TA, should become in-phase. In particular, when the wave propagates using a horn antenna as a feed, the

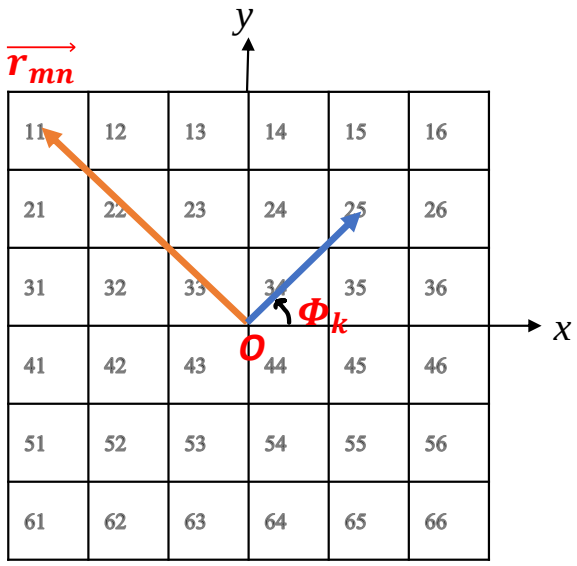

FIGURE 6.3 : The schematic of a simplified TA including m×n=6×6 elements to demonstrate the variables of Equation (6.1).

electric fields on the TA plane present different phase differences relative to each other. Thus, with regard to the simulated values for *l*, it is possible to make all the fields in-phase.

In the second step, desired OAM modes are selected and by paying attention to the second sentence of the equation, the other required phase for each unit cell is calculated. Therefore, summation of two phases achieved from the equation provides the precise compensating phase values for one OAM mode. In order to obtain mixed OAM modes, the centered 10×10 TA is assigned for mode -1, and the rest of the TA is bestowed to mode -2. In the other words, from 20×20 TA, the centered 10×10 sub-TA generates OAM mode -1 and the remaining part produces mode -2.

After calculating all the necessary compensating phases, it is time to utilize quantized values according to Equation (6.2).

$$\phi^c_{mn,quantized} = \begin{cases} 0 & -22.5 < \phi^c_{mn} \leq 22.5 \\ 45 & 22.5 < \phi^c_{mn} \leq 67.5 \\ 90 & 67.5 < \phi^c_{mn} \leq 112.5 \\ 135 & 112.5 < \phi^c_{mn} \leq 157.5 \\ 180 & 157.5 < \phi^c_{mn} \leq 202.5 \\ 225 & 202.5 < \phi^c_{mn} \leq 247.5 \\ 270 & 247.5 < \phi^c_{mn} \leq 292.5 \\ 315 & 292.5 < \phi^c_{mn} \leq 337.5 \end{cases} \tag{6.2}$$

Based on the above equation, only eight values of phases are considered during the simulation process, making the design complexity less. Furthermore, the proposed quantized technique paves the way for later investigations regarding the reconfigurable OAM generating TAs using Varactor diodes or PIN diodes.

6.4 Experimental verification

The prototype of the designed TA including 20×20 unit cells are fabricated on Rogers 4003C with a thickness of 60 mils as shown in figure 6.4a,b. The centered TA having 10×10 unit cells helps create OAM mode -1, and the rest of the unit cells are responsible for exiting OAM mode -2. In the figure, the mentioned sections are separated by square shapes. To verify the generation

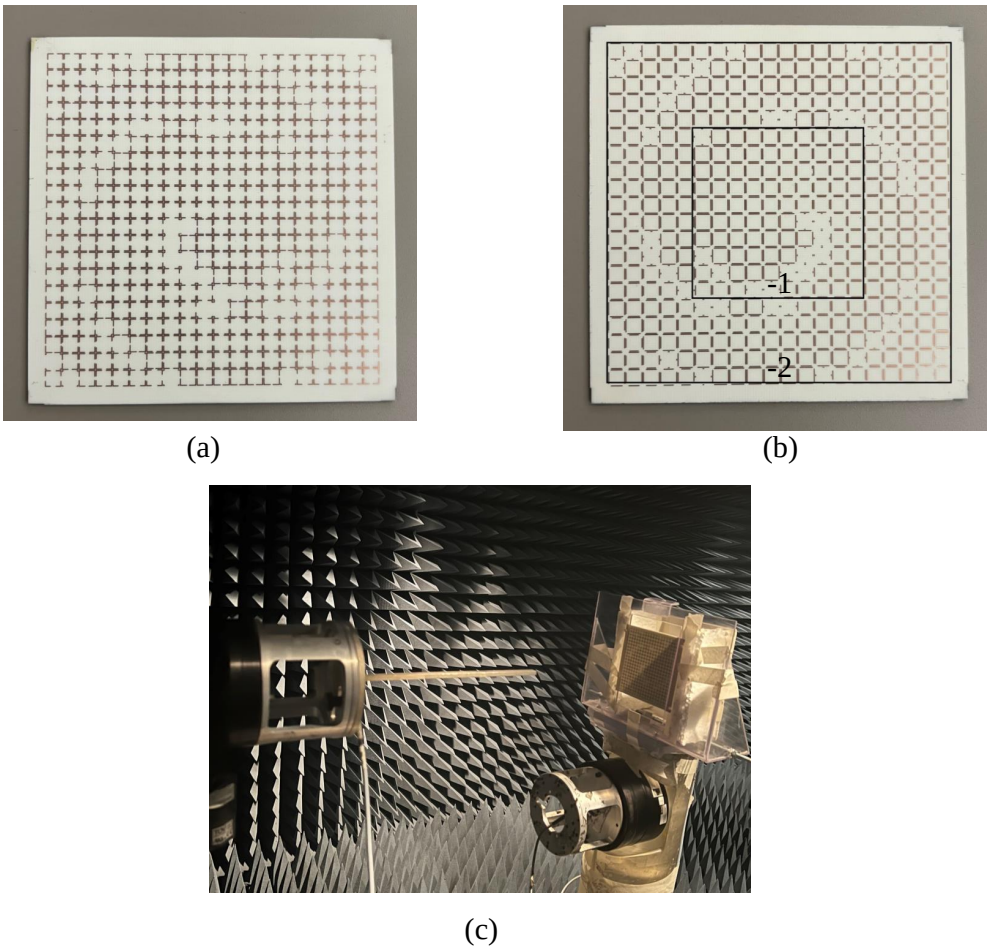

(a) (b)

(c)

FIGURE 6.4 : Configuration of the fabricated structure : (a) front side, and (b) back side.

of mixed OAM modes, a setup as illustrated in figure 6.4 has been utilized. A probe scanning the square area with 15×15 cm^2 has been placed at 15 *cm* away from the proposed TA. The position of the TA (antenna under test) is fixed, while the probe (transmitter) scans the square area and each time transmits the signal. Thus, the amplitude and phase of the transmitted signal is detected by the TA at each position. Figure 6.5 depicts the phase front and amplitude response of the TA. As evident, there is a null at the center of the scanning area and two OAM modes (-1 and -2) are mixed together in the helical phase fronts.

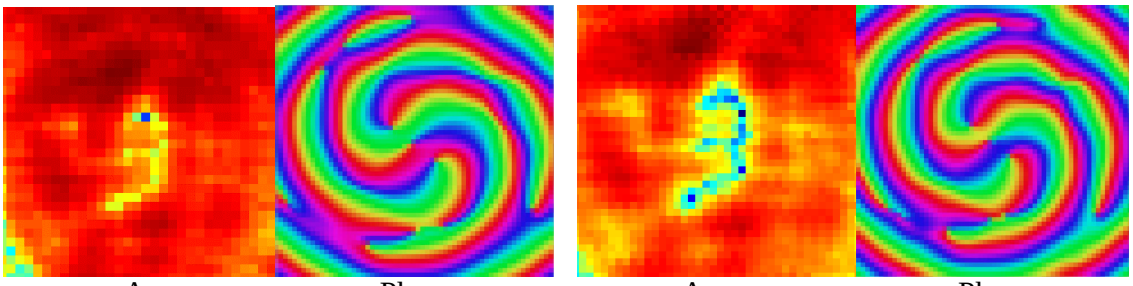

(a) (b)

FIGURE 6.5 : Amplitude and phase response for (a) X-polarization, and (b) Y-polarization.

Concerning the far-field radiation pattern of the proposed TA, figure 6.6 has been provided. Maximum gain of around 16 dBi has been achieved while measured process for both X and Y-polarization cases, confirming the TA being dual-polarized. The existence of null at Theta=0 is obvious as well.

Mode purity analysis is a factor which explores the validity of the generation of OAM modes. In a structure providing a single OAM mode, this value is 1 in theory. However, since the proposed TA excites two mixed OAM modes, this value depends on the circle in which the mode purity is calculated. According to [158], the mode purity in both X and Y-polarization has been calculated. If we assign a circle with r=4λ, taking into consideration inside the circle, the purity of around 0.65 has been obtained for mode -1. As th circle becomes bigger, the purity of OAM mode -1 decreases and for -2 increases. Some results have been presented in figure 6.7. As the results for X and Y-polarization cases were almost the same, we only provided X-polarization scenario. It is worth pointing out that in an ideal situation, the mode purity should be 0.5 for modes -1 and -2. However, owing to fabrication and quantization errors, some impurities exist.

6.5 Discussion

As mentioned, OAM antennas are mainly categorized in four groups. The first group is reconfigurable structures that generate one predefined mode at each time. More specifically, according to the state of PIN diodes or varactor diodes, the desired OAM mode is excited. These kind of antennas can be useful as a spatial filter. To demonstrate, if a mode-tunable antenna is utilized in a receiver side, it is possible to catch the signals having the corresponding mode and refuse other unwanted modes. The second group is related to the antenna arrays that have their own feeding networks. Each feed helps create the necessary phase distribution for one OAM mode. Due to the fact that every OAM mode has its own feeding structure, the complexity of network increases. It should be pointed out that such antennas can be used in a case that multiple streams of data are going to be sent at the same time and frequency. The data streams are not combined to each other because of the orthogonality of OAM modes. Concerning the third group, the single antenna elements that can generate vortex beams own a low gain. Further, theses types of OAM antennas are

able to produce two OAM modes at a specific frequency, limiting their application in high data rate wireless systems. As the fourth group of OAM antennas, transmitarrays and reflectarrays including various kind of metamaterials excite only one OAM mode. In this case, increasing the channel capacity does not make any sense since it is not possible to send different versions of a signal or multiple data streams at the same time and frequency. To enable the metamaterial-based OAM antennas for improving the channel capacity, one should provide mixed-OAM modes. In this manner, different versions of a signal are transmitted using different OAM modes, and consequently the possibility of receiving high quality signal in the reception side increases. In this regard, a few works have been carried out [14, 153, 154]. However, they either suffer from the fabrication complexity or not being dual-polarized structures. Moreover, none of them use quantized phase values during design process. This feature tremendously simplifies the unit cell design for TA.

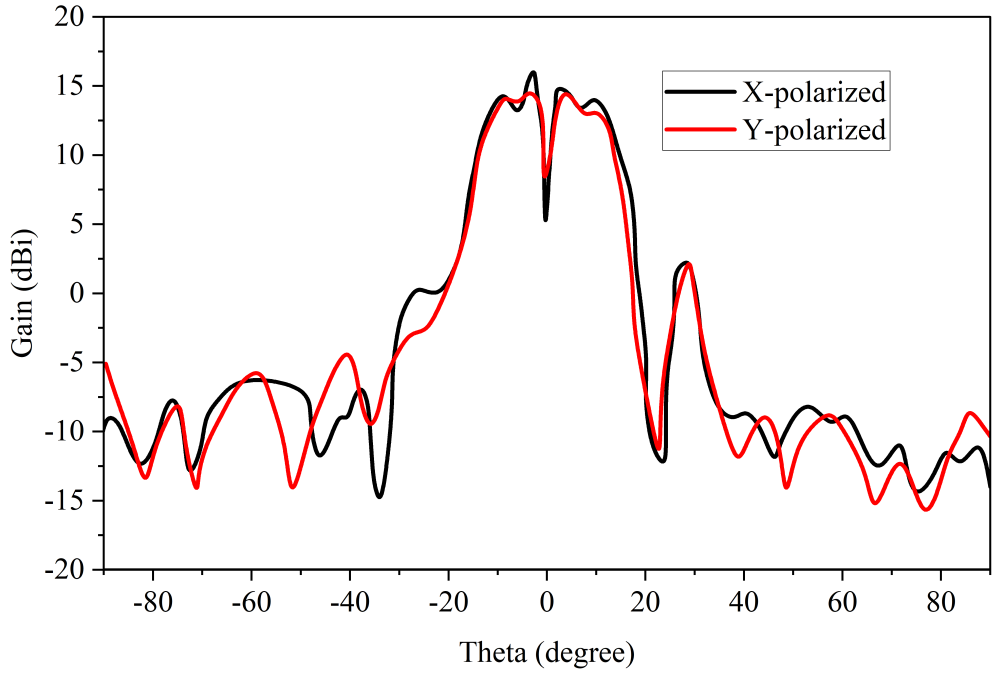

FIGURE 6.6 : The far-field measured patterns for suggested TA.

Beside the TAs generating mixed OAM modes at the broadside, there exist some which can create a desired mode at an off-axis position [155, 156]. Superimposing the phase values on the TA or reflectarray, it is possible to excite two OAM modes at two different positions. With regard to the reciprocity law, in case the horn antennas are located at the off-axis position corresponding to the OAM mode direction, the mixed OAM modes propagate at the on-axis direction. Taking advantage of the mentioned feature, the multiplexing-demultiplexing link using two copies of the structure (for transmission and reception) is obtained. These type of structures can not support the generation of more than two mixed OAM modes, as the technique of superimposing the phases on the TA deteriorates the purity of mode. However, in our structure by increasing the sub-TAs, the number of mixed OAM modes can be easily increased as done in [14]. Furthermore, utilizing two feeding sources in applications requiring the reduction of multipath fading effect, makes the system

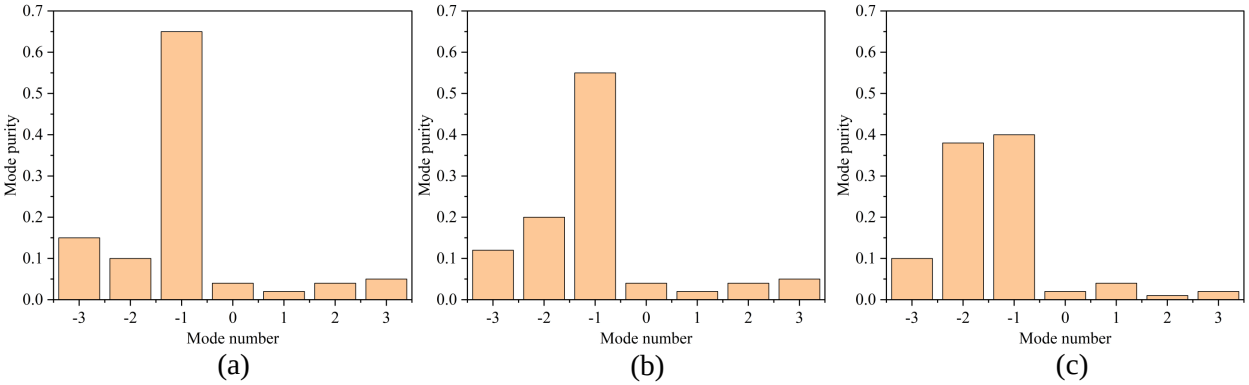

FIGURE 6.7 : The mode purity analysis for X-polarization once (a) r=4λ, (b) r=8λ, and (c) r=12λ

complicated. Moreover, they do not provide dual-polarized characteristic as described in our work. Concerning some applications for our structure, it is worth pointing out that our structure provides the generation of two mixed OAM modes. Since these two modes are orthogonal together and propagate simultaneously, two versions of the data stream are transmitted. These two versions are not combined and consequently the possibility of achieving a high-quality signal at the receiver side increases. This feature is similar to the MIMO application (multipath fading reduction). According to the channel capacity for MIMO structure, our structure offers a high-capacity communication as well. Another example of application for using mixed OAM modes is related to imaging applications. In fact, more information from the object being imaged is going to be available using mixed OAM modes from a shared aperture. This gives rise to a high-resolution imaging in next-coming wireless systems.

To summarized the above mentioned discussion, it is required to clarify that the novelty of our structure is related to its being polarization independent. This is because of the fact that the unit cells are dual-polarized. Also, during the design process we used quantized values for the phases which simplifies the configuration of structure as well as its design complexity in comparison with similar works [14, 153, 154]. Further, this feature paves the way for introducing mode tunable OAM generating TAs, since creating quantized values by embedding active components such as pin diodes and varactor diodes is much easier than creating continuous phase values. Moreover, the fabrication cost of the suggested structure is low in comparison with the mentioned references due to having ultrathin unit cells designed on a cheap substrate. However, [14] needs state-of-the-art equipment for fabrication and [154] has used cascaded substrates. About the applications for the proposed structure, point-to-point high data rate communications, high resolution imaging, and high quality sensing can be taken into consideration.

6.6 Conclusions

This study has presented a dual-polarized tramsmitarray (TA) that can generate mixed Orbital Angular Momentum (OAM) modes. The proposed structure comprises two concentrically embed-

ded TAs, where the inner TA has 10×10 Huygens' metasurfaces to generate OAM mode -1 and the outer TA excites mode -2. The generation of OAM modes has been achieved by adjusting the angular position of each unit cell and the necessary phase compensation for converting the propagating spherical wave to a planar one. The measured results demonstrate helical phase fronts composed of mixed -1 and -2 modes and radiation patterns that show null at broadside. The maximum gains of 16 dBi have been obtained in both X- and Y-polarization. Moreover, the mode purity analysis has been evaluated, confirming the equality of mode -1 and -2 purity taking into account a larger calculating circle. Therefore, it is suggested that this proposed TA can be a potential candidate for enhancing the channel capacity of next-generation wireless communication systems and acquiring high resolution images in imaging systems.

7 CONCLUSION AND FUTURE WORK

7.1 Conclusion

Traditionally, increasing the channel capacity of wireless communication systems has relied on enhancing the BW and the SNR. Indeed, achieving high data transfer rates has required a wide impedance BW and an acceptable level of SNR. However, current communication systems have increasingly failed to meet the growing demand for high-speed connectivity. This shortfall has stemmed from inherent limitations in BW—often constrained by gain or AR bandwidths—and from fluctuations in SNR caused by environmental changes and other uncontrollable factors. These challenges have highlighted the need for novel antenna designs that can contribute to improving channel capacity through alternative means.

OAM antennas have offered a promising solution by enabling the generation of multiple orthogonal donut-shaped beams from a single aperture, owing to their helical phase fronts. This orthogonality has allowed the simultaneous transmission of multiple data streams over the same frequency band, thereby significantly increasing spectral efficiency.

In this context, reconfigurable OAM antennas have emerged as key enablers of intelligent wireless systems. These antennas have provided reconfigurability in mode number, polarization, and operating frequency. The present thesis has aimed to design and develop novel OAM antenna systems that exhibit such reconfigurability, with a view toward their integration in future intelligent wireless networks.

Chapter 1 has introduced the fundamental principles of OAM modes and their generation mechanisms, along with three widely adopted excitation methods. Chapter 2 has presented the initial design of a mode-reconfigurable OAM antenna based on a UCA and a 1×4 feeding network. This system has utilized embedded phase shifters to generate either +1 or -1 OAM modes. Although effective, the use of patch antennas has limited polarization control post-fabrication, and the single-port input has restricted the system to one mode at a time—thereby constraining its overall potential for enhancing channel capacity.

To overcome these limitations, Chapter 3 has introduced a new antenna system capable of independently controlling both polarization and operating frequency for each OAM mode. Chapter 4 has extended this design by enabling simultaneous mode generation and dynamic assignment of mode numbers to different polarizations, while maintaining frequency tunability. This multidimensional reconfigurability has marked a significant step toward achieving the thesis's central objective.

Chapter 5 has further advanced this work by proposing an antenna system capable of generating three OAM modes (0, -1, and +1), each with selectable vertical or horizontal polarization. This has further elevated the level of reconfigurability and flexibility required for practical OAM-based systems.

Subsequently, Chapter 6 has addressed the development of high-gain, multi-mode OAM antennas to enable long-range communication—an essential feature for real-world deployment.

Finally, Chapter 7 has summarized the findings and contributions of this four-year research journey and has outlined future research directions. These include the development of more compact architectures, integration with MIMO systems, and the implementation of real-time adaptive control strategies—paving the way for the next generation of intelligent wireless communication systems.

7.2 Future works

In this section we will discuss potential future works that can be very useful for researchers following this thesis.

7.2.1 Mode augmentation technique in generating OAM modes

The number of generated OAM modes are limited by the number of antenna elements in the uniform circular array. To demonstrate, if we have four antenna elements in the UCA, we can excite mode 0, -1 and +1. In order to overcome this limitation, we proposed a new technique explained below; Considering a UCA with *N* antenna elements as depicted in figure 7.1, Equation (7.1) can be expressed for calculating the electric filed of the whole structure.

$$E_{total} = E_N \times AF \tag{7.1}$$

where E_N represents the electric field associated with one of the antenna elements. It is worth

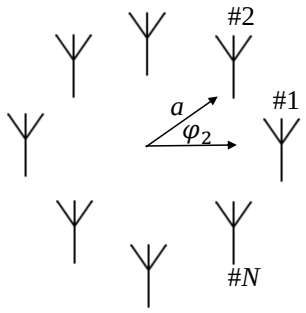

FIGURE 7.1 : Schematic of the UCA including tunable OAM generating antenna elements.

mentioning that all the antenna elements are the same in this configuration. Further, *AF* is the array factor of the UCA.

If the antenna elements are selected to be one generating dual-mode OAM modes, Equation (7.1) would be in the form of Equation (7.2).

$$E_{Total} = E_0 \times e^{\pm jl\phi} \times AF \tag{7.2}$$

In the above equation, *l* is the OAM mode number and E_0 is the total amplitude of the electric field.

Calculating the *AF*, Equation (7.3) gives rise to complete form of the total electric filed.

$$E_{Total} = E_0 \times e^{\pm jl\varphi} \times \sum_{N=1}^{N} e^{-jk_0 \times a \times sin(\theta) cos(\varphi - \varphi_N) - j\Phi_N} \tag{7.3}$$

where k_0 is the wave number, θ is the direction of propagation relative to the normal vector of UCA plane, and φ_N is the angular position of each element. Moreover, Φ_N is he primary phase of each antenna elements.

Simplifying the Equation (7.3), Equation (7.4) is obtained.

$$E_{Total} = E_0 \times e^{\pm jl\varphi} \times e^{j\grave{l}\varphi} \times J_N(\frac{2\pi a sin\theta}{\lambda}) = E.e^{\pm j(l+\acute{l})\varphi} \tag{7.4}$$

J_k is the Bessel function of the first kind.

Equation (7.4) indicates that in case an OAM mode generating antenna element is used to create a UCA, the mode number of the single element is added to the mode number of the UCA. For instance, if a single antenna exciting a tunable OAM +1 and -1 exists, and we create a 2×2 UCA generating modes 0 and -1, it is possible to have OAM modes 0, -1, +1, -2.

The researchers interested in OAM design can use the introduced technique and the other methods discussed in the chapters of this thesis to come up with multi-mode tunable designs to provide more reconfigurablities to the OAM antennas.

7.2.2 OAM mode with beam-steering capabilities

To provide OAM communication in non-line of sight scenarios, the structure should be able to steer the vortex beams in different directions. This is really challenging and the way we propose is utilization of active metasurfaces. Thus, beside providing the necessary phase shifts for specific OAM mode, the active unit cells should be able to provide phase differences for changing the beam directions as well.

7.2.3 Multi-mode OAM generation

The more we can generate OAM modes, the more we can increase the channel capacity. In UCA, the challenge is to provide different phase differences in the outputs. This requires increased number of phase shifters, resulting in sophisticated feeding networks. The solution we suggest is the utilization of Butler Matrix. To illustrate, if we design a 8×8 Butler Matrix, we can receive eight different phase gradients. These phase gradients can lead to excitation of OAM modes if they follow Equation (1.1) and feed eight antennas.

7.2.4 Limitations of OAM communication

Even though OAM is a promising way for ultra-high speed communication, there are limitations as mentioned below :

1-Distance : Due to the existence of null in the radiation pattern of the OAM modes, the communication distance becomes shorter. This is because of the fact that if we put the receiver far from the transmitter, it will be in the null of the pattern and loose communication. Consider this fact that there is divergence angle in radiation and null becomes bigger and bigger by distance.

2-Mode crosstalk : In reality, the OAM modes are not perfectly orthogonal together and this can degrade the performance of systems.

3-Hardware complexity : As you saw from our designs, the systems become more complex as we need to feed antenna elements with different phases according to each mode.

4-perfect line of sight alignment : Due to the fact that we have null in the radiation pattern, a slight misalignment can lead to the communication failure.

BIBLIOGRAPHIE

[1] M. S. Sharawi, "Current misuses and future prospects for printed multiple-input, multiple-output antenna systems [wireless corner]," *IEEE Antennas and Propagation Magazine*, vol. 59, no. 2, pp. 162–170, 2017.

[2] B. Gao, F. Zhang, G. Sun, Y. Xiang, and S. Pan, "Microwave photonic mimo radar for high-resolution imaging," *Journal of Lightwave Technology*, vol. 39, no. 24, pp. 7726–7733, 2021.

[3] X. Liu, T. Huang, N. Shlezinger, Y. Liu, J. Zhou, and Y. C. Eldar, "Joint transmit beamforming for multiuser mimo communications and mimo radar," *IEEE Transactions on Signal Processing*, vol. 68, pp. 3929–3944, 2020.

[4] H. Liu, Y. Wang, J. Wang, K. Liu, and H. Wang, "Electromagnetic vortex enhanced imaging using fractional oam beams," *IEEE Antennas and Wireless Propagation Letters*, vol. 20, no. 6, pp. 948–952, 2021.

[5] H. Liu, K. Liu, Y. Cheng, and H. Wang, "Microwave vortex imaging based on dual coupled oam beams," *IEEE Sensors Journal*, vol. 20, no. 2, pp. 806–815, 2019.

[6] H. Wu, Y. Yuan, Z. Zhang, and J. Cang, "Uca-based orbital angular momentum radio beam generation and reception under different array configurations," in *2014 Sixth International Conference on Wireless Communications and Signal Processing (WCSP)*, pp. 1–6, IEEE, 2014.

[7] X. Bai, R. Jin, L. Liu, J. Geng, and X. Liang, "Generation of oam radio waves with three polarizations using circular horn antenna array," *International Journal of Antennas and Propagation*, vol. 2015, no. 1, p. 132549, 2015.

[8] C. Sun, S. Yang, Y. Chen, J. Guo, and S. Qu, "Realization of multiple orbital angular momentum modes simultaneously through four-dimensional antenna arrays," *Scientific reports*, vol. 8, no. 1, p. 149, 2018.

[9] Z. Zhao, Y. Yan, L. Li, G. Xie, Y. Ren, N. Ahmed, Z. Wang, C. Liu, A. J. Willner, P. Song, *et al.*, "A dual-channel 60 ghz communications link using patch antenna arrays to generate data-carrying orbital-angular-momentum beams," in *2016 IEEE International Conference on Communications (ICC)*, pp. 1–6, IEEE, 2016.

[10] D. Liu, L. Gui, Z. Zhang, H. Chen, G. Song, and T. Jiang, "Multiplexed oam wave communication with two-oam-mode antenna systems," *IEEE Access*, vol. 7, pp. 4160–4166, 2018.

[11] F. Qin, L. Li, Y. Liu, W. Cheng, and H. Zhang, "A four-mode oam antenna array with equal divergence angle," *IEEE Antennas and Wireless Propagation Letters*, vol. 18, no. 9, pp. 1941–1945, 2019.

[12] Y.-M. Zhang and J.-L. Li, "Analyses and full-duplex applications of circularly polarized oam arrays using sequentially rotated configuration," *IEEE Transactions on Antennas and Propagation*, vol. 66, no. 12, pp. 7010–7020, 2018.

[13] J. Wu, Z. Huang, X. Ren, W. E. Sha, and X. Wu, "Wideband millimeter-wave dual-mode dual circularly polarized oam antenna using sequentially rotated feeding technique," *IEEE Antennas and Wireless Propagation Letters*, vol. 19, no. 8, pp. 1296–1300, 2020.

[14] L. Cheng, W. Hong, and Z.-C. Hao, "Generation of electromagnetic waves with arbitrary orbital angular momentum modes," *Scientific reports*, vol. 4, no. 1, p. 4814, 2014.

[15] N. Gagnon, A. Petosa, and D. A. McNamara, "Research and development on phase-shifting surfaces (psss)," *IEEE Antennas and Propagation Magazine*, vol. 55, no. 2, pp. 29–48, 2013.

[16] D. Zelenchuk and V. Fusco, "Split-ring fss spiral phase plate," *IEEE Antennas and Wireless Propagation Letters*, vol. 12, pp. 284–287, 2013.

[17] Y. Chen, S. Zheng, Y. Li, X. Hui, X. Jin, H. Chi, and X. Zhang, "A flat-lensed spiral phase plate based on phase-shifting surface for generation of millimeter-wave oam beam," *IEEE Antennas and Wireless Propagation Letters*, vol. 15, pp. 1156–1158, 2015.

[18] S. Yu, L. Li, G. Shi, C. Zhu, and Y. Shi, "Generating multiple orbital angular momentum vortex beams using a metasurface in radio frequency domain," *Applied Physics Letters*, vol. 108, no. 24, 2016.

[19] B. Allen, T. Drysdale, S. Zhang, D. Isakov, A. Tennant, W. Whittow, C. Stevens, J. Vardaxoglou, and J. Coon, "Reduction of orbital angular momentum radio beam divergence using a 3d printed planar graded index lenses," in *12th European Conference on Antennas and Propagation (EuCAP 2018)*, p. 83, IET, 2018.

[20] Y. Yao, X. Liang, W. Zhu, J. Li, J. Geng, R. Jin, and K. Zhuang, "Realizing orbital angular momentum (oam) beam with small divergence angle by luneberg lens," in *2017 IEEE International Symposium on Antennas and Propagation & USNC/URSI National Radio Science Meeting*, pp. 367–368, IEEE, 2017.

[21] Z. Zhao, G. Xie, L. Li, H. Song, C. Liu, K. Pang, R. Zhang, C. Bao, Z. Wang, S. Sajuyigbe, *et al.*, "Performance of using antenna arrays to generate and receive mm-wave orbital-angular-momentum beams," in *GLOBECOM 2017-2017 IEEE Global Communications Conference*, pp. 1–6, IEEE, 2017.

[22] M. Barbuto, F. Trotta, F. Bilotti, and A. Toscano, "Circular polarized patch antenna generating orbital angular momentum," *Progress In Electromagnetics Research*, vol. 148, pp. 23–30, 2014.

[23] Y. Huang, Z. Qi, Q. Li, H. Zhu, X. Li, X. Li, and X. Jiang, "A broadband multi-oam-mode four-feed circular patch antenna with high mode purity," in *2018 IEEE Asia-Pacific Conference on Antennas and Propagation (APCAP)*, pp. 494–495, IEEE, 2018.

[24] H. Tang, C. Yu, S. Xiao, Z. Yi, Y. Wu, and K. Kang, "Single-fed oam antenna based on half-mode substrate integrated waveguide," in *2018 IEEE Asia-Pacific Conference on Antennas and Propagation (APCAP)*, pp. 116–117, IEEE, 2018.

[25] S. Singh, M. D. Upadhayay, and S. Pal, "Oam wave generation using square-shaped patch antenna as slot array equivalence," *IEEE Antennas and Wireless Propagation Letters*, vol. 19, no. 4, pp. 680–684, 2020.

[26] S. Loyka and C. D. Charalambous, "A General Formula for Compound Channel Capacity," *IEEE Transactions on Information Theory*, vol. 62, no. 7, pp. 3971–3991, 2016.

[27] N. Melouki, A. Hocini, F. Z. Fegriche, P. PourMohammadi, H. Naseri, A. Iqbal, and T. A. Denidni, "High-gain wideband circularly polarised fabry–perot resonator array antenna using a single-layered pixelated prs for millimetre-wave applications," *Micromachines*, vol. 13, no. 10, p. 1658, 2022.

[28] Z. Mousavirazi, M. M. M. Ali, H. N. Gheisanab, and T. A. Denidni, "Analysis and design of ultra-wideband PRGW hybrid coupler using PEC/PMC waveguide model," *Scientific reports*, vol. 12, no. 1, p. 14214, 2022.

[29] P. PourMohammadi, H. Naseri, R. Alwahishi, G. A. Vandenbosch, and T. A. Denidni, "A 2×3 high-gain coupled patch array for body area network applications," in *2022 IEEE International Symposium on Antennas and Propagation and USNC-URSI Radio Science Meeting (AP-S/URSI)*, pp. 2068–2069, IEEE, 2022.

[30] Y. Yan, G. Xie, M. P. Lavery, H. Huang, N. Ahmed, C. Bao, Y. Ren, Y. Cao, L. Li, Z. Zhao, A. F. Molisch, M. Tur, M. J. Padgett, and A. E. Willner, "High-capacity millimetre-wave communications with orbital angular momentum multiplexing," *Nature Communications*, vol. 5, pp. 1–9, 2014.

[31] X. Bai, X. Liang, R. Jin, and J. Geng, "Generation of OAM radio waves with three polarizations using circular horn antenna array," *2015 9th European Conference on Antennas and Propagation, EuCAP 2015*, 2015.

[32] H. Wu, Y. Yuan, Z. Zhang, and J. Cang, "UCA-based orbital angular momentum radio beam generation and reception under different array configurations," *2014 6th International Conference on Wireless Communications and Signal Processing, WCSP 2014*, pp. 1–6, 2014.

[33] B. Palacin, K. Sharshavina, K. Nguyen, and N. Capet, "An 8×8 Butler matrix for generation of waves carrying Orbital Angular Momentum (OAM)," *8th European Conference on Antennas and Propagation, EuCAP 2014*, no. EuCAP, pp. 2814–2818, 2014.

[34] Z. G. Guo and G. M. Yang, "Radial uniform circular antenna array for dual-mode OAM communication," *IEEE Antennas and Wireless Propagation Letters*, vol. 16, pp. 404–407, 2017.

[35] W. Wei, K. Mahdjoubi, C. Brousseau, and O. Emile, "Generation of OAM waves with circular phase shifter and array of patch antennas," *Electronics Letters*, vol. 51, no. 6, pp. 442–443, 2015.

[36] C. Sun, S. Yang, Y. Chen, J. Guo, and S. Qu, "Realization of multiple orbital angular momentum modes simultaneously through four-dimensional antenna arrays," *Scientific Reports*, vol. 8, no. 1, pp. 1–8, 2018.

[37] T. Zhang, J. Hu, Q. Zhang, D. Zhu, Y. Ma, B. Lin, and W. Wu, "A Compact Multimode OAM Antenna Using Sequentially Rotated Configuration," *IEEE Antennas and Wireless Propagation Letters*, vol. 21, no. 1, pp. 134–138, 2022.

[38] Z. Zhao, Y. Yan, L. Li, G. Xie, Y. Ren, N. Ahmed, Z. Wang, C. Liu, A. J. Willner, P. Song, H. Hashemi, H. Yao, D. Macfarlane, R. Henderson, N. Ashrafi, S. Ashrafi, S. Talwar, S. Sajuyigbe, M. Tur, A. F. Molisch, and A. E. Willner, "A dual-channel 60 GHz communications link using patch antenna arrays to generate data-carrying orbital-angular-momentum beams," *2016 IEEE International Conference on Communications, ICC 2016*, 2016.

[39] B. Liu, G. Lin, Y. Cui, and R. L. Li, "An Orbital Angular Momentum (OAM) Mode Reconfigurable Antenna for Channel Capacity Improvement and Digital Data Encoding," *Scientific Reports*, vol. 7, no. 1, pp. 1–9, 2017.

[40] Q. Liu, Z. N. Chen, Y. Liu, F. Li, Y. Chen, and Z. Mo, "Circular Polarization and Mode Reconfigurable Wideband Orbital Angular Momentum Patch Array Antenna," *IEEE Transactions on Antennas and Propagation*, vol. 66, no. 4, pp. 1796–1804, 2018.

[41] J. Wu, Z. Zhang, X. Ren, Z. Huang, and X. Wu, "A Broadband Electronically Mode-Reconfigurable Orbital Angular Momentum Metasurface Antenna," *IEEE Antennas and Wireless Propagation Letters*, vol. 18, no. 7, pp. 1482–1486, 2019.

[42] H. Li, L. Kang, and K. Dong, "Generating Tunable Orbital Angular Momentum Radio Beams with Dual-Circular-Polarization and Dual-Mode Characteristics," *IEEE Access*, vol. 8, pp. 211248–211254, 2020.

[43] L. Kang, H. Li, J. Zhou, and S. Zheng, "An OAM-Mode Reconfigurable Array Antenna with Polarization Agility," *IEEE Access*, vol. 8, pp. 40445–40452, 2020.

[44] H. F. Huang and Z. P. Zhang, "A single fed wideband mode-reconfigurable OAM metasurface CP antenna array with simple feeding scheme," *International Journal of RF and Microwave Computer-Aided Engineering*, vol. 31, no. 2, pp. 1–8, 2021.

[45] H. Naseri, P. Pourmohammadi, Z. Mousavirazi, A. Iqbal, and T. A. Denidni, "Full azimuth beam steering by means of radiation pattern with the narrow beamwidth," in *2022 IEEE International Symposium on Antennas and Propagation and USNC-URSI Radio Science Meeting (AP-S/URSI)*, pp. 1630–1631, IEEE, 2022.

[46] H. Nasseri, M. Bemani, and A. Ghaffarlou, "A new method for arbitrary amplitude distribution generation in 4 × 8 butler matrix," *IEEE Microwave and Wireless Components Letters*, vol. 30, no. 3, pp. 249–252, 2020.

[47] Z. Liao, Y. Che, L. Liu, B. C. Pan, B. G. Cai, J. N. Zhou, G. Q. Luo, and Y. Liu, "Reconfigurable vector vortex beams using spoof surface plasmon ring resonators," *IEEE Transactions on Antennas and Propagation*, 2022.

[48] L. Davoli, L. Belli, A. Cilfone, and G. Ferrari, "From micro to macro iot : Challenges and solutions in the integration of ieee 802.15. 4/802.11 and sub-ghz technologies," *IEEE Internet of Things Journal*, vol. 5, no. 2, pp. 784–793, 2017.

[49] F. Meneghello, M. Calore, D. Zucchetto, M. Polese, and A. Zanella, "Iot : Internet of threats? a survey of practical security vulnerabilities in real iot devices," *IEEE Internet of Things Journal*, vol. 6, no. 5, pp. 8182–8201, 2019.

[50] M. Mercuri, G. Sacco, R. Hornung, P. Zhang, H. J. Visser, M. Hijdra, Y.-H. Liu, S. Pisa, B. van Liempd, and T. Torfs, "2-d localization, angular separation and vital signs monitoring using a siso fmcw radar for smart long-term health monitoring environments," *IEEE Internet of Things Journal*, vol. 8, no. 14, pp. 11065–11077, 2021.

[51] J. Hwang, L. Nkenyereye, N. Sung, J. Kim, and J. Song, "Iot service slicing and task offloading for edge computing," *IEEE Internet of Things Journal*, vol. 8, no. 14, pp. 11526–11547, 2021.

[52] J. An, F. Le Gall, J. Kim, J. Yun, J. Hwang, M. Bauer, M. Zhao, and J. Song, "Toward global iot-enabled smart cities interworking using adaptive semantic adapter," *IEEE Internet of Things Journal*, vol. 6, no. 3, pp. 5753–5765, 2019.

[53] X. Zhang, M. Pipattanasomporn, T. Chen, and S. Rahman, "An iot-based thermal model learning framework for smart buildings," *IEEE Internet of Things Journal*, vol. 7, no. 1, pp. 518–527, 2019.

[54] R. Hussain, "Shared-aperture slot-based sub-6-ghz and mm-wave iot antenna for 5g applications," *IEEE Internet of Things Journal*, vol. 8, no. 13, pp. 10807–10814, 2021.

[55] C. Li, Y. Duan, B. Du, and X. Tao, "Adjustable dielectric resonator antenna with parasitic elements for 5g sagoi-iot applications," *IEEE Internet of Things Journal*, 2022.

[56] P. P. Shome, T. Khan, A. A. Kishk, and Y. M. Antar, "Quad-element mimo antenna system using half-cut miniaturized uwb antenna for iot-based smart home digital entertainment network," *IEEE Internet of Things Journal*, 2023.

[57] N. Hussain and N. Kim, "Integrated microwave and mm-wave mimo antenna module with 360 pattern diversity for 5g internet of things," *IEEE Internet of Things Journal*, vol. 9, no. 24, pp. 24777–24789, 2022.

[58] S. M. Mohammadi, L. K. Daldorff, K. Forozesh, B. Thidé, J. E. Bergman, B. Isham, R. Karlsson, and T. D. Carozzi, "Orbital angular momentum in radio : Measurement methods," *Radio Science*, vol. 45, no. 4, pp. 565–572, 2010.

[59] O. Edfors and A. J. Johansson, "Is orbital angular momentum (oam) based radio communication an unexploited area?," *IEEE Transactions on Antennas and Propagation*, vol. 60, no. 2, pp. 1126–1131, 2011.

[60] L. Wang, H. Shi, X. Chen, B. Qu, J. Yi, A. Zhang, Z. Xu, and H. Liu, "Multibeam metasurface antenna enabled by orbital angular momentum demultiplexing feeding for iot communication," *IEEE Internet of Things Journal*, 2023.

[61] C. Guo, X. Zhao, C. Zhu, P. Xu, and Y. Zhang, "An oam patch antenna design and its array for higher order oam mode generation," *IEEE Antennas and Wireless Propagation Letters*, vol. 18, no. 5, pp. 816–820, 2019.

[62] H. Naseri, P. Pourmohammadi, M. S. Bizan, N. Melouki, F. Ahmed, A. Iqbal, and T. A. Denidni, "Reconfigurable dielectric resonator oam antenna with augmented modes," in *2023 IEEE International Symposium on Antennas and Propagation and USNC-URSI Radio Science Meeting (USNC-URSI)*, pp. 703–704, IEEE, 2023.

[63] G. Xie, Z. Zhao, Y. Yan, L. Li, Y. Ren, N. Ahmed, Y. Cao, A. J. Willner, C. Bao, Z. Wang, C. Liu, M. Ziyadi, S. Talwar, S. Sajuyigbe, S. Ashrafi, M. Tur, A. F. Molisch, and A. E. Willner, "Demonstration of Tunable Steering and Multiplexing of Two 28 GHz Data Carrying Orbital Angular Momentum Beams Using Antenna Array," *Scientific Reports*, vol. 6, no. November, pp. 1–9, 2016.

[64] L. Fang, H. Yao, and R. M. Henderson, "OAM antenna arrays at E-band," *IEEE MTT-S International Microwave Symposium Digest*, pp. 658–661, 2017.

[65] X. D. Bai, X. L. Liang, Y. T. Sun, P. C. Hu, Y. Yao, K. Wang, J. P. Geng, and R. H. Jin, "Experimental Array for Generating Dual Circularly-Polarized Dual-Mode OAM Radio Beams," *Scientific Reports*, vol. 7, no. November 2016, pp. 1–8, 2017.

[66] B. Liu, Y. Cui, and R. Li, "A broadband dual-polarized dual-oam-mode antenna array for oam communication," *IEEE Antennas and Wireless Propagation Letters*, vol. 16, pp. 744–747, 2016.

[67] H. Li, L. Kang, F. Wei, Y. M. Cai, and Y. Z. Yin, "A Low-Profile Dual-Polarized Microstrip Antenna Array for Dual-Mode OAM Applications," *IEEE Antennas and Wireless Propagation Letters*, vol. 16, pp. 3022–3025, 2017.

[68] F. Qin, L. Li, Y. Liu, W. Cheng, and H. Zhang, "A four-mode OAM antenna array with equal divergence angle," *IEEE Antennas and Wireless Propagation Letters*, vol. 18, no. 9, pp. 1941–1945, 2019.

[69] D. Liu, L. Gui, Z. Zhang, H. Chen, G. Song, and T. Jiang, "Multiplexed OAM Wave Communication with Two-OAM-Mode Antenna Systems," *IEEE Access*, vol. 7, pp. 4160–4166, 2019.

[70] L. Kang, H. Li, J. Zhou, and S. Zheng, "An OAM-Mode Reconfigurable Array Antenna with Polarization Agility," *IEEE Access*, vol. 8, pp. 40445–40452, 2020.

[71] J. Ming and Y. Shi, "A Mode Reconfigurable Orbital Angular Momentum Water Antenna," *IEEE Access*, vol. 8, pp. 89152–89160, 2020.

[72] Y. Y. Wang, Y. X. Du, L. Qin, and B. S. Li, "An electronically mode reconfigurable orbital angular momentum array antenna," *IEEE Access*, vol. 6, pp. 64603–64610, 2018.

[73] Y. X. Du, H. Liu, L. Qin, and B. S. Li, "Integrated Multimode Orbital Angular Momentum Antenna Based on RF Switch," *IEEE Access*, vol. 8, pp. 48599–48606, 2020.

[74] H. Song, H. Zhou, K. Zou, R. Zhang, K. Pang, H. Song, A. Minoofar, X. Su, N. Hu, C. Liu, *et al.*, "Demonstration of generating a 100 gbit/s orbital-angular-momentum beam with a tunable mode order over a range of wavelengths using an integrated broadband pixel-array structure," *Optics Letters*, vol. 46, no. 19, pp. 4765–4768, 2021.

[75] G. Xie, Y. Yan, Z. Zhao, L. Li, Y. Ren, N. Ahmed, A. J. Willner, C. Bao, Z. Wang, C. Liu, *et al.*, "Tunable generation and angular steering of a millimeter-wave orbital-angular-momentum

beam using differential time delays in a circular antenna array," in *2016 IEEE International Conference on Communications (ICC)*, pp. 1–6, IEEE, 2016.

[76] Y. Shi, Q. W. Wu, and J. Ming, "An archimedean spiral antenna for generation of tunable angular momentum wave," *IEEE Access*, vol. 9, pp. 63122–63130, 2021.

[77] C. Deng, K. Zhang, and Z. Feng, "Generating and measuring tunable orbital angular momentum radio beams with digital control method," *IEEE Transactions on Antennas and Propagation*, vol. 65, no. 2, pp. 899–902, 2016.

[78] H. Naseri, P. PourMohammadi, N. Melouki, A. Iqbal, and T. A. Denidni, "A Low-profile Antenna System for Generating Reconfigurable OAM-carrying Beams," *IEEE Antennas and Wireless Propagation Letters*, pp. 1–5, 2022.

[79] Y. Wang, K. Zhang, Y. Yuan, X. Ding, G. Yang, J. Fu, and Q. Wu, "Generation of High-Efficiency Vortex Beam Carrying OAM Mode Based on Miniaturized Element Frequency Selective Surfaces," *IEEE Transactions on Magnetics*, vol. 55, no. 10, pp. 1–4, 2019.

[80] D. Zelenchuk and V. Fusco, "Split-ring FSS spiral phase plate," *IEEE Antennas and Wireless Propagation Letters*, vol. 12, pp. 284–287, 2013.

[81] Y. Chen, S. Zheng, Y. Li, X. Hui, X. Jin, H. Chi, and X. Zhang, "A Flat-Lensed Spiral Phase Plate Based on Phase-Shifting Surface for Generation of Millimeter-Wave OAM Beam," *IEEE Antennas and Wireless Propagation Letters*, vol. 15, pp. 1156–1158, 2016.

[82] A. V. Shahmirzadi, Z. Badamchi, B. Badamchi, and H. Subbaraman, "Generating concentrically embedded spatially divided oam carrying vortex beams using transmitarrays," *IEEE Transactions on Antennas and Propagation*, vol. 69, no. 12, pp. 8436–8448, 2021.

[83] A. V. Shahmirzadi and A. A. Kishk, "OAM Carrying Vortex Beam Mode Interconversion Using Modular Cascaded Transmitarrays," *IEEE Transactions on Microwave Theory and Techniques*, pp. 1–15, 2022.

[84] K. Guo, Q. Zheng, Z. Yin, and Z. Guo, "Generation of mode-reconfigurable and frequency-adjustable oam beams using dynamic reflective metasurface," *IEEE Access*, vol. 8, pp. 75523–75529, 2020.

[85] H. Naseri, P. PourMohammadi, N. Melouki, F. Ahmed, A. Iqbal, and T. A. Denidni, "Generation of mixed-oam-carrying waves using huygens' metasurface for mm-wave applications," *Sensors*, vol. 23, no. 5, p. 2590, 2023.

[86] Y. Zhao, Z. Wang, Y. Lu, and Y. L. Guan, "Multi-mode oam convergent transmission with co-divergent angle tailored by airy wavefront," *IEEE Transactions on Antennas and Propagation*, 2023.

[87] W. Iqbal, H. Abbas, M. Daneshmand, B. Rauf, and Y. A. Bangash, "An in-depth analysis of iot security requirements, challenges, and their countermeasures via software-defined security," *IEEE Internet of Things Journal*, vol. 7, no. 10, pp. 10250–10276, 2020.

[88] K.-Y. Lam, S. Mitra, F. Gondesen, and X. Yi, "Ant-centric iot security reference architecture—security-by-design for satellite-enabled smart cities," *IEEE Internet of Things Journal*, vol. 9, no. 8, pp. 5895–5908, 2021.

[89] E. Erdil, K. Topalli, M. Unlu, O. A. Civi, and T. Akin, "Frequency tunable microstrip patch antenna using rf mems technology," *IEEE transactions on antennas and propagation*, vol. 55, no. 4, pp. 1193–1196, 2007.

[90] S.-S. Oh, W.-K. Park, Y.-B. Jung, T.-I. Choi, and Y.-H. Lee, "Frequency-tunable open-ring microstrip antenna with optimally-positioned varactors for radiated-power in situ measurements," *AEU-International Journal of Electronics and Communications*, vol. 68, no. 9, pp. 841–845, 2014.

[91] S. P. Lavadiya, S. K. Patel, and R. Maria, "High gain and frequency reconfigurable copper and liquid metamaterial tooth based microstrip patch antenna," *AEU-International Journal of Electronics and Communications*, vol. 137, p. 153799, 2021.

[92] N. C. Pradhan and S. Koziel, "Shielded hmsiw-based frequency-tunable self-quadruplexing antenna using different solid/liquid dielectrics," *AEU-International Journal of Electronics and Communications*, p. 155071, 2023.

[93] V. Rajeshkumar and S. Raghavan, "A compact metamaterial inspired triple band antenna for reconfigurable wlan/wimax applications," *AEU-International Journal of Electronics and Communications*, vol. 69, no. 1, pp. 274–280, 2015.

[94] H. Naseri, P. PourMohammadi, A. Iqbal, A. A. Kishk, and T. A. Denidni, "Siw-based self-quadruplexing antenna for microwave and mm-wave frequencies," *IEEE Antennas and Wireless Propagation Letters*, vol. 21, no. 7, pp. 1482–1486, 2022.

[95] E. Cano, B. Allen, Q. Bai, and A. Tennant, "Generation and detection of OAM signals for radio communications," *2014 Loughborough Antennas and Propagation Conference, LAPC 2014*, no. November, pp. 637–640, 2014.

[96] O. Edfors and A. J. Johansson, "Is orbital angular momentum (oam) based radio communication an unexploited area?," *IEEE Transactions on Antennas and Propagation*, vol. 60, no. 2, pp. 1126–1131, 2011.

[97] H. Naseri, P. PourMohammadi, N. Melouki, F. Ahmed, A. Iqbal, and T. A. Denidni, "Generation of mixed-oam-carrying waves using huygens' metasurface for mm-wave applications," *Sensors*, vol. 23, no. 5, p. 2590, 2023.

[98] L. Wang, X. Ge, R. Zi, and C.-X. Wang, "Capacity analysis of orbital angular momentum wireless channels," *IEEE Access*, vol. 5, pp. 23069–23077, 2017.

[99] P. PourMohammadi, H. Naseri, N. Melouki, F. Ahmed, A. Iqbal, G. A. Vandenbosch, and T. A. Denidni, "Compact siw-based self-quadruplexing antenna for microwave and mm-wave communications," *IEEE Transactions on Circuits and Systems II : Express Briefs*, vol. 21, no. 7, pp. 1482–1486, 2023.

[100] M. H. Hassan, M. Al-Mulla, B. Sievert, A. Rennings, and D. Erni, "Evaluation of different phased array approaches for orbital angular momentum beam steering," in *2020 German Microwave Conference (GeMiC)*, pp. 44–47, IEEE, 2020.

[101] H. Nasseri, M. Bemani, and A. Ghaffarlou, "A new method for arbitrary amplitude distribution generation in 4×8 butler matrix," *IEEE Microwave and Wireless Components Letters*, vol. 30, no. 3, pp. 249–252, 2020.

[102] T. Qi, S. He, Z. Dai, and W. Shi, "Novel unequal dividing power divider with 50 ohm characteristic impedance lines," *IEEE Microwave and Wireless Components Letters*, vol. 26, no. 3, pp. 180–182, 2016.

[103] D. Yang, Y. Yuan, Q. Wu, and K. Zhang, "High gain oam antenna with low profile utilizing integrated reflective metasurface," *IEEE Antennas and Wireless Propagation Letters*, vol. 23, no. 1, pp. 294–298, 2023.

[104] S. M. Mohammadi, L. K. Daldorff, J. E. Bergman, R. L. Karlsson, B. Thidé, K. Forozesh, T. D. Carozzi, and B. Isham, "Orbital angular momentum in radio—a system study," *IEEE transactions on Antennas and Propagation*, vol. 58, no. 2, pp. 565–572, 2009.

[105] B. Liu, G. Lin, Y. Cui, and R. Li, "An orbital angular momentum (oam) mode reconfigurable antenna for channel capacity improvement and digital data encoding," *Scientific reports*, vol. 7, no. 1, p. 9852, 2017.

[106] M. Jie and S. Yan, "A mode reconfigurable orbital angular momentum water antenna [j]," *IEEE Access*, vol. 8, pp. 89152–89160, 2020.

[107] Y.-X. Du, H. Liu, L. Qin, and B.-S. Li, "Integrated multimode orbital angular momentum antenna based on rf switch," *IEEE Access*, vol. 8, pp. 48599–48606, 2020.

[108] L. Kang, H. Li, J. Zhou, and S. Zheng, "An oam-mode reconfigurable array antenna with polarization agility," *IEEE Access*, vol. 8, pp. 40445–40452, 2020.

[109] Q. Liu, Z. N. Chen, Y. Liu, F. Li, Y. Chen, and Z. Mo, "Circular polarization and mode reconfigurable wideband orbital angular momentum patch array antenna," *IEEE Transactions on Antennas and Propagation*, vol. 66, no. 4, pp. 1796–1804, 2018.

[110] J. Wu, M. Fan, X. Lu, J. Hu, G. Xie, and Z. Huang, "Circularly polarized and linear polarized mode multiplexing oam antenna using sequentially rotated technique," *IEEE Antennas and Wireless Propagation Letters*, vol. 23, no. 4, pp. 1261–1265, 2024.

[111] H. Naseri, P. PourMohammadi, N. Melouki, F. Ahmed, A. Iqbal, and T. A. Denidni, "Reconfigurable oam antenna with flexibility on mode numbers, polarization and frequency," *IEEE Antennas and Wireless Propagation Letters*, 2024.

[112] Y. Cui, R. Li, and H. Fu, "A broadband dual-polarized planar antenna for 2g/3g/lte base stations," *IEEE transactions on antennas and propagation*, vol. 62, no. 9, pp. 4836–4840, 2014.

[113] Y. Yan, G. Xie, M. P. Lavery, H. Huang, N. Ahmed, C. Bao, Y. Ren, Y. Cao, L. Li, Z. Zhao, *et al.*, "High-capacity millimetre-wave communications with orbital angular momentum multiplexing," *Nature Communications*, vol. 5, no. 1, p. 4876, 2014.

[114] X. Hui, S. Zheng, Y. Chen, Y. Hu, X. Jin, H. Chi, and X. Zhang, "Multiplexed millimeter wave communication with dual orbital angular momentum (oam) mode antennas," *Scientific Reports*, vol. 5, no. 1, p. 8578, 2015.

[115] H. Li, L. Kang, and K. Dong, "Generating tunable orbital angular momentum radio beams with dual-circular-polarization and dual-mode characteristics," *IEEE Access*, vol. 8, pp. 211248–211254, 2020.

[116] W. Li, L. Zhang, S. Yang, K. Zhuo, L. Ye, and Q. H. Liu, "A reconfigurable second-order oam patch antenna with simple structure," *IEEE Antennas and Wireless Propagation Letters*, vol. 19, no. 9, pp. 1531–1535, 2020.

[117] H. Huang and Z. Zhang, "A single fed wideband mode-reconfigurable oam metasurface cp antenna array with simple feeding scheme," *International Journal of RF and Microwave Computer-Aided Engineering*, vol. 31, no. 2, p. e22499, 2021.

[118] J. Wu, Z. Zhang, X. Ren, Z. Huang, and X. Wu, "A broadband electronically mode-reconfigurable orbital angular momentum metasurface antenna," *IEEE Antennas and Wireless Propagation Letters*, vol. 18, no. 7, pp. 1482–1486, 2019.

[119] L. Kang, H. Li, J. Zhou, S. Zheng, and S. Gao, "A mode-reconfigurable orbital angular momentum antenna with simplified feeding scheme," *IEEE Transactions on Antennas and Propagation*, vol. 67, no. 7, pp. 4866–4871, 2019.

[120] Z. Wang, X. Pan, F. Yang, S. Xu, and M. Li, "Real-time mode switching and beam scanning of high-gain oam waves using a 1-bit reconfigurable reflectarray antenna," *Electronics*, vol. 9, no. 12, p. 2181, 2020.

[121] B. Liu, S. Li, Y. He, Y. Li, and S.-W. Wong, "Generation of an orbital-angular-momentum-mode-reconfigurable beam by a broadband 1-bit electronically reconfigurable transmitarray," *Physical Review Applied*, vol. 15, no. 4, p. 044035, 2021.

[122] L. Li and X. Zhou, "Mechanically reconfigurable single-arm spiral antenna array for generation of broadband circularly polarized orbital angular momentum vortex waves," *Scientific Reports*, vol. 8, no. 1, p. 5128, 2018.

[123] J. Ming and Y. Shi, "A mode reconfigurable orbital angular momentum water antenna," *IEEE Access*, vol. 8, pp. 89152–89160, 2020.

[124] H. Naseri, P. PourMohammadi, N. Melouki, A. Iqbal, and T. A. Denidni, "A low-profile antenna system for generating reconfigurable oam-carrying beams," *IEEE Antennas and Wireless Propagation Letters*, 2022.

[125] H. Li, L. Kang, F. Wei, Y.-M. Cai, and Y.-Z. Yin, "A low-profile dual-polarized microstrip antenna array for dual-mode oam applications," *IEEE Antennas and Wireless Propagation Letters*, vol. 16, pp. 3022–3025, 2017.

[126] X. Xu, A. Mazzinghi, A. Freni, and J. Hirokawa, "Simultaneous generation of three oam modes by using a rlsa fed by a waveguide circuit for 60 ghz-band radiative near-field region oam multiplexing," *IEEE Transactions on Antennas and Propagation*, vol. 69, no. 3, pp. 1249–1259, 2020.

[127] Z.-G. Guo and G.-M. Yang, "Radial uniform circular antenna array for dual-mode oam communication," *IEEE Antennas and Wireless Propagation Letters*, vol. 16, pp. 404–407, 2016.

[128] J. Yoo and H. Son, "Quad-mode radial uniform circular array antenna for oam multiplexing," *IET Microwaves, Antennas and Propagation*, vol. 14, no. 8, pp. 728–733, 2020.

[129] B. Palacin, K. Sharshavina, K. Nguyen, and N. Capet, "An 8× 8 butler matrix for generation of waves carrying orbital angular momentum (oam)," in *The 8th European Conference on Antennas and Propagation (EuCAP 2014)*, pp. 2814–2818, IEEE, 2014.

[130] X.-D. Bai, X.-L. Liang, Y.-T. Sun, P.-C. Hu, Y. Yao, K. Wang, J.-P. Geng, and R.-H. Jin, "Experimental array for generating dual circularly-polarized dual-mode oam radio beams," *Scientific reports*, vol. 7, no. 1, p. 40099, 2017.

[131] A. Mazzinghi and A. Freni, "Simultaneous generation of pseudo-bessel vortex modes with a rlsa," *IEEE Antennas and Wireless Propagation Letters*, vol. 16, pp. 1747–1750, 2017.

[132] W. Zhang, S. Zheng, X. Hui, Y. Chen, X. Jin, H. Chi, and X. Zhang, "Four-oam-mode antenna with traveling-wave ring-slot structure," *IEEE Antennas and Wireless Propagation Letters*, vol. 16, pp. 194–197, 2016.

[133] J. Liang and S. Zhang, "Orbital angular momentum (oam) generation by cylinder dielectric resonator antenna for future wireless communications," *IEEE Access*, vol. 4, pp. 9570–9574, 2016.

[134] Y. Yang, Z. Wang, S. Wang, Q. Zhou, F. Shen, H. Jiang, Z. Wu, B. Zeng, Z. Guo, and Y. Gong, "Designing a water-immersed rectangular horn antenna for generating underwater oam waves," *Electronics*, vol. 8, no. 11, p. 1224, 2019.

[135] L. Wang, H. Chen, K. Guo, F. Shen, and Z. Guo, "An inner-and outer-fed dual-arm archimedean spiral antenna for generating multiple orbital angular momentum modes," *Electronics*, vol. 8, no. 2, p. 251, 2019.

[136] S. Zheng, X. Hui, X. Jin, H. Chi, and X. Zhang, "Transmission characteristics of a twisted radio wave based on circular traveling-wave antenna," *IEEE Transactions on Antennas and Propagation*, vol. 63, no. 4, pp. 1530–1536, 2015.

[137] Q. Zhang, W. Chen, H. Sun, J. Fu, Y. Zhao, H. Feng, and K. Zhang, "A circular-polarized vortex beams generation with orbital angular momentum based on a leaky-wave antenna," *IEEE Antennas and Wireless Propagation Letters*, 2023.

[138] M. Esfandiyari, A. Lalbakhsh, S. Jarchi, M. Ghaffari-Miab, H. Noori Mahtaj, and R. B. Simorangkir, "Tunable terahertz filter/antenna-sensor using graphene-based metamaterials," *Materials and Design*, vol. 220, p. 110855, 2022.

[139] A. Lalbakhsh, M. U. Afzal, T. Hayat, K. P. Esselle, and K. Mandal, "All-metal wideband metasurface for near-field transformation of medium-to-high gain electromagnetic sources," *Scientific Reports*, vol. 11, no. 1, p. 9421, 2021.

[140] P. Das, K. Mandal, and A. Lalbakhsh, "Beam-steering of microstrip antenna using single-layer fss based phase-shifting surface," *International Journal of RF and Microwave Computer-Aided Engineering*, vol. 32, no. 3, p. e23033, 2022.

[141] S. Adibi, M. A. Honarvar, and A. Lalbakhsh, "Gain enhancement of wideband circularly polarized uwb antenna using fss," *Radio Science*, vol. 56, no. 1, pp. 1–8, 2021.

[142] A. Lalbakhsh, M. U. Afzal, K. P. Esselle, and S. L. Smith, "All-metal wideband frequency-selective surface bandpass filter for te and tm polarizations," *IEEE Transactions on Antennas and Propagation*, vol. 70, no. 4, pp. 2790–2800, 2022.

[143] F. Qin, L. Wan, L. Li, H. Zhang, G. Wei, and S. Gao, "A transmission metasurface for generating oam beams," *IEEE Antennas and Wireless Propagation Letters*, vol. 17, no. 10, pp. 1793–1796, 2018.

[144] J. Xu, K. Bi, R. Zhang, Y. Hao, C. Lan, K. D. McDonald-Maier, X. Zhai, Z. Zhang, and S. Huang, "A small-divergence-angle orbital angular momentum metasurface antenna," *Research*, 2019.

[145] Y. Li, X. Li, L. Chen, M. Pu, J. Jin, M. Hong, and X. Luo, "Orbital angular momentum multiplexing and demultiplexing by a single metasurface," *Advanced Optical Materials*, vol. 5, no. 2, p. 1600502, 2017.

[146] X. Yang, Y. Zhou, and G. Wang, "A wideband transmission metasurface for generating bessel beam carrying orbital angular momentum," *International Journal of RF and Microwave Computer-Aided Engineering*, vol. 29, no. 11, p. e21941, 2019.

[147] H.-F. Huang and H.-M. Huang, "Millimeter-wave wideband high efficiency circular airy oam multibeams with multiplexing oam modes based on transmission metasurfaces," *Progress In Electromagnetics Research*, vol. 173, pp. 151–159, 2022.

[148] H. Wang, S. Yu, N. Kou, Z. Ding, and Z. Zhang, "Cylindrical holographic impedance metasurface for oam vortex wave generation," *Applied Physics Letters*, vol. 120, no. 14, p. 143504, 2022.

[149] L. Wang, H. Shi, J. Yi, L. Dong, H. Liu, A. Zhang, and Z. Xu, "Suspended metasurface for broadband high-efficiency vortex beam generation," *Materials*, vol. 15, no. 3, p. 707, 2022.

[150] M. R. Akram, X. Bai, R. Jin, G. A. Vandenbosch, M. Premaratne, and W. Zhu, "Photon spin hall effect-based ultra-thin transmissive metasurface for efficient generation of oam waves," *IEEE Transactions on Antennas and Propagation*, vol. 67, no. 7, pp. 4650–4658, 2019.

[151] H.-H. Lv, Q.-L. Huang, X.-J. Yi, J.-Q. Hou, and X.-W. Shi, "Low-profile transmitting metasurface using single dielectric substrate for oam generation," *IEEE Antennas and Wireless Propagation Letters*, vol. 19, no. 5, pp. 881–885, 2020.

[152] H. Shi, L. Wang, G. Li, J. Yi, H. Liu, A. Zhang, and Z. Xu, "Guided-wave inspired metasurfaces for multifunctional vortex beam generation and manipulation," *Journal of Lightwave Technology*, 2022.

[153] A. V. Shahmirzadi, Z. Badamchi, B. Badamchi, and H. Subbaraman, "Generating concentrically embedded spatially divided oam carrying vortex beams using transmitarrays," *IEEE Transactions on Antennas and Propagation*, vol. 69, no. 12, pp. 8436–8448, 2021.

[154] A. V. Shahmirzadi and A. A. Kishk, “Oam carrying vortex beam mode interconversion using modular cascaded transmitarrays,” *IEEE Transactions on Microwave Theory and Techniques*, 2022.

[155] Q. Feng, X. Kong, M. Shan, Y. Lin, L. Li, and T. J. Cui, “Multi-orbital-angular-momentum-mode vortex wave multiplexing and demultiplexing with shared-aperture reflective metasurfaces,” *Physical Review Applied*, vol. 17, no. 3, p. 034017, 2022.

[156] H. Chung, D. Kim, E. Choi, and J. Lee, “E-band metasurface-based orbital angular momentum multiplexing and demultiplexing,” *Laser and Photonics Reviews*, vol. 16, no. 6, p. 2100456, 2022.

[157] C. Xue, J. Sun, L. Niu, and Q. Lou, “Ultrathin dual-polarized huygens’ metasurface : Design and application,” *Annalen der Physik*, vol. 532, no. 7, p. 2000151, 2020.

[158] H. Xue, J. Han, S. Zhang, Y. Tian, J. Hou, and L. Li, “Co-modulation of spin angular momentum and high-order orbital angular momentum based on anisotropic holographic metasurfaces,” *IEEE Transactions on Antennas and Propagation*, 2023.